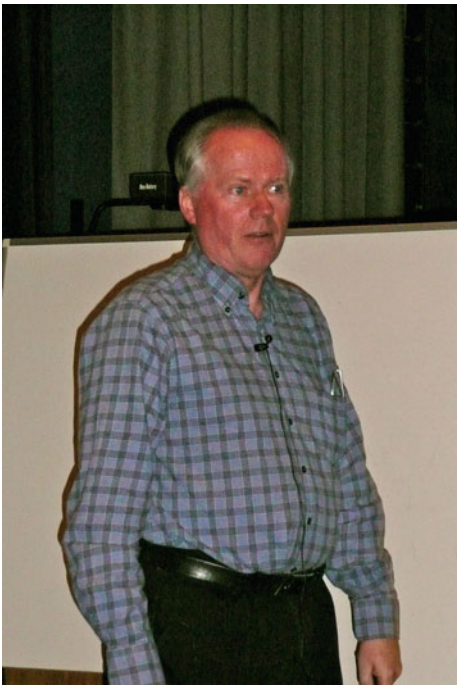

Multi-Messenger Astronomy and Dark Matter

Lars Bergström

1 Preamble

Astrophysics, and more specifically astroparticle physics, has been going through tremendous progress during the last two decades. Still, one of the main problems, that of the nature of the dark matter, remains unsolved. With the help of accelerator experiments (at CERN's Large Hadron Collider (LHC) in particular, which started operation in 2010 and which is currently gathering an impressive integrated luminosity) we could soon hope to get a first indication of the mass scale for the new physics that is associated with dark matter. However, to actually prove that a particle discovered at accelerators has the right properties to constitute the astrophysical dark matter, complementary methods are needed. The fact that a candidate for dark matter is electrically neutral (as not to emit nor absorb light—that is what we mean with the term "dark") can plausibly be determined at accelerators. However, the coupling of the dark matter particles to other matter needs to be weak, and the lifetime of the dark matter particle needs to be at least of the order of the age of the universe. This cannot be tested at accelerators—the dark matter particles would leave the detector in some 100 ns. There could be very useful information still gathered at the LHC, as possibly decays of more massive states in the "dark sector" would be observable, and the missing energy could be estimated.

Fortunately, through observations of various types of messengers—radio waves, microwaves, IR, optical and UV radiation, X-rays, γ-rays and neutrinos, there is great hope that we could get an independent indication of the mass scale of dark matter. This variety of possible methods of indirect detection methods is a part of multi-messenger astronomy, and it is the second way by which we approach the dark matter problem. In particular, for models where the dark matter particles are

L. Bergström
Department of Physics, The Oskar Klein Centre, AlbaNova, Stockholm University,
SE-106 91 Stockholm, Sweden
e-mail: lbe@fysik.su.se

F. Aharonian et al., *Astrophysics at Very High Energies*,
Saas-Fee Advanced Course 40, DOI: 10.1007/978-3-642-36134-0_2,

involved in breaking the electroweak symmetry of the Standard Model, so-called WIMP models (for weakly interacting massive particles), prospects of detection in the near future look promising. We will look in some detail on the properties of WIMP candidates, where the fact that they are massive means that they move non-relativistically in galactic halos, and form so-called cold dark matter (CDM). One thought earlier that neutrinos could be the dark matter, but they would constitute hot dark matter (HDM), which is not favoured by observations. Due to free-streaming motion, they would only form very large structures first, which then fragment into smaller scales, like galaxies. This scenario does not agree with observations, as it gives too little power on small scales. Of course, one may also consider an in-between scenario, warm dark matter, usually consisting of having a sterile neutrino (i.e., with no direct Standard Model couplings) in the keV mass region. These may perhaps have some virtue of explaining possible anomalies in dark matter distribution on the very smallest scales, but reliable methods are so far lacking to probe the dark matter distribution, and its couplings to baryons, on these scales.

As a third approach, ingenious experiments for direct detection employing solid state devices, liquid noble gases, etc. can be used to tell us about other important properties of dark matter, like the spin-dependent or spin-independent cross section of dark matter particle scattering on nucleons. Once signals start to be found (and there are some, however not undisputed ones, already), an exciting puzzle will present itself, putting all these pieces of information together. For indirect detection, astrophysical backgrounds that could mask or mimic dark matter signatures will often be a great challenge to overcome. It should therefore be useful to the reader to study also the accompanying articles by Felix Aharonian and Chuck Dermer in this volume—not the least to understand the very interesting aspects of those processes in their own right.

In this set of lectures, I will treat all of the dark matter-related aspects in some detail, and also cover some other current problems of astroparticle physics and cosmology. The sections in these lectures correspond roughly to the lectures at the Saas-Fee Course in Les Diablerets in March, 2010, i.e.,

- The particle universe: introduction, cosmological parameters.
- Basic cross sections for neutrinos and γ-rays; IceCube.
- Density of relic particles from the early universe.
- Dark matter: direct and indirect detection methods; the galactic centre & other promising DM sources.
- Neutrinos and antimatter from dark matter, Sommerfeld enhancement.
- Supersymmetric dark matter, DarkSUSY.
- Particular dark matter candidates (WIMPS, Kaluza-Klein particles, sterile neutrinos . . .).
- Diffuse extragalactic γ-rays, Primordial black holes, Hawking radiation.
- Gravitational waves.

The order has been slightly changed (cf. the Table of Contents), and in many cases I have updated the material since the time of the lectures, referring to important developments (actually, quite a number of them) that have appeared after the time

of the Course. This is of course mandatory in a field that evolves so rapidly. For the more basic parts of this review, I have relied heavily on the textbook by Ariel Goobar and myself [1]. Also material from various reviews I have written over the last few years [2–5] has come to use, but also a lot of new material. With these lecture notes, I hope to convey at least some of the excitement I feel for this topic, which relates to some of the outstanding questions still with us in particle physics and cosmology.

2 The Particle Universe: Introduction

2.1 Introduction

One of the most impressive achievements of science is the development of a quite detailed understanding of the physical properties of the universe, even at its earliest stages. Thanks to the fruitful interplay between theoretical analysis, astronomical observations and laboratory experiments we have today very successful 'Standard Models' of both particle physics and cosmology. The Standard Model of particle physics involves matter particles: quarks which always form bound states such as neutrons and protons, and leptons like the electron which is charged and therefore can make up neutral matter when bound to nuclei formed by neutrons and protons. There are also neutral leptons, neutrinos, which do not form bound states but which play a very important role in cosmology and particle astrophysics as we will see throughout these lecture notes. The other important ingredients in the Standard Model of particle physics are the particles which mediate the fundamental forces: the photon, the gluons and the W and Z bosons.

The Standard Model of cosmology is the hot model, which states that the universe is not infinitely old but rather came into existence some 13.7 billion years ago. There may have been a short period with extremely rapid expansion, inflation, which diluted all matter, radiation and other structures (like magnetic monopoles) that might have existed before inflation. When inflation ended, there was a rapid heating (or, thus, rather re-heating) which meant a re-start of expansion, now governed by the relativistic degrees of freedom of our universe, i.e., radiation. The expansion started out in a state which after this small fraction of a second was enormously compressed and very hot (the relation between the density and the temperature can be determined by near-equilibrium thermodynamics at this epoch, when the expansion was "slow" and adiabatic). No bound states could exist because of the intense heat which caused immediate dissociation even of protons and neutrons into quarks if they were formed in the quark-gluon plasma. Subsequently, the universe expanded and cooled, making possible the formation of a sequence of ever more complex objects: protons and neutrons, nuclei, atoms, molecules, clouds, stars, planets,.... As we will see, the observational support for the big bang model is overwhelming, but it contains new elements, of dark matter and dark energy, that were not entirely expected. The key observations are:

- The present expansion of the universe.
- The existence of the cosmic microwave background radiation (CMBR), i.e. the relic radiation from the hot stage of the early universe, and measurements of the temperature variations therein.
- The presence of related structure in the late-time distribution of galaxies, so-called "baryon acoustic oscillations" (BAO).
- Supernova cosmology that measures the expansion history, with the surprising result that the cosmic expansion is accelerating.
- The successful calculations of the relative abundance of light elements in the universe, which accurately agrees with what would be synthesized in an initially hot, expanding universe.
- The concept of cosmological inflation, which successfully predicted the geometric flatness of the universe, (thus that the average density is near the critical density, i.e., $\Omega_{tot} = 1$ to an excellent approximation) and gave an explanation of the form of the nearly scale invariant, gaussian temperature fluctuations.
- The discovery of dark matter, pioneered by Zwicky in the 1930s, has stood the test of time and is now an established piece of the cosmological standard model. Dark energy, in its simplest form just a constant vacuum energy, is the other part which explains $\Omega_{tot} = 1$ and the accelerated expansion of the universe.

Several of these observations have been awarded the Nobel Prize, the latest thus being the prize for the discovery of the accelerated expansion of the universe through supernova observations (S. Perlmutter, B. Schmidt and A. Riess, 2011).

As another piece of evidence in favour of the big bang scenario, can be taken the fact that the oldest objects found in the universe—globular clusters of stars and some radioactive isotopes—do not seem to exceed an age around 13 billion years. This gives strong evidence for a universe with a finite age, such as the big bang model predicts.

In some areas, there are new pieces of information to await. For instance, one of the main objectives of the Planck satellite, which will present cosmological data in early 2013, is to search for non-gaussian features, which could tell us more about the mechanism of inflation.

Although there are still many puzzles and interesting details to fill in, both in the Standard Model of particle physics and in the big bang model, they do remarkably well in describing a majority of all phenomena we can observe in nature. Combined, they allow us to follow the history of our universe back to only about 10^{-10} s after the big bang using established physical laws that have been checked in the laboratory. Extending the models, there are inflationary scenarios that describe the evolution back to 10^{-43} s after the big bang!

Behind this remarkable success are the theories of General Relativity and Quantum Field Theory, which we use in these lecture notes. However, many fundamental aspects of the laws of nature remain uncertain and are the subject of present-day research. The key problem is, as it has been for many decades, to find a valid description of quantized gravity, something which is needed to push our limit of knowledge even closer to (and maybe eventually explaining?) the big bang itself.

In this section we will review some of the most striking observational facts about our universe.

2.2 Basic Assumptions

A basic concept in modern cosmology is that of the "Copernican principle", i.e. the supposition that the universe on the average is homogeneous and isotropic. Although this is definitely not true on galactic scales and smaller, the distribution of matter seems to become more and more smooth on large scales, and on the largest scales we can observe, probed by the CMBR, isotropy and homogeneity seems to be fulfilled. The inhomogeneities seem to be 10^{-5} or smaller, apart from a dipole component in the CMBR, which however has a natural interpretation in terms of motion of our galaxy towards other massive galaxies. Given isotropy and homogeneity, the most general line element is the one found by Friedmann, Lemaître, Robertson and Walker (FLRW),

$$ds^2 = dt^2 - a^2(t)\left(\frac{dr^2}{1-kr^2} + r^2 d\theta^2 + r^2 \sin^2\theta d\phi^2\right). \tag{1}$$

Measurements on the cosmic microwave background gives (and inflationary theories predicted) $k = 0$, i.e., a geometrically flat universe on large scales, to good accuracy. (There have been suggestions that some of the features of the homogeneous and isotropic model can be alternatively explained if we live in an inhomogeneous universe with large "bubbles" of atypical density. Although a logical possibility, combined constraints from galaxy surveys, supernova data, and the CMBR mean that we would have to live at a fine-tuned location near the centre of such a bubble [6]. We will thus not consider these scenarios.)

The scale factor $a(t)$ follows equations first derived by Friedmann from Einstein's equations in general relativity:

$$H(t)^2 \equiv \left(\frac{\dot{a}}{a}\right)^2 = \frac{8\pi G_N}{3}\rho_{tot}. \tag{2}$$

Here G_N is Newton's gravitational constant, and ρ_{tot} is the total average energy density of the universe. The time-dependent Hubble parameter $H(t)$, has a value today which is known as the Hubble constant,

$$H(t_0) \equiv H_0 = h \cdot 100 \text{ km s}^{-1}\text{Mpc}^{-1}. \tag{3}$$

This defines the dimensionless quantity $h \sim 0.7$, which has to be given by measurement.

The equation which determines the acceleration of the scale factor is also derived from Einstein's equations:

$$\frac{2\ddot{a}}{a} + \left(\frac{\dot{a}}{a}\right)^2 = -8\pi G_N p, \tag{4}$$

with p being the total pressure.

2.3 Energy and Pressure

In general, there are several components contributing to the energy density, at least matter, radiation and dark energy, where the simplest possibility is a constant vacuum energy—the modern version of Einstein's cosmological constant:

$$\rho_{tot} = \rho_m + \rho_{rad} + \rho_\Lambda. \tag{5}$$

For an isotropic and homogeneous model, the relevant elements of the energy-momentum tensor are

$$T^{ij} = p\delta_{ij} \tag{6}$$

$$T^{i0} = 0 \tag{7}$$

$$T^{00} = \rho_{tot} \tag{8}$$

and there is for each component contributing to p and ρ_{tot} a relation

$$p_i = w_i \cdot \rho_i \tag{9}$$

called the equation of state, which enables one to make predictions for the time evolution of the expansion of the universe and for the relative weights of the different energy components. For non-relativistic matter, the pressure is proportional to $(v/c)^2$, and therefore negligible, $p = 0$, i.e. $w_M = 0$. For radiation on the other hand, $p = \rho/3$, so $w_R = 1/3$. What is the equation of state for vacuum energy? This is easy to motivate from symmetry reasons (as was done already by Lemaître in the 1930s). The energy momentum tensor has to be proportional to the only available rank-2 tensor in empty space-time, namely the Minkowski metric tensor in the cosmic rest frame:

$$T^{\mu\nu}_\Lambda = \rho_\Lambda \begin{pmatrix} 1 & 0 & 0 & 0 \\ 0 & -1 & 0 & 0 \\ 0 & 0 & -1 & 0 \\ 0 & 0 & 0 & -1 \end{pmatrix} = \begin{pmatrix} \rho_\Lambda & 0 & 0 & 0 \\ 0 & -\rho_\Lambda & 0 & 0 \\ 0 & 0 & -\rho_\Lambda & 0 \\ 0 & 0 & 0 & -\rho_\Lambda \end{pmatrix}. \tag{10}$$

This form is thus dictated by the requirement of Lorentz invariance. Comparing with the general form of the energy-momentum tensor which has ρ and p in the diagonal,

we thus see that the equation of state is $p = -\rho$, i.e., $w_\Lambda = -1$. The vacuum energy thus acts as a fluid with negative pressure.

2.4 Contributions to Vacuum Energy

How do we describe the contents of the universe, including vacuum energy? Based on its success in particle physics, we try to do it by using quantum field theory, with its particles and fields. A field is a dynamical quantity which is defined in all points of space and at all times. Particles are the lowest excitations of the fields. A particle is characterized by the mass m, spin s, charge Q, and maybe other internal quantum numbers.

The lowest excitations of the field, carrying energy E and three-momentum p can be quantized as harmonic oscillators fulfilling, in the cosmic rest frame (the reference frame where the CMBR looks maximally isotropic), the mass shell condition

$$p_\mu p^\mu = m^2, \tag{11}$$

where the four momentum

$$p^\mu = (E, \mathbf{p}) \tag{12}$$

and

$$p_\mu = (E, -\mathbf{p}). \tag{13}$$

For each possible momentum mode, there will, as for the simple quantum mechanical harmonic oscillator, be a zero-point energy

$$E_i = \omega(p_i)\left(n + \frac{1}{2}\right)_{n=0} = \sqrt{p_i^2 + m^2}\left(n + \frac{1}{2}\right)_{n=0} = \frac{1}{2}\sqrt{p_i^2 + m^2}. \tag{14}$$

However, for a given field, these have to be summed for all modes, meaning that there will be a huge zero-energy density

$$\rho_\Lambda = \frac{1}{2}\frac{1}{(2\pi)^3}\int d^3p\sqrt{p^2 + m^2}. \tag{15}$$

The highly divergent integral has to be cut-off at some large energy scale, and the first guess is the Planck mass, $m_{Pl} \sim 10^{19}$ GeV, thus

$$\rho_\Lambda = \frac{1}{2}\frac{1}{(2\pi)^3}\int^{m_{Pl}} d^3p\sqrt{p^2 + m^2} \sim m_{Pl}^4. \tag{16}$$

Unfortunately, this is orders of magnitude too large, and is the same disastrous result one would get by using simple dimensional analysis. Namely, what is the natural

scale of ρ_Λ? We see here that it is governed by the cut-off mass scale when new physics appears, and dimensional analysis gives that in units where $c = 1$ so that length is proportional to an inverse mass, and thus energy per unit volume becomes $[\rho_\Lambda] = [M^4]$. The only mass scale in gravity is m_{Pl}, thus

$$\rho_\Lambda^{th} \sim m_{Pl}^4. \tag{17}$$

Unlike other guesses in physics based on dimensional analysis, this is a terrible prediction. The present-day vacuum energy density of the universe is given by measurements of supernovae and the CMBR and is (using $k = 0$)

$$\rho_\Lambda^{obs} \sim 10^{-122} m_{Pl}^4 \ll m_{Pl}^4 \sim \rho_\Lambda^{th}. \tag{18}$$

To go back to our field theory result, the zero-point energy is really a consequence of the quantum mechanical commutator between the field and its canonical momentum. However, for fermions, anticommutators are used, meaning the sign of the vacuum energy is changed. So, introducing the fermion number $F = 1$ for fermions, $F = 0$ for bosons, one gets

$$\rho_\Lambda = \sum (-1)^F \frac{1}{2} \frac{1}{(2\pi)^3} \int^{m_{Pl}} d^3p \sqrt{p^2 + m^2}. \tag{19}$$

Remarkably, if there are as many fermionic degrees of freedom as bosonic, and they pairwise have the same mass, the vacuum energy would vanish. Examples of theories having this property are supersymmetric theories, with unbroken supersymmetry. However, since we do not see 0.511 MeV scalar electrons (selectrons), supersymmetry has to be broken. Therefore large effects of the zero-point energy remain, and $\rho_\Lambda \sim m_{SUSY}^4$ with m_{SUSY} (1000 GeV, say) the scale of SUSY breaking. Better, but still enormously much "too high".

In summary, we have encountered one of the most severe problems of cosmology and particle astrophysics: Why is the cosmological constant so small, but still not zero? (By the way, nobody found a good reason that it should be exactly zero, anyway...) Supersymmetry alleviates the problem somewhat, but since supersymmetry is broken there remains large mass terms still giving a value some 50–60 orders of magnitude different from the observed value.

In cosmology the cosmological constant has a dramatic effect. Since it is related to the energy density of the vacuum, and the vacuum is growing in size due to the expansion, it will eventually dominate completely. Matter is on the other hand more and more diluted and becomes less and less important, and radiation is also diluted plus red-shifted:

$$\rho_m \sim (1+z)^3, \quad \rho_r \sim (1+z)^4, \quad \rho_\Lambda \sim (1+z)^0. \tag{20}$$

We see that in the early universe (large redshifts), vacuum energy was irrelevant. Today matter and vacuum energy are almost equal (why now?). In the future, the

expansion rate will grow exponentially, as we will see in the section on inflation, Sect. 3.2.

To explain the smallness of Λ some people resort to (almost) non-scientific reasoning: the anthropic principle, or the landscape of string theory vacua. There the argument goes roughly like this: There exist an amazingly large number of different vacua, i.e., ground states, of the theory, and maybe all of these are realized somewhere in nature. But of course, those with very large values of Λ would accelerate so quickly that structure would not form in the universe and therefore no life could appear. But since we exist, we have to do so in one of the very few universes where life did evolve. Of course, this sounds more like post-dicting the properties of our universe rather than predicting them, which perhaps just shows the desperation in front of the problem of the size of the cosmological constant.

Let us have another look at Planck-mass phenomena. Consider the scattering of a photon on an electron, Compton scattering (we will treat this in detail later, see Fig. 3). The relation between the incident and outgoing wavelength as a function of scattering angle is given by

$$\lambda' - \lambda = \frac{2\pi\hbar}{m_e c}(1 - \cos\theta) = \frac{2\pi}{m_e}(1 - \cos\theta) \equiv \lambda_c (1 - \cos\theta)\,. \tag{21}$$

Here $\lambda_c \equiv 2\pi/m_e$ is called the Compton wavelength (or radius) of the particle (the electron in this case). Note that we use here and onwards units such that $c = \hbar = 1$. This implies that time and length have the same dimension which is inversely proportional to the dimension of mass.

We will see in Sect. 9 the expression for the Schwarzschild radius (the radius which marks the limit of where light can leave the black hole)

$$r_S = \frac{2G_N M}{c^2} = 2G_N M \tag{22}$$

Thus, the Compton radius decreases with mass, but the Schwarzschild radius increases with mass. When are the two equal, i.e., how big must the mass be for the Compton radius to be smaller than the Schwarzschild radius? This is when quantum gravity should be important. (All details of particle properties are smeared out by quantum fluctuations on the order of the Compton wavelength or less, so for $\lambda_c > r_s$ the black hole properties should be unnoticeable.) We see

$$\frac{\lambda_c}{r_S} = \frac{\pi}{G_N M^2} \sim \frac{m_{Pl}^2}{M^2}. \tag{23}$$

Thus, when the mass of an elementary particle is larger than the Planck mass, its Compton radius is smaller than its Schwarzschild radius, which implies that we need quantum gravity! None exists yet, but perhaps string theory is the best bet for such a fundamental theory at the Planck scale? For an electron, $\lambda_c/r_S \sim 10^{45}$, so quantum

gravity effects are completely negligible at the particle level. The same is true for all other Standard Model particles.

2.5 Summary of Observations

To end this section where the main theoretical lines for describing the universe have been laid out, we summarize what we know about the cosmological parameters of the universe from the impressive recent measurements. Analyses combining high-redshift supernova luminosity distances, microwave background fluctuations (from the satellite WMAP) and baryon acoustic oscillations (BAO) in the galaxy distribution give tight constraints [7] on the present mass density of matter in the universe. This is usually expressed in the ratio

$$\Omega_M = \rho_M/\rho_c, \tag{24}$$

normalized to the critical density,

$$\rho_c = 3H_0^2/(8\pi G_N) = h^2 \times 1.9 \cdot 10^{-29}\ \mathrm{g\,cm^{-3}}. \tag{25}$$

The value obtained for the 7-year WMAP data [7] for cold dark matter for the (unknown) particle X making up the dark matter is $\Omega_X h^2 = 0.113 \pm 0.004$, which is around 5 times higher than the value obtained for baryons, $\Omega_B h^2 = 0.0226 \pm 0.0005$. Here $h = 0.704 \pm 0.014$ is the derived [7] present value of the Hubble constant in units of 100 km s^{-1} Mpc^{-1}. In addition, the WMAP data is consistent within a percent with a flat universe ($\Omega_{tot} = 1$) and a value for the dark energy component, e.g. the cosmological constant Λ, of $\Omega_\Lambda = 0.73 \pm 0.02$.

One of the main problems for cosmology and particle physics is to explain the measured density of dark matter, and to give candidates for the identity of the dark matter particles. The fact that dark matter is definitely needed on the largest scales (probed by WMAP), on galaxy cluster scales (as pointed out by Zwicky already in 1933 [8], and verified by gravitational lensing and the temperature distribution of X-ray emitting gas) all the way down to the smallest dwarf galaxies, means that solutions based on changing the laws of gravity seem less natural. In particular, the direct empirical proof of the existence of dark matter given by the "Bullet Cluster" [9] is very difficult to circumvent, as the X-ray signal from the baryonic matter and the gravitational lensing signal from dark matter are clearly separated.

Although the existence of a non-zero cosmological constant (or some similar form of dark energy) in the present-day universe came as a big surprise to most cosmologists and particle physicists, the most successful models of evolution in the universe do make use of a similar effect in models of inflation, as we will see in Sect. 3.2.

3 Relic Density of Particles

There are several important examples of freeze-out in the early universe, for instance at the synthesis of light elements one second to a few minutes after the big bang, and the microwave photons from the "surface of last scattering" several hundred thousand years later. Before we calculate freeze-out, it is convenient to introduce a formalism which considers freeze-out in general: that is, what happens when a particle species goes out of equilibrium. A rigorous treatment has to be based on the Boltzmann transport equation in an expanding background, but here we give a simplified treatment (see, for example [1] for a more complete discussion).

There are several different contributions to $\Omega = \rho/\rho_c$, like radiation Ω_R, matter Ω_M and vacuum energy Ω_Λ.

The equations of motion for the matter in the universe are given by the vanishing of the covariant divergence of the energy-momentum tensor

$$T^{\alpha\beta}_{;\beta} = 0 \tag{26}$$

This gives, for the FLRW metric,

$$\frac{d}{dt}(\rho a^3) = -p\frac{d}{dt}a^3 \tag{27}$$

which shows that the change of energy in a comoving volume element is equal to minus the pressure times the change in volume. This can be rewritten as

$$a^3\frac{dp}{dt} = \frac{d}{dt}[a^3(\rho + p)] \tag{28}$$

which can be interpreted as a conservation law for the entropy in a volume $a^3(T)$. For radiation, where $p = \rho/3$, (27) gives $\rho \sim a^{-4}$. Note that all particles fulfilling $mc^2 \ll k_B T$ have the equation of state of radiation.

The Friedmann equation is

$$H^2(t) = \frac{8\pi G_N \rho}{3} \tag{29}$$

where as a good approximation only the relativistic species contribute appreciably to ρ. Note that the Hubble parameter $H(t)$ has units of 1/(time). This means in our units that it has dimensions of mass. The age of the universe at a given time t is simply of the order of $H^{-1}(t)$, at least when the scale factor increases as a power of t.

We now treat schematically the thermodynamics of the expanding universe. We assume, which is true if reactions between different species of particles are rapid enough, that we can use the thermodynamical quantities, temperature T, pressure p, entropy density s, and other quantities, at each time t to describe the state of the universe. The constituents have number density n and typical relative velocities v,

and scattering or annihilation cross-section σ, meaning that the interaction rate per particle Γ is given by

$$\Gamma = n\sigma v. \tag{30}$$

The condition that the interactions maintain equilibrium is that the interaction rate is larger than the expansion rate of the universe:

$$\Gamma \gg H \tag{31}$$

Typically, the number density of particles decreases faster with temperature and therefore with time than the Hubble parameter does. This means that at certain epochs some of the particle species will leave thermodynamic equilibrium. Their number density will be "frozen" at some particular value which then only changes through the general dilution due to the expansion. This "freeze-out" of particles is an important mechanism which explains the particle content of the universe we observe today.

Using relativistic statistical mechanics in the cosmic rest frame, the distribution function $f_i(\mathbf{p})$ for particle species of type i is

$$f_i(\mathbf{p}) = \frac{1}{e^{\frac{(E_i-\mu_i)}{T}} \pm 1} \tag{32}$$

with $E_i = \sqrt{\mathbf{p}^2 + m_i^2}$ the energy, μ_i is the chemical potential and T the temperature (we put $k_B = 1$). The minus sign is for particles that obey Bose-Einstein statistics (bosons) and the plus sign is for particles obeying the exclusion principle and therefore Fermi-Dirac statistics (fermions). To a good approximation the chemical potentials can be neglected in the very early universe.

We denote by g_i the number of internal degrees of freedom of particle i. The photon has two polarization states and therefore $g_\gamma = 2$. The neutrinos only have one polarization state, giving $g_\nu = 1$, electrons and muons have $g_{e,\mu} = 2$ (and the same numbers for the antiparticles).

With these definitions, the number density for species i is

$$n_i = \frac{g_i}{(2\pi)^3} \int f_i(\mathbf{p}) d^3p, \tag{33}$$

and its energy density is

$$\rho_i = \frac{g_i}{(2\pi)^3} \int E_i(\mathbf{p}) f_i(\mathbf{p}) d^3p. \tag{34}$$

The expression for the pressure is

$$p_i = \frac{g_i}{(2\pi)^3} \int \frac{|\mathbf{p}|^2}{3E_i(\mathbf{p})} f_i(\mathbf{p}) d^3p. \tag{35}$$

In the nonrelativistic limit $T/m \ll 1$ we can solve the integrals analytically, and the result both for Fermi-Dirac and Bose-Einstein particles is

$$n_{NR} = g_i \left(\frac{mT}{2\pi}\right)^{\frac{3}{2}} e^{-\frac{m}{T}}, \tag{36}$$

$$\rho_{NR} = m \cdot n_{NR}, \tag{37}$$

and

$$p_{NR} = T \cdot n_{NR} \ll \rho_{NR} \tag{38}$$

For nonrelativistic matter, $\langle E \rangle = m + 3T/2$.

In the ultrarelativistic approximation, $T/m \gg 1$, the integrals can also be performed with the results

$$\rho_R = \frac{g_i}{6\pi^2} \int_0^\infty \frac{E^3 dE}{e^{\frac{E}{T}} \pm 1} = \begin{cases} \frac{\pi^2}{30} g_i T^4, & \textit{Bose-Einstein} \\ \frac{7}{8}\left(\frac{\pi^2}{30} g_i T^4\right), & \textit{Fermi-Dirac}, \end{cases} \tag{39}$$

$$n_R = \begin{cases} \frac{\zeta(3)}{\pi^2} g_i T^3, & \textit{Bose-Einstein} \\ \frac{3}{4}\left(\frac{\zeta(3)}{\pi^2} g_i T^3\right), & \textit{Fermi-Dirac}, \end{cases} \tag{40}$$

with $\zeta(x)$ is the Riemann zeta function, $\zeta(3) = 1.20206\ldots$ The average energy ρ/n for a relativistic particle is

$$\langle E \rangle_{BE} \sim 2.7T \tag{41}$$

and

$$\langle E \rangle_{FD} \sim 3.15T \tag{42}$$

For photons, with the mass $m_\gamma = 0$, and $g_\gamma = 2$, the expression for $\rho_\gamma(T) \sim T^4$ is the famous Stefan Boltzmann law for electromagnetic black-body radiation.

The total contribution to the energy and number density of all kinds of particles in the early universe is to a good approximation (since the energy and number density of a nonrelativistic species is exponentially suppressed),

$$\rho_R(T) = \frac{\pi^2}{30} g_{\text{eff}}(T) T^4 \tag{43}$$

$$p_R(T) = \frac{1}{3}\rho_R(T) = \frac{\pi^2}{90} g_{\text{eff}}(T) T^4 \tag{44}$$

where $g_{\rm eff}(T)$ counts the total number of internal degrees of freedom (such as spin, colour, etc.) of the particles whose mass fulfill $m \ll T$, and which are in thermodynamic equilibrium with the "primordial cosmic soup" of particles in the early universe. The expression for $g_{\rm eff}(T)$ has the factor 7/8 for fermions.

As an example, we calculate $g_{\rm eff}(T)$ for a temperature of, say, 1 TeV when all the particles of the Standard Model were relativistic and in thermal equilibrium. The total number of internal degrees of freedom of the fermions is 90 and for the gauge and Higgs bosons 28, so the total expression for $g_{\rm eff}$ is

$$g_{\rm eff}(T \sim 1\,{\rm TeV}) = 28 + \frac{7}{8} \cdot 90 = 106.75 \tag{45}$$

If we insert the expression for the energy density into the Friedmann equation (29) we get for the radiation-dominated epoch in the early universe

$$H^2 = \frac{8\pi G_N}{3}\rho_R = \frac{8\pi G_N}{3}\frac{\pi^2}{30}g_{\rm eff}T^4 = 2.76\frac{g_{\rm eff}T^4}{m_{Pl}^2} \tag{46}$$

or

$$H = 1.66\sqrt{g_{\rm eff}}\frac{T^2}{m_{Pl}} \tag{47}$$

This is a very important formula governing the physics of the early universe.

For radiation domination, it can be shown that

$$a(t) \sim \sqrt{t} \tag{48}$$

deriving from the equation of state $p = \rho/3$. For matter domination, that is, for $p \sim 0$, one has

$$a(t) \sim t^{\frac{2}{3}}. \tag{49}$$

So for radiation domination,

$$H = \frac{\dot{a}}{a} = \frac{1}{2t} \tag{50}$$

and the time-temperature relation becomes

$$t = 0.30\frac{m_{Pl}}{\sqrt{g_{\rm eff}}T^2} \sim \left(\frac{1\,{\rm MeV}}{T}\right)^2 {\rm s} \tag{51}$$

We now have to determine which particles are in thermal equilibrium at a given temperature, so that we can calculate $g_{\rm eff}(T)$. The entropy $S(V, T)$ is introduced through

$$dS(V, T) = \frac{1}{T}\left[d(\rho(T)V) + p(T)dV\right] \tag{52}$$

this gives (see [1])

$$S(V, T) = \frac{V}{T}(\rho(T) + p(T)) \tag{53}$$

and from the conservation of the energy-momentum tensor follows

$$\frac{d}{dt}\left(\frac{a^3}{T}[\rho(T) + p(T)]\right) = 0. \tag{54}$$

Identifying the volume V with $a^3(t)$ and comparing with (53) we find the law of conservation of entropy in the volume $a^3(t)$. Sometimes it is more useful to work with the entropy density $s(T)$ rather than the total entropy $S(V, T)$ within the volume V. The definition is thus:

$$s(T) \equiv \frac{S(V, T)}{V} = \frac{\rho(T) + p(T)}{T} \tag{55}$$

In the early universe, both the energy density and the pressure were dominated by relativistic particles with the equation of state $p = \rho/3$. Using (55) and the relativistic expressions for the energy density and the pressure (Eqs. (43) and (44)), gives density s

$$s = \frac{2\pi^2}{45} g^s_{\text{eff}} T^3 \tag{56}$$

where g^s_{eff} is defined in a similar way as g_{eff}.

Since s and n_γ both vary as T^3 there is a simple relationship between them. With

$$n_\gamma = \frac{2\zeta(3)}{\pi^2} T^3 \tag{57}$$

from Eq. (40), we find

$$s = \frac{\pi^4}{45\zeta(3)} g^s_{\text{eff}} n_\gamma \sim 1.8 g^s_{\text{eff}} n_\gamma \tag{58}$$

Following [1] we now consider a case of great interest for the dark matter problem. Suppose that there exists some kind of unknown particle χ, with antiparticle $\bar{\chi}$, that can annihilate each other and be pair created through processes $\chi + \bar{\chi} \leftrightarrow X + \bar{X}$, where X stands for any type of particle to which the χs can annihilate.[1] We further assume that the X particles have zero chemical potential and that they are kept in thermal equilibrium with the photons and the other light particles in the early universe (the X particles can be quarks, leptons etc.)

[1] The supersymmetric neutralino is actually its own antiparticle (just as the photon is its own antiparticle). The formalism is very similar in this case. In particular, a neutralino can annihilate with another neutralino giving other, non-supersymmetric particles in the final state.

How will the number density n_χ evolve with time (and therefore with temperature)? It is clear that in exact thermal equilibrium the number of χ particles in a comoving volume $N_\chi = a^3 n_\chi$ will be given by the equilibrium value $n_\chi^{EQ}(T)$ (see (40)). (In exact thermal equilibrium the rate for the process $\chi + \bar{\chi} \leftrightarrow X + \bar{X}$ is the same in both directions.) If the actual number density $n_\chi(T)$ is larger than the equilibrium density the reaction will go faster to the right: that is, the χ particles will annihilate faster than they are created. The depletion rate of χ should be proportional to $\sigma_{\chi\bar{\chi}\to X\bar{X}}|\mathbf{v}|n_\chi^2$ (quadratic in the density, since it should be proportional to the product of n_χ and $n_{\bar{\chi}}$, and these are equal). However, χ particles are also created by the inverse process, with a rate proportional to $(n_\chi^{EQ})^2$. We have thus 'derived' the basic equation that governs the departure from equilibrium for the species χ:

$$\frac{dn_\chi}{dt} + 3Hn_\chi = -\langle\sigma_{\chi\bar{\chi}\to X\bar{X}}|\mathbf{v}|\rangle[n_\chi^2 - (n_\chi^{EQ})^2]. \tag{59}$$

The left-hand side comes from $\frac{1}{a^3}\frac{d}{dt}[n_\chi a^3]$; the term proportional to $3H$ just expresses the dilution that automatically comes from the Hubble expansion. The expression $\langle\sigma_{\chi\bar{\chi}\to X\bar{X}}|\mathbf{v}|\rangle$ stands for the thermally averaged cross section times velocity. This averaging is necessary, since the annihilating particles have random thermal velocities and directions. Summing over all possible annihilation channels gives

$$\frac{dn_\chi}{dt} + 3Hn_\chi = -\langle\sigma_A|\mathbf{v}|\rangle[n_\chi^2 - (n_\chi^{EQ})^2], \tag{60}$$

where σ_A is the total annihilation cross section.

Using the time-temperature relation of Eq. (51) (for radiation dominance)

$$t = 0.30\frac{m_{Pl}}{T^2\sqrt{g_{\text{eff}}}} \tag{61}$$

this can be converted to an evolution equation for n_χ as a function of temperature. Introducing the dimensionless variable $x \equiv m_\chi/T$, and normalizing n_χ to the entropy density:

$$Y_\chi = \frac{n_\chi}{s} \tag{62}$$

gives after some intermediate steps

$$\frac{dY_\chi}{dx} = -\frac{m_\chi m_{Pl} c_{\text{eff}}}{x^2}\sqrt{\frac{\pi}{45}}\langle\sigma_A|\mathbf{v}|\rangle(Y_\chi^2 - (Y_\chi^{EQ})^2) \tag{63}$$

where

$$c_{\text{eff}} = \frac{g_{\text{eff}}^s}{\sqrt{g_{\text{eff}}}} \tag{64}$$

or, after some rearrangement,

$$\frac{x}{Y_\chi^{EQ}}\frac{dY_\chi}{dx} = -\frac{\Gamma_A}{H}\left[\left(\frac{Y_\chi}{Y_\chi^{EQ}}\right)^2 - 1\right], \tag{65}$$

where $\Gamma_A = n_\chi^{EQ}\langle\sigma_A|\mathbf{v}|\rangle$. This equation can be solved numerically with the boundary condition that for small x, $Y_\chi \sim Y_\chi^{EQ}$ (since at high temperature the χ particles were in thermal equilibrium with the other particles). We see from (65) that the evolution is governed by the factor Γ_A/H, the interaction rate divided by the Hubble expansion rate.

The solutions to these equations have to be obtained numerically in the general case to find the temperature T_f and therefore the value of x_f of freeze-out and the asymptotic value $Y_\chi(\infty)$ of the relic abundance of the species χ. There are, however, some simple limiting cases. If the species χ is relativistic at freeze-out, then Y_χ^{EQ} is not changing with time during the period of freeze-out, and the resulting $Y_\chi(\infty)$ is just the equilibrium value at freeze-out,

$$Y_\chi(\infty) = Y_\chi^{EQ}(x_f) = \frac{45\zeta(3)}{2\pi^4}\frac{g_{eff}}{g^s_{\rm eff}(x_f)} \tag{66}$$

where $g_{eff} = g$ for bosons and $3g/4$ for fermions. A particle that was relativistic at freeze-out is called a hot relic. A typical example is the neutrino. The present mass density of a hot relic with mass m is

$$\Omega_\chi h^2 = 7.8\cdot 10^{-2}\frac{g_{eff}}{g^s_{\rm eff}(x_f)}\left(\frac{m_\chi}{1\ \text{eV}}\right) \tag{67}$$

Note that today the motion of a particle with mass greater than the small number $T_0 = 2.73\ \text{K} = 2.4\cdot 10^{-4}\ \text{eV}$ is of course non-relativistic and therefore the contribution to the energy density is dominated by its rest mass energy. A Standard Model neutrino has $g_{eff} = 2\cdot 3/4 = 1.5$ and decoupled at a few MeV when $g^s_{\rm eff} = g_{\rm eff} = 10.75$. We find

$$\Omega_{\nu\bar{\nu}}h^2 = \frac{\sum_i m_{\nu_i}}{(93\ \text{eV})}. \tag{68}$$

As we will see, present estimates of the neutrinos masses, based on the observation of neutrino oscillations, give a sum much less than 1 eV, which means that neutrinos are not the main form of dark matter. On the other hand, we are now rather certain that they do contribute a small fraction of non-baryonic dark matter!

This analysis has been valid for hot relics, or hot dark matter. For cold relics (particles that were non-relativistic at freeze-out) the Eq. (65) has to be solved numerically. There one finds that for massive particles in the mass range between, say, 10 GeV and a few TeV, $x_f \sim 1/20$, and moreover to a good approximation the relic density only depends on the cross section times velocity,

$$\Omega_X h^2 \simeq 0.11 \times \frac{2.8 \cdot 10^{-26}\ \mathrm{cm}^3\ \mathrm{s}^{-1}}{\langle \sigma_A |\mathbf{v}| \rangle}. \tag{69}$$

Another striking result is that, if one gives typical gauge couplings to the particle X, and a mass of typical weak interaction magnitude (100–300 GeV, say), then $\langle \sigma_A v \rangle$ is such that the resulting $\Omega_X h^2 \sim 0.11$. This is the essence of what is sometimes called the "WIMP miracle".

As can be understood, the value of x_f when Y_χ leaves the equilibrium curve is lower for a smaller cross section σ_A. This is because of the fact that in thermal equilibrium, massive particles will eventually be exponentially suppressed. That is, more weakly interacting particles decouple earlier, and since the equilibrium curve for a non relativistic species drops fast with increasing x, more weakly coupled particles will have a higher relic abundance.

Going through the numerical analysis one finds that a hypothetical neutrino with mass $m_\nu \sim 3$ GeV would also have about the right mass to close the universe. On the other hand, the range between 90 eV and 3 GeV is cosmologically disallowed for a stable neutrino. There are arguments from large-scale structure formation that favour cold relics over hot relics, so such a neutrino would be a good dark matter candidate. Data from the LEP accelerator at CERN have, however, excluded any ordinary neutrino with a mass in the GeV range.

3.1 Coannihilations

There are instances when the simple treatment discussed here has to be improved. One example is for instance the possibility that entropy may be generated by other particles than those of the Standard Model, before, at, or after decoupling. Another example, which for instance appears in some supersymmetric models, is that of coannihilations. This was first discussed in [10], here we follow the more detailed treatment in [11].

We will here outline the procedure developed in [2, 11] which is used in DarkSUSY [144]. For more details, see [2, 11]. DarkSUSY is a free FORTRAN package that can be used to compute a variety of dark matter related quantities, such the relic density and the scattering and annihilation rates to many different channels. It was developed for computations in the Minimal Supersymmetric extension to the Standard Model (MSSM), but it is modular and can be adapted to most WIMP models.

We consider annihilation of N particles with mass m_i and internal degrees of freedom g_i. For convenience, we may order them such that $m_1 \leq m_2 \leq \cdots \leq m_{N-1} \leq m_N$. For the lightest particle (which is the dark matter candidate, if a symmetry is guaranteeing the stability, like what is called R-parity for supersymmetry, see Sect. 5), we use both the notation m_1 and m_χ.

All heavier particles will eventually decay to the lightest, stable, and therefore we add the number densities up,

$$n = \sum_{i=1}^{N} n_i .$$

The scattering rate of particles on particles in the thermal background "soup" is generally much faster than the annihilation rate, since the background particle densities of Standard Model particles, n_{SM} is much larger than each of the particle densities in the dark sector n_i. The important SM particles are, as we have seen, those that are relativistic and cold dark matter particles (WIMPs) are nonrelativistic, and thus suppressed by the Boltzmann factor. Thus, the n_i distributions remain in thermal equilibrium during their ("chemical") freeze-out.

We then get

$$\frac{dn}{dt} = -3Hn - \langle \sigma_{\rm eff} v \rangle \left(n^2 - n_{\rm eq}^2 \right) \tag{70}$$

where

$$\langle \sigma_{\rm eff} v \rangle = \sum_{ij} \langle \sigma_{ij} v_{ij} \rangle \frac{n_i^{\rm eq}}{n^{\rm eq}} \frac{n_j^{\rm eq}}{n^{\rm eq}} . \tag{71}$$

with

$$v_{ij} = \frac{\sqrt{(p_i \cdot p_j)^2 - m_i^2 m_j^2}}{E_i E_j} . \tag{72}$$

Using the Maxwell-Boltzmann approximation for the velocity distributions one can derive the following expression for the thermally averaged annihilation cross section [11]

$$\langle \sigma_{\rm eff} v \rangle = \frac{\int_0^\infty dp_{\rm eff}\, p_{\rm eff}^2 W_{\rm eff} K_1 \left(\frac{\sqrt{s}}{T} \right)}{m_1^4 T \left[\sum_i \frac{g_i}{g_1} \frac{m_i^2}{m_1^2} K_2 \left(\frac{m_i}{T} \right) \right]^2} . \tag{73}$$

where K_1 (K_2) is the modified Bessel function of the second kind of order 1 (2), T is the temperature, s is the usual Mandelstam variable and

$$\begin{aligned} W_{\rm eff} &= \sum_{ij} \frac{p_{ij}}{p_{\rm eff}} \frac{g_i g_j}{g_1^2} W_{ij} \\ &= \sum_{ij} \sqrt{\frac{[s - (m_i - m_j)^2][s - (m_i + m_j)^2]}{s(s - 4m_1^2)}} \frac{g_i g_j}{g_1^2} W_{ij} . \end{aligned} \tag{74}$$

Here,

$$p_{ij} = \frac{\left[s - (m_i + m_j)^2 \right]^{1/2} \left[s - (m_i - m_j)^2 \right]^{1/2}}{2\sqrt{s}} , \tag{75}$$

and the invariant annihilation rate is

$$W_{ij} = 4p_{ij}\sqrt{s}\sigma_{ij} = 4\sigma_{ij}\sqrt{(p_i \cdot p_j)^2 - m_i^2 m_j^2} = 4E_i E_j \sigma_{ij} v_{ij} \tag{76}$$

and, finally, the effective momentum

$$p_{\text{eff}} = p_{11} = \frac{1}{2}\sqrt{s - 4m_1^2}. \tag{77}$$

Since $W_{ij}(s) = 0$ for $s \leq (m_i + m_j)^2$, the terms in (74) are non-negative. For a two-body final state, W_{ij} is given by the expression

$$W_{ij}^{2-\text{body}} = \frac{|\mathbf{k}|}{16\pi^2 g_i g_j S_f \sqrt{s}} \sum_{\text{internal d.o.f.}} \int |\mathcal{M}|^2 \, d\Omega, \tag{78}$$

that after some manipulations leads to (63). Here $\mathbf{k}$ is the final center-of-mass momentum, S_f is a symmetry factor equal to 2 for identical final particles.

So, what could the dark matter be? It turns out that in particle physics, there are hypothetical particles, like supersymmetric partners of ordinary particles, that have the right interaction strength and mass range to be promising dark matter candidates. In particular, the neutralino has all the properties of a good dark matter candidate. Since it is electrically neutral it does not emit or absorb radiation which makes it 'dark' (invisible matter is thus a better term than dark matter). The couplings of neutralinos are generally of weak interaction strength, but the large number of possible annihilation channels, which depends on the unknown supersymmetry breaking parameters, makes an exact prediction of mass and relic abundance uncertain. Scans of parameter space show, however, that a neutralino in the mass range between 30 GeV and a few TeV could give a relic density close to the critical density. We will later in these notes have much more to say about this.

3.2 Inflation

An important ingredient in today's cosmology is, as mentioned, the concept of inflation, which was introduced by Alan Guth in the early 1980s. Here we use the near constancy of H to write $a_2/a_1 = \exp(\int_{t_1}^{t_2} H(t)dt)$: that is, Einstein's equations including a cosmological constant read

$$R_{\mu\nu} - \frac{1}{2}g_{\mu\nu}\mathcal{R} = 8\pi G T_{\mu\nu} + \Lambda g_{\mu\nu}. \tag{79}$$

Here we have put the Λ term on the right hand side, which shows that a cosmological term acts as a stress-energy tensor, albeit with the unusual equation of state $p_{vac} = -\rho_{vac}$. (We have already used that one may trivially include vacuum energy in

the term proportional to G, with $\rho_\Lambda = \Lambda/(8\pi G)$.) The equation of state implies that the entropy density according to (55) is $s \sim \rho + p = 0$. This means that, when vacuum energy dominates, the entropy vanishes. This can be understood from statistical mechanics. Entropy is related to the total number of degrees of freedom, and the vacuum (at least if it is unique) is just one state, that is only one degree of freedom. Of course, the entropy that was in a patch before inflation will still be there after inflation—but it will be diluted by an exponentially large factor due to the expansion.

In the situation when the constant vacuum energy dominates the expansion, the Friedmann equation (2) becomes very simple:

$$H^2 = \left(\frac{\dot{a}}{a}\right)^2 = \frac{\Lambda}{3} \tag{80}$$

or

$$H = \frac{\dot{a}}{a} = \sqrt{\frac{\Lambda}{3}} = \text{const} \tag{81}$$

with the (de Sitter) solution

$$a \sim e^{Ht}. \tag{82}$$

In inflation, the expansion rate is constant, which causes an exponential growth of the scale factor.

In many models of inflation, the phase transition involving a scalar field, the inflation field, took place at temperatures around the hypothetical Grand Unification scale $T_{GUT} \sim 10^{15}$ GeV, at the corresponding Hubble time $H^{-1} \sim 10^{-34}$ s. If the universe stayed in the inflationary state for a short time, say 10^{-32} s, many e-folds of inflation took place. When inflation stopped, the huge vacuum energy of the inflation field went into creation of ordinary particles, and a reheating of the universe took place. The reheating temperature is of the order of the temperature of the phase transition, $T_{RH} \sim 10^{15}$ GeV if the inflation is strongly enough coupled to ordinary matter, as it is in many successful models of inflation.

Let us see what happened to a small region with radius of for example 10^{-23} cm before inflation. The entropy within that volume was only around 10^{14}, but after inflation the volume of the region has increased by a factor given by the cube of the scale factor, $(e^{100})^3 = 10^{130}$. Thus, after the entropy generated by reheating, the total entropy within the inflated region had grown to around 10^{144}. Entropy was generated because the equation of state changed from $p = -\rho$ to $p = \rho/3$, meaning that the entropy density $s \sim p + \rho$ increased dramatically.

This huge entropy increase solves many problems of cosmology. The "horizon problem"—i.e., how came that regions of the universe that are too far from each other to be causally connected today, still have exactly the same microwave background temperature—is solved since our whole observable universe arose from a very small thermalized volume before inflation, and the smooth region after inflation had sufficient entropy to encompass our observable universe.

During inflation the energy density, and the negative pressure, of the universe were constant, whereas the scale factor a increased exponentially. This means that the total Ω after inflation was exponentially close to unity. (Like a balloon which would inflate to be as big as the Earth would locally look very flat.) Thus, the present value should also be equal to unity with an accuracy of many decimal places, perhaps the most important successful prediction of inflation.

Even if $\Omega = 1$ is predicted, there is nothing telling us the subdivision of Ω into contributions from radiation, matter and vacuum energy. As we have noted, however, the 'natural' contribution of Ω_Λ is either extremely small or extremely large. Only during very brief epochs can Ω_Λ be of similar magnitude as the matter contribution Ω_M. This is actually a still unsolved problem, why is it that the energy density in matter ρ_M is about the same as ρ_Λ today?

The period of inflation and reheating is strongly non-adiabatic, since there was an enormous generation of entropy at reheating. After the end of inflation, the universe 'restarted' in an adiabatic phase with the standard conservation of aT, and it is because the universe automatically restarts from very special initial conditions given by inflation that the horizon and flatness problems are solved.

It is instructive to see how inflation can be produced in field theory. A Lagrangian density of the form

$$\mathcal{L} = \frac{1}{2}\partial^\mu\phi\partial_\mu\phi - V(\phi) \tag{83}$$

can be shown to give a contribution to the energy-momentum tensor $T^{\mu\nu}$ of the form

$$T^{\mu\nu} = \partial^\mu\phi\partial^\nu\phi - \mathcal{L}g^{\mu\nu}. \tag{84}$$

For a homogeneous state, the spatial gradient terms vanish, meaning that $T^{\mu\nu}$ becomes that of the perfect fluid type. If one would keep the gradient terms, one sees that they are divided by $a(t)^2$, which means that after a short period of inflation they are exponentially suppressed. The resulting ρ and p are

$$\rho = \frac{\dot{\phi}^2}{2} + V(\phi) \tag{85}$$

and

$$p = \frac{\dot{\phi}^2}{2} - V(\phi), \tag{86}$$

and we see that the equation of state $\rho = -p$ will be fulfilled if we can neglect the kinetic term $\sim \dot{\phi}^2$ (this is called "slow-roll" inflation).

The exact equations of motion of ϕ can be derived from the condition of vanishing covariant divergence of the energy-momentum tensor, $T^{\mu\nu}_{\ \ \nu} = 0$, which gives

$$\ddot{\phi} + 3H\dot{\phi} + V'(\phi) = 0 \tag{87}$$

This is similar to the equation of motion of a ball in a potential well with friction $\sim 3H\dot{\phi}$, and can be solved by elementary methods. We assume that at very high temperatures, $\phi = 0$ gives the locations of the minimum of the potential. Temperature dependent terms in the effective potential then generate another minimum for $\phi = \phi_{vac} \neq 0$, an example of what is called spontaneous symmetry breakdown. To produce a long enough period of inflation and a rapid reheating after inflation, the potential $V(\phi)$ has as mentioned to be of the "slow-roll" type, with the field spending a long time on the nearly flat, horizontal part of the potential. In the beginning, on the almost horizontal slow 'roll' towards a deep potential well, $\ddot{\phi}$ can be neglected, and the slow-roll equation of motion is

$$3H\dot{\phi} + V'(\phi) = 0, \tag{88}$$

together with the Friedmann equation

$$H^2 = \frac{8\pi G_N}{3}\left[\frac{1}{2}\dot{\phi}^2 + V(\phi)\right], \tag{89}$$

which during slow roll, when $\dot{\phi}^2$ is small, can be approximated by

$$H^2 = \frac{8\pi G_N}{3}V(\phi). \tag{90}$$

One can from this get an expression for the number N_ϕ of e-folds of the scale factor,

$$N_\phi \equiv \log\left(\frac{a_2}{a_1}\right) = \int H dt \sim \int_{\phi_1}^{\phi_2} \frac{V(\phi)}{V'(\phi)} d\phi. \tag{91}$$

Thus, for a large growth of the scale factor, $V(\phi)$ has to be very flat ($V'(\phi) \sim 0$). This may be unnatural except perhaps in some supersymmetric theories where 'flat directions' can occur because of the pattern of supersymmetry breaking. In a situation of such a slow roll of the inflation field, the exact form of the potential does not matter so much, and the relevant physics can be expressed in terms of the so-called slow-roll parameters

$$\varepsilon = -\frac{\dot{H}}{H^2} = 4\pi G_N \frac{\dot{\phi}^2}{H^2} = \frac{1}{16\pi G_N}\left(\frac{V'}{V}\right)^2 \tag{92}$$

$$\eta = \frac{1}{8\pi G_N}\left(\frac{V''}{V}\right) = \frac{V''}{3H^2} \tag{93}$$

where the second equation in (92) comes from taking the derivative of (89) and inserting into (87). The variable ε is a measure of the change of the Hubble expansion during inflation; for inflation to happen at all, $\varepsilon < 1$ is needed.

In the picture of the rolling ball, reheating corresponds to oscillations in the potential well. Thus, for enough entropy to be generated the well has to be rather steep. The problem of constructing a suitable potential is to simultaneously have it flat near $\phi = 0$ and steep near $\phi = \phi_{min}$.

A way to avoid a phase transition, and in fact the simplest model of inflation is the chaotic inflation model of Andrei Linde [12]. It relies on the fact that the key ingredient for inflation to occur is that the field is rolling slowly, so that the energy density is nearly constant during a sufficient number of e-foldings of the scale factor. Since the rolling is damped by the presence of the term proportional to H in (87), and H according to the Friedmann equation is given by the height of the potential (if kinetic terms can be neglected), inflation will be possible for any positive, power-law potential $V(\phi)$, for example the simplest $V(\phi) = \frac{1}{2}m^2\phi^2$, as long as the field values start out large. As Linde has argued, this may not be unreasonable since these initial values may be given stochastically ("chaotically") at the Planck epoch, and those regions where the field values are large start to inflate rapidly dominating the volume of the universe. There are also constructions relying on the existence of more than one scalar field, keeping the same general features but with changes in the details.

Since the value of the total energy density $\Omega = 1$ is found observationally in current measurements of the CMBR anisotropy which yield $\Omega = 1.003 \pm 0.010$, the most natural explanation seems to be that the universe has indeed gone through a period of inflation. An important test of inflation may be produced by the upcoming measurements from the Planck satellite of the detailed pattern of temperature fluctuations in the CMBR. Inflation predicts a nearly but not perfect scale-invariant spectrum of fluctuations (which is when the index of scalar fluctuations $n_s = 1$), and present measurements from WMAP give $n_s \sim 0.96$, in excellent agreement. Inflation could also have generated gravitational (tensor) waves during the phase transitions which would give a particular pattern ("B-modes") in the microwave sky. However, the amplitude of tensor to scalar fluctuations depends rather strongly on the model. It will be interesting to see whether the Planck satellite, when cosmological data are released in early 2013, will detect such a B-mode pattern.

4 Basic Cross Sections for Neutrinos and γ-Rays

Among the various messengers from the Galaxy and structures further away, neutrinos and γ-rays have the advantage that they follow straight lines (or to be more exact, geodesics; the deviations from straight lines can in almost all cases be safely neglected—exceptions are given for particles originating or travelling very near black holes). This is in contrast to all other cosmic rays, electrons, protons, nuclei, and antimatter (positrons, antiprotons and some antinuclei like antideuterons). Neutrons would in principle also travel rectilinearly apart from effects of their magnetic moment. However, their finite lifetime (of the order of 10 min in the rest frame) means that for energies less than a few TeV which is the energy range we will

generally be concerned with, they cannot travel over astrophysical distances. They β-decay to a proton, an electron and an (anti-)neutrino.

Although neutrinos and γ-rays (high-energy photons) are both encompassed in the Standard Model of particle physics and therefore in principle should interact with similar strengths given by gauge couplings, this is in practice not so. The reason is the difference that the photon is a massless, spin-1 gauge particle, i.e., a mediator of a force (the electromagnetic force, i.e., it couples to electrons and protons, and all other particles with electric charge) while the neutrino is a spin-1/2 matter particle which in turn interacts through the weak force mediated by the heavy W and Z bosons. The large, important difference of masses between weak bosons and the photon is due to the hitherto experimentally unverified, but hopefully soon to be verified mechanism, the Higgs mechanism. This breaks the gauge group of the Standard Model, leaving only the electromagnetic $U(1)_{em}$ unbroken and therefore the photon massless. It means that for energies up to 1 TeV or so, neutrinos have very small cross section, which however rises with energy, until the centre-of-mass energy is of the order of the W and Z masses, at which point neutrinos start to react roughly as strongly as photons. Let us now discuss in some more detail how some simple particle cross sections are computed.

4.1 Estimates of Cross Sections

The calculation of collision and annihilation cross sections, and decay rates of particles, is an important task in particle physics. Here we will present only a brief outline of how this is done, and focus on 'quick-and-dirty' estimates which may be very useful in cosmology and astrophysics. For the local microphysics in the FLRW model, only three interactions—electromagnetic, weak and strong—between particles need to be considered. The gravitational force is completely negligible between individual elementary particles—for instance, the gravitational force between the proton and the electron in a hydrogen atom is around 10^{40} times weaker than the electromagnetic force. However, gravity, due to its coherence over long range, still needs to be taken into account through its influence on the metric. This means that the dilution of number densities due to the time dependence of the scale factor $a(t)$ has to be taken into account. In the next section we will see how this is done.

Let us begin with the interaction strengths. The strength of the electromagnetic interaction is governed by the electromagnetic coupling constant g_{em}, which is simply the electric charge. As usual, we take the proton charge e as the basic unit and can thus write

$$g_{em} = Qe \tag{94}$$

where Q is the charge of the particle in units of the proton charge (for a u-quark, for example, $Q_u = +2/3$). In our system of units,

$$\frac{e^2}{4\pi} \equiv \alpha_{em} \tag{95}$$

where α_{em} is the so-called fine structure constant which has the value of around $1/137$ at low energies.[2] The weak coupling constant is of similar magnitude:

$$g_w = \frac{e}{\sin\theta_W} \tag{96}$$

with θ_W the weak interaction (or Weinberg) angle, which has the numerical value $\sin^2\theta_W \sim 0.23$. The fact that the weak and electromagnetic coupling constants are of the same order of magnitude is of course related to the fact that they are unified in the Standard Model to the 'electroweak' interaction.

The coupling constant of the strong interaction, g_s, is somewhat higher. Also, it runs faster (it decreases) with energy than the electromagnetic coupling. At energies of a few GeV,

$$\alpha_s \equiv \frac{g_s^2}{4\pi} \sim 0.3 \tag{97}$$

Let us look at the Feynman diagram for a simple process like $e^+e^- \to \mu^+\mu^-$ (Fig. 1). The amplitude will be proportional to the coupling constants at both vertices, which in this case are both equal to e. The cross section, being proportional to the square of the amplitude, is thus proportional to $e^4 \propto \alpha^2$.

The total energy of the e^+e^- pair in the centre of momentum frame is $E_{cm}(e^+) + E_{cm}(e^-)$, which is conventionally noted with the Mandelstam variable as $\sqrt{s}$. Since the total momentum in this frame is zero, the four-momentum $p^\mu = (\sqrt{s}, 0, 0, 0)$ is identical to that of a massive particle of mass $M = \sqrt{s}$ which is at rest. Energy and momentum conservation then tells us that the photon in the intermediate state has this four-momentum. However, a freely propagating photon is massless, which means that the intermediate photon is virtual by a large amount. In quantum field theory one can show that the appearance of an intermediate state of virtual mass $\sqrt{s}$ for a particle with real rest mass M_i is suppressed in amplitude by a factor (called the propagator factor)

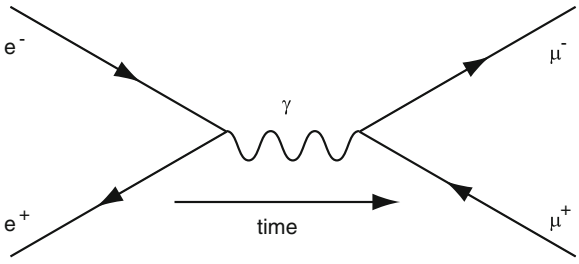

Fig. 1 A Feynman diagram representing the annihilation of an electron and a positron to a muon pair

[2] This coupling constant usually denoted just α without the subscript, as all others, depends on the energy scale, for example, the energy transfer, of the process. At 100 GeV energy α_{em} is $\sim 1/128$.

$$P(s) = 1/(s - m_i^2) \tag{98}$$

In this case ($m_\gamma = 0$), we have a factor of $1/s$. (If one does this rigorously, one should insert a small imaginary part in the denominator, which defines how the singularity on the mass shell is treated.) The outgoing particles (in this case the muons) have a large number of possible final states to enter (for example, all different scattering angles in the centre of momentum frame). This is accounted for by the so-called phase space factor ϕ, which generally grows as s for large energies. For the cross section σ

$$\sigma(e^+e^- \to \mu^+\mu^-) \propto \phi\left(\frac{\alpha^2}{s^2}\right) \tag{99}$$

with ϕ the phase space factor. If s is large compared to m_e^2 and m_μ^2, $\phi \propto s$, and

$$\sigma(e^+e^- \to \mu^+\mu^-) \sim \frac{\alpha^2}{s} \tag{100}$$

This is not an exact expression. A careful calculation (see next section) gives $4\pi\alpha^2/(3s)$, but it is surprisingly accurate and often accurate enough for the estimates we need in big bang cosmology.

Since the weak coupling strength is similar to the electromagnetic strength, the same formula is valid for, e.g., $\nu_e + e \to \nu_\mu + \mu$ which goes through W exchange (see Fig. 2). The only replacement we need is $1/s \to 1/(s - m_W^2)$ for the propagator, thus

$$\sigma(\bar{\nu}_e + e^- \to \bar{\nu}_\mu + \mu^-) \sim \frac{\alpha^2 s}{(s - m_W^2)^2} \tag{101}$$

When $s \ll m_W^2$, this gives $\sigma_w \sim \alpha^2 s/m_W^4$, which is a very small cross section, e.g., for MeV energies. One should notice, however, the fast rise with energy due to the factor s. This is the historical reason for the name 'weak interaction', which is really not appropriate at high energies (much larger than m_W), where the two types of cross sections become of similar size.

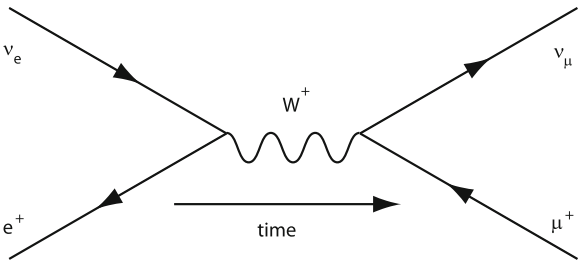

Fig. 2 A Feynman diagram representing the annihilation of an electron neutrino and a positron to a muon neutrino and a muon

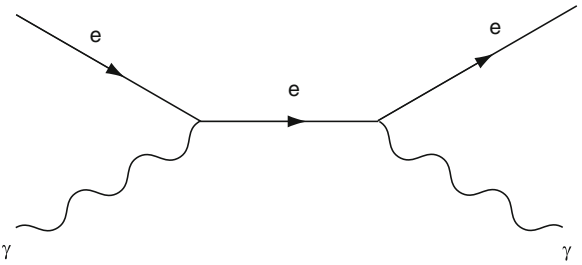

Fig. 3 A Feynman diagram representing the $\gamma e \to \gamma e$ process. In the classical limit, this is called Thomson scattering. The quantum version is called Compton scattering, and in the relativistic regime, the result is given by the Klein-Nishina formula

Note that once one remembers the factors of coupling constants and the propagators, the magnitude of cross sections can often be estimated by simple dimensional analysis. A cross section has the dimension of area, which in our units means $(\text{mass})^{-2}$. It is very useful to check that the expressions (100) and (101) have the correct dimensions.

A decay rate Γ can be estimated in a similar way. If a collection of identical unstable particles decay, their number density decreases as $e^{-\Gamma t}$ which means that Γ has the dimensions of mass.

A fermion has a propagator that behaves as $1/m$ (instead of $1/m^2$) at low energies. This means that the Thomson cross section $\sigma(\gamma e \to \gamma e)$ at low energies $E_\gamma \ll m_e$ can be estimated to be (see Fig. 3)

$$\sigma_T \equiv \sigma(\gamma e \to \gamma e) \sim \frac{\alpha^2}{m_e^2} \tag{102}$$

4.2 Examples of Cross Section Calculations

The estimates we have given are in many cases sufficient for cosmological and astrophysical applications. However, there are cases when one would like to have a more accurate formula. We now provide only a couple of examples and summarize the general framework for calculation and the main results.

4.3 Definition of the Cross Section

The differential cross section $d\sigma/dt$ for $2 \to 2$ scattering $a + b \to c + d$ is given by the expression

$$\frac{d\sigma}{dt} = \frac{|\widetilde{T}|^2}{16\pi\lambda\left(s, m_a^2, m_b^2\right)} \tag{103}$$

where the Lorentz invariant Mandelstam variables are $s = (p_a + p_b)^2, t = (p_a - p_c)^2$ and $u = (p_a - p_d)^2$. $|\widetilde{T}|^2$ is the polarization-summed and squared quantum mechanical transition amplitude, while the function λ is defined as

$$\lambda(x, y, z) \equiv x^2 + y^2 + z^2 - 2xy - 2xz - 2yz\,. \tag{104}$$

For a $2 \to 2$ process, the kinematically allowed region in s is

$$s > (m_c + m_d)^2 \tag{105}$$

which can be understood from energy conservation: In the centre of momentum system (cms), where $\sqrt{s}$ corresponds to the total energy, at least the rest mass energy $m_c + m_d$ has to be provided.

The kinematical limits for t can be obtained from the condition $|\cos\theta_{ac}^{\rm cms}| \leq 1$, with

$$\cos\theta_{ac}^{\rm cms} = \frac{s(t-u) + (m_a^2 - m_b^2)(m_c^2 - m_d^2)}{\sqrt{\lambda(s, m_a^2, m_b^2)}\sqrt{\lambda(s, m_c^2, m_d^2)}}. \tag{106}$$

A typical calculation (following the treatment of [1]) involves computing the matrix element in terms of s and t and carrying out the t integration to obtain the total cross section.

In the one-photon exchange approximation, the cross section for the annihilation process $e^+e^- \to \mu^+\mu^-$ is

$$\sigma(e^+e^- \to \mu^+\mu^-) = \frac{2\pi\alpha^2}{s}\beta\left(1 - \frac{\beta^2}{3}\right) \tag{107}$$

where the only approximation made is to neglect m_e (this is allowed, since $m_e^2/m_\mu^2 \ll 1$). Here β is the velocity of one of the outgoing muons in the centre of momentum system, $\beta = \sqrt{1 - 4m_\mu^2/s}$. In the relativistic limit of $s \gg m_\mu^2$, ($\beta \to 1$), this becomes

$$\sigma\left(e^+e^- \to \mu^+\mu^-\right)_{\text{large } s} = \frac{4\pi\alpha^2}{3s} \tag{108}$$

in agreement with our simple estimate (100).

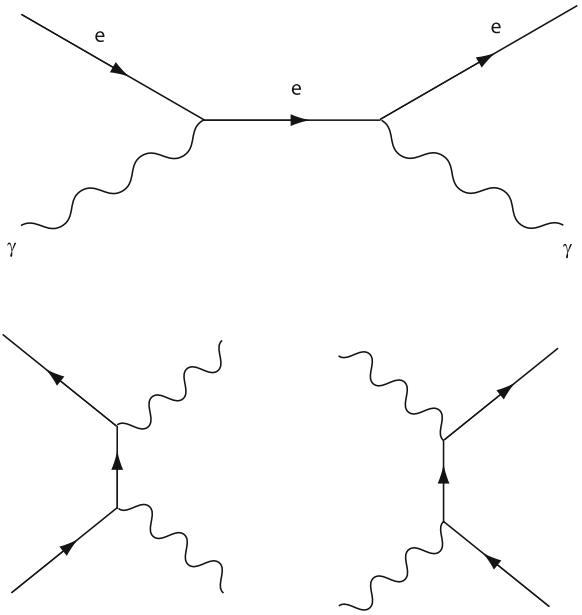

Fig. 4 The same Feynman diagram can, after rotation of the external legs, describe both $e\gamma \to e\gamma$, $e^+e^- \to \gamma\gamma$, and $\gamma\gamma \to e^+e^-$. Here time is as usual flowing from *left* to *right*

4.4 The $\gamma\gamma ee$ System

By different permutations of the incoming and outgoing particles, the basic $\gamma\gamma ee$ interaction (shown in Fig. 3) can describe all of the astrophysically important processes (see the contributions by F. Aharonian and C. Dermer in this volume) $\gamma\gamma \to e^+e^-$, $e^+e^- \to \gamma\gamma$, and $\gamma e^\pm \to \gamma e^\pm$, see Fig. 4.

For $\gamma\gamma \to e^+e^-$ the result is

$$\sigma\left(\gamma\gamma \to e^+e^-\right) = \frac{\pi\alpha^2}{2m_e^2}\left(1-\beta^2\right)\left[\left(3-\beta^4\right)\ln\left(\frac{1+\beta}{1-\beta}\right) + 2\beta\left(\beta^2-2\right)\right] \tag{109}$$

where β now is the velocity of one of the produced electrons in the centre-of-momentum frame, $\beta = \sqrt{1-4m_e^2/s}$. Near threshold, i.e. for small β, the expression in square brackets can be series expanded to $2\beta + \mathcal{O}(\beta^2)$, and thus

$$\sigma\left(\gamma\gamma \to e^+e^-\right)_{\text{small }\beta} \simeq \frac{\pi\alpha^2}{m_e^2} \tag{110}$$

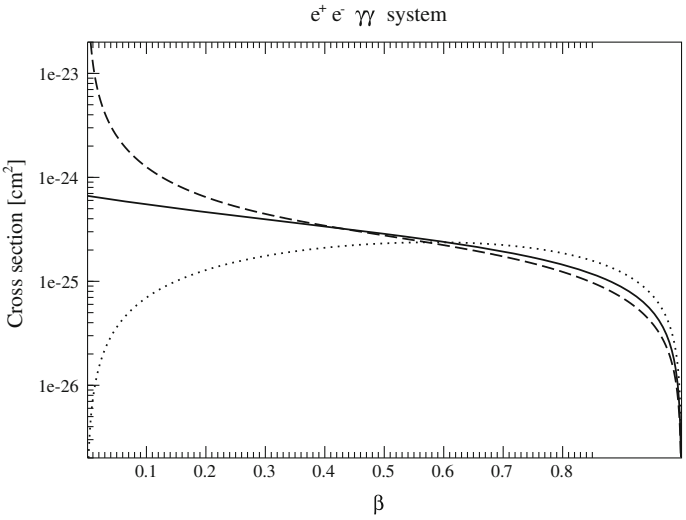

Fig. 5 The cross sections (in cm^2) for photon–photon annihilation (*dotted line*), $e^+e^- \to \gamma\gamma$ (*dashed line*) and Compton scattering (*solid line*) as a function of the cms velocity β of the electron

In the other extreme, $\beta \to 1$,

$$\sigma\left(\gamma\gamma \to e^+e^-\right)_{s\gg 4m_e^2} \simeq \frac{4\pi\alpha^2}{s}\left[\ln\left(\frac{\sqrt{s}}{m_e}\right) - 1\right] \tag{111}$$

One could in fact have guessed most of this to a fair amount of accuracy by the simple dimensional and vertex-counting rules. At low energy, the only available mass scale is m_e, so the factor α^2/m_e^2 could have been guessed for that reason. The factor β could also have been inferred with some more knowledge of non-relativistic partial wave amplitudes. At low energy, the $\ell = 0$ (S-wave) amplitude should dominate, and this contributes to the cross section proportionally to β. A partial wave ℓ contributes to the total cross section with a term proportional to $\beta^{2\ell+1}$. We see from Eq. (107) that in the case of $e^+e^- \to \mu^+\mu^-$ the S-wave dominates at low energy, but when $\beta \to 1$, the P-wave contribution is $1/3$. At high energy, when m_e can be neglected, the dimensions have to be carried by s. Only the logarithmic correction factor in (111) could not have been easily guessed.

These formulas show that the $\gamma\gamma \to e^+e^-$ cross section rises from threshold to a maximum at intermediate energies and then drops roughly as $1/s$ at higher β, i.e., higher cms energy in the process (see Fig. 5).

The results for the reverse process $e^+e^- \to \gamma\gamma$ are of course extremely similar. Now, the process is automatically always above threshold. For $\beta \to 0$ (with β now the velocity of one of the incoming particles in the cm-system, still given by the formula $\beta = \sqrt{1 - 4m_e^2/s}$), the flux factor $\sim 1/\beta$ implicit in Eq. (103) diverges. Since the

outgoing photons move away with $\beta = c = 1$ there is no partial-wave suppression factor, and we can thus expect the cross section at low energy to behave as

$$\sigma\left(e^+e^- \to \gamma\gamma\right)_{\text{low energy}} \sim \frac{\alpha^2}{\beta m_e^2} \tag{112}$$

and the high-energy behavior by the same formula, with m_e^2 replaced by s (and possibly a logarithmic factor). These expectations are borne out by the actual calculation, which gives

$$\sigma\left(e^+e^- \to \gamma\gamma\right) = \frac{\pi\alpha^2\left(1-\beta^2\right)}{2\beta m_e^2}\left[\frac{3-\beta^4}{2\beta}\ln\left(\frac{1+\beta}{1-\beta}\right) - 2 + \beta^2\right] \tag{113}$$

Note the similarity with Eq. (109). The $1/\beta$ behavior of the cross section (see the dashed curve in Fig. 5) was noted by Arnold Sommerfeld in the 1930s, and he showed how one can make an improved calculation valid at very small velocities by not only treating the annihilating particles as plane waves, but using wave functions appropriate for the attractive Coulomb interaction between the electron and positron. He thereby described a generic mechanism, the so-called Sommerfeld enhancement mechanism, which recently has played an important role for dark matter calculations, as we will see later in Sect. 6.3.

Compton and Inverse Compton Scattering

As the final example, we consider Compton scattering $\gamma + e^- \to \gamma + e^-$. Historically, this was first computed for an incoming beam of photons of energy ω which hit electrons at rest. Later on, the related process of a very high energy electron or positron colliding with a low-energy photon (such as coming from the cosmic microwave background, or from infrared or optical radiation created in stellar processes) and upscattering that photon to high, maybe GeV energy or higher, has been found to be very important in astrophysics. Despite being really one and the same process, the latter situation is often referred to as the inverse Compton or IC process. In fact, the inverse Compton process is one purely leptonic process of creating high-energy γ-rays, and could be important for the emission γ-rays in several cases, such as AGNs, GRBs and various supernova remnants. However, to completely prove such a scenario, it is important to search for, or give upper limits on, neutrino emission. In competing hadronic models of emission, where γ-rays mainly come from π^0 decays, one should also have essentially the same amount of charged pions which decay into a leptons and neutrinos. Also for some "leptophilic" models of dark matter, where electrons and muons are main annihilation products, inverse Compton processes may be quite important, e.g., near the galactic centre where radiation fields are large.

For scattering of a photon by an angle θ with respect to the incident photon direction, the outgoing photon energy ω' is given by energy-momentum conservation

$$\omega' = \frac{m_e \omega}{m_e + \omega\,(1 - \cos\theta)} \tag{114}$$

In this frame, the unpolarized differential cross section, the Klein-Nishina formula as it was first computed by Klein and Nishina shortly after Dirac had presented his equation describing relativistic electrons (and positrons), is

$$\frac{d\sigma}{d\Omega} = \frac{\alpha^2}{2m_e^2}\left(\frac{\omega'}{\omega}\right)^2\left[\frac{\omega'}{\omega} + \frac{\omega}{\omega'} - \sin^2\theta\right] \tag{115}$$

Integrated over all possible scattering angles this gives the total cross section

$$\begin{aligned}\sigma(\gamma + e \to \gamma + e) &= \frac{\pi\alpha^2\,(1-\beta)}{m_e^2\beta^3} \\ &\times\left[\frac{4\beta}{1+\beta} + \left(\beta^2 + 2\beta - 2\right)\ln\left(\frac{1+\beta}{1-\beta}\right) - \frac{2\beta^3\,(1+2\beta)}{(1+\beta)^2}\right]\end{aligned} \tag{116}$$

where β is now the incoming electron velocity in the centre of momentum frame, $\beta = (s - m_e^2)/(s + m_e^2)$. If one expands this result around $\beta = 0$, one recovers the Thomson scattering result

$$\sigma_{\text{Thomson}} = \frac{8\pi\alpha^2}{3m_e^2} \sim 6.65 \cdot 10^{-25}\ \text{cm}^2 \tag{117}$$

and the large-s, so-called Klein Nishina regime gives

$$\sigma_{\text{KN}} = \frac{2\pi\alpha^2}{s}\left[\ln\left(\frac{s}{m_e^2}\right) + \frac{1}{2}\right] \tag{118}$$

We see that for photon energies much larger than m_e—that is, in the Klein-Nishina regime—the Compton cross section falls quite rapidly.

In the classical Compton scattering situation, the outgoing photon energy is always less than the incoming one. Thus, energetic photons traveling through a gas of cold electrons will be 'cooled' by Compton scattering. In the IC case (for example for the cosmic microwave background radiation passing through a galaxy cluster with hot gas) energetic electrons may instead transfer energy to photons, thereby 'heating' them. For CMBR this is called the Sunyaev-Z'eldovich effect, and has a large range of applicability (for instance, it has recently been used to find galaxy clusters).

When computing actual numbers for the cross sections (which should have the dimensions of area) in our units, a useful conversion factor is

$$1\ \text{GeV}^{-2} = 0.389 \cdot 10^{-27}\ \text{cm}^2 \tag{119}$$

In Fig. 5 the numerical results are summarized. The cross sections are shown (in cm^2) for $\gamma\gamma \to ee$, $ee \to \gamma\gamma$ and $\gamma e \to \gamma e$ as a function of the cms velocity β of the electron. We see in the figure the different behaviour at low cms velocity already discussed, but that they show a similar decrease at high energy.

Another process of great astrophysical importance is bremsstrahlung. By this is meant the emission of photons from charged particles which are accelerated or decelerated. If this acceleration is due to circular motion in a magnetic field, the term synchrotron radiation is used. Through these processes (unlike Compton scattering) the number of photons can change. This is needed, for instance in the early universe, if thermal equilibrium is to be maintained, since the number density of photons has to vary, as it depends strongly on temperature. Most of the produced photons have very low energy (long wavelength). If fast electrons pass through a region where synchrotron radiation and bremsstrahlung occur, these low-energy photons may be upscattered in energy through the inverse Compton process. This may for example explain the observations of very high-energy photons in active galactic nuclei.

For a detailed discussion of these and other quantum electrodynamic (QED) processes, see standard textbooks in quantum field theory, for example, [13], or a simplified treatment along the lines given here, in [1]. And, of course, for good examples of the use of these processes in astrophysics, see the accompanying lectures by F. Aharonian and C. Dermer in this volume.

4.5 Processes Involving Hadrons

Since protons and neutrons belong to the most common particles in the universe, it is of course of great interest to compute processes where these and other hadrons (such as pions) are involved. This is, however, not easy to do from first principles. The reason that in the previous section we could compute so accurately weak and electromagnetic processes is that we could use perturbation theory (as summarized, for example, in Feynman diagrams). The expansion parameter, the electroweak gauge coupling constant g or rather $\alpha_{ew} = g^2/(4\pi) \sim 10^{-2}$, is small enough that a lowest-order calculation is enough to obtain very accurate results.

In quantum chromodynamics (QCD), which also is a gauge theory just as QED, we also have a coupling constant α_s. Due to the fact that the gauge group of QCD is SU(3), which involves self-interactions of the 8 spin-1 gluons, there are important differences. We say that QCD is a non-abelian gauge theory whereas QED is based on the abelian group U(1) with only one spin-1 gauge field, the photon. One consequence of this difference is that QCD has what is called asymptotic freedom meaning that the coupling strength which is of order unity at a few hundred MeV, "runs" to smaller values for large energies. The energy scale is set, for example, by the energy or momentum transfer Q ($Q^2 \equiv -t$ with t the usual Mandelstam variable) in the process. Thus, for processes with large Q^2, we should be able to use low-order perturbative QCD, although with lower accuracy than for QED due to the possible importance of higher-order corrections. At low energies when the QCD coupling

becomes of the order unity perturbation theory breaks down. In the nonperturbative regime we have to rely on empirical methods, such as "QCD sum rules" [14] or large computer simulations, where one tries to solve QCD by formulating it as a field theory on a lattice. Although the problem is notoriously difficult, the agreement between the spectrum of hadrons, i.e., the masses and quantum numbers of the lowest-lying states with experimentally measured quantities, is quite satisfactory for the most recent numerical simulations [15].

For processes like proton-proton scattering at low energies, the picture of strong interactions being due to the exchange of gluons breaks down. Instead one may approximate the exchange force as being due to pions and other low-mass mesons with surprisingly good results (this is in fact what motivated Yukawa to predict the existence of pions). If one wants to make crude approximations of the strong interaction cross section in this regime, $\sigma_s \sim 1/m_\pi^2$ is a good estimate.

In the perturbative regime at high Q^2, the scattering, for example, of an electron off a proton ('deep inelastic scattering') can be treated by the successful parton model. Here, the momentum of a hadron at high energy is shared between its different constituents. Among the constituents are of course the quarks that make up the hadron (two u and one d quarks in the case of the proton), i.e., the valence quarks. In addition, there may be pairs of quarks and antiquarks produced through quantum fluctuations at any given "snapshot" of the hadron. The incoming exchange photon sent out from an electron in ep scattering may hit these "sea quarks", which will therefore contribute to the scattering process.

Since the partons interact with each other, they can share the momentum of the proton in many ways. Thus, there will be a probability distribution, $f_i(x, Q^2)$, for a parton of type i (where i denotes any quark, antiquark or gluon) to carry a fraction x of the proton momentum. These functions cannot be calculated from first principles. However, once determined (by guess or by experimental information from various scattering and annihilation processes) at a particular value of Q_0^2, the evolution of the structure functions with Q^2 can be predicted. This analysis, as first convincingly performed by Altarelli and Parisi [16], gives rise to a predicted variation of the deep inelastic scattering probability with Q^2 (so-called scaling violations) which has been successfully compared with experimental data. The success of the perturbative QCD program, including the running of α_s in agreement with the asymptotic freedom prediction, and the agreement of scaling violations in several processes with data, resulted in a Nobel Prize for Gross, Wilczek and Politzer in 2004.

With the successful QCD parton model, we can now compute many electromagnetic and weak processes, including those when hadrons are involved. For instance, the neutrino-proton scattering cross section is be given by the scattering of a neutrino on a single quark or antiquark. This calculation is easily done in a way similar to how we computed the $\bar{\nu}_e + e^- \to \bar{\nu}_\mu + \mu^-$ cross section. The only change is that the contributions from all partons have to be summed over, and an integral of x performed.

As an example, we give the expression for the electromagnetic cross section $p + p \to \mu^+ + \mu^-$, which is called the Drell-Yan process, in the QCD parton model. The fundamental process must involve charged partons, i.e., quarks (since

we assume that strong interactions dominate and thus neglect the weak contribution), $q+\bar{q} \to \gamma^* \to \mu^+ + \mu^-$, with the (valence) quark taken from one of the protons and the (sea) antiquark from the other. The momentum transfer in the process is $Q^2 = \hat{s}$, where $\hat{s} = (p_{\mu^+} + p_{\mu^-})^2$. We know from (108) that the parton level cross section is $4\pi\alpha e_q^2/3\hat{s}$ (where we have to take into account that the quark charge e_q is not the unit charge). Since the parton from proton 1 carries the fraction x_1 and that from proton 2 x_2 of the respective parent proton, $\hat{s} = x_1 x_2 s$, with $s = (p_1 + p_2)^2$. The total cross section for producing a muon pair of momentum transfer $\hat{s}$ is thus

$$\frac{d\sigma}{d\hat{s}} = \frac{4\pi\alpha^2}{3\hat{s}} k_c \sum_q e_i^2 \int_0^1 dx_1 \int_0^1 dx_2 \times \left[f_q(x_1, \hat{s}) f_{\bar{q}}(x_2, \hat{s}) + f_{\bar{q}}(x_1, \hat{s}) f_q(x_2, \hat{s}) \right] \delta(\hat{s} - x_1 x_2 s)$$

Here k_c is a colour factor, which takes into account that for a given quark of a given colour, the probability to find in the other proton an antiquark with a matching (anti-) colour is 1/3. Thus, in this case $k_c = 1/3$. In the reverse process, $\mu^+ + \mu^- \to q + \bar{q}$, all the quark colours in the final state have to be summed over (each contributes to the cross section), so in that case $k_c = 3$.

4.6 Neutrinos

Neutrinos are the neutral counterparts of the charged leptons: e, μ and τ. There are therefore three types of "active" neutrinos in the Standard Model of particle physics: ν_e, ν_μ and ν_τ. Neutrinos are fermions, i.e., spin-$\frac{1}{2}$ particles. Apart from their possible gravitational interactions, they interact with matter only through the exchange of the mediators of the weak force, the W and Z bosons. They are fundamental particles without constituents, as far as is known, have extremely small masses and lack electric charge. Among the most spectacular events in astrophysics are supernova explosions. In a few seconds, more energy is released in neutrinos from the forming neutron star than all the electromagnetic emission from an entire galaxy over a decade.

Neutrinos would provide an important contribution to the total energy density of the universe if they had a mass in the eV range. Present-day analyses of the microwave background and the matter distribution favour as we mentioned, cold dark matter over hot dark matter which eV-scale Standard Model neutrinos would constitute. However, neutrinos are plausibly part of dark matter, as one of the most important discoveries of the last 15 years has been the definitive demonstration that neutrinos are not massless. It has been shown that neutrinos species can transform into each other through quantum mechanical mixing, which means that in principle they could also decay into each other, e.g., by emitting a photon. The huge mass scale of the W and Z bosons means, however, that the lifetime even for the heaviest neutrino is much longer than the age of the universe, so they are effectively stable. Their production through thermal processes in the early universe would then mean

that their number density is of the same order of magnitude today as that of the microwave background photons, and since they are electrically neutral they qualify as dark matter. This was in fact one of the most studied candidates for dark matter in the 1970s, when one did not know how many different neutrino types there were (this was fixed in the 1990s to 3 standard species, thanks to the CERN LEP experiments), neither very much about their mass. Today's knowledge give estimates of far less than a percent for their contribution to Ω.

There is of course a possibility that there may exist neutrinos with weaker couplings than standard model ones, and if they have mass in the keV range they would qualify as "warm" dark matter, that would still be allowed from structure formation. However, this involves some fine-tuning to get the correct relic density and to avoid other experimental bounds [17].

Neutrinos are also very important information carriers from violent astrophysical processes, which is why neutrino astrophysics is a very active field of research at the present time. An attractive property of neutrinos is in fact their feeble interactions at low energies, which means that they may penetrate regions with dense matter, e.g., the solar interior, or near remnants of supernovae, without being absorbed. Where other particles become trapped or can only propagate through very slow diffusive processes (for instance, it takes on the order of a million years for a photon created near the centre of the sun to diffuse out to the solar surface), neutrinos are able to escape. Neutrinos can thus connect regions of matter that would otherwise be isolated from each other. Because they are almost massless, they move effectively with the speed of light, which makes energy transfer (i.e., radiative heat conduction) very efficient, e.g., from the interior of the sun. Unfortunately, the fact that neutrinos are so weakly interacting, also means that they are extremely difficult to detect. As of today, the only neutrinos of astrophysical interest that have been detected are those created in the fusion processes in the solar interior, and the exceptional supernova in 1987, where a handful of neutrinos was detected a few hours before it was spotted optically in the Southern sky.

Neutrino interactions with matter are divided into two kinds, neutral current (NC) interactions mediated by the neutral Z bosons, and charged current (CC) interactions involving the exchange of W^+ and W^- bosons. NC interactions are responsible for annihilation reactions involving neutrinos,

$$e^+ + e^- \to \nu_\mu + \bar{\nu}_\mu$$

or for example, and elastic scattering interactions such as

$$\nu_\mu + e^- \to \nu_\mu + e^-.$$

In CC interactions there is a change of fermion type, of "flavour". For example, an antineutrino can be absorbed by a proton, producing a neutron and a positron in the final state. This comes about because at the parton level a u-quark in the proton is changed into a d-quark, which means it is transformed to a neutron. In this process

charge is transferred, both for the leptons as the neutrino becomes a charged lepton, and for the hadrons as the positively charged proton becomes a neutron.

4.7 Neutrino Interactions

For the neutrino process (the flavour-changing charged current interaction) $\bar{\nu}_e e^- \to \bar{\nu}_\mu \mu^-$ the cross section at low energies (but still high enough to produce the heavier muon) is

$$\sigma\left(\bar{\nu}_e e^- \to \bar{\nu}_\mu \mu^-\right) \sim \frac{g_w^4 s}{96\pi m_W^4} \tag{120}$$

Before it was known that W bosons existed, Enrico Fermi[3] had written a phenomenological theory for weak interactions with a dimensionful constant (the Fermi constant) G_F. The relation between Fermi's constant and the gauge theory quantities is

$$\frac{G_F}{\sqrt{2}} = \frac{g_w^2}{8m_W^2} \simeq 1.166 \cdot 10^{-5}\ \text{GeV}^{-2} \tag{121}$$

Using the Fermi constant, the cross section can now be written

$$\sigma\left(\bar{\nu}_e e^- \to \bar{\nu}_\mu \mu^-\right) = \frac{G_F^2 s}{3\pi}. \tag{122}$$

We note that the cross section rises with $s \simeq 2E_\nu m_e$ and thus linearly with neutrino energy. When s starts to approach m_W^2, the W propagator $1/(s - m_W^2)$ has to be treated more carefully. It can be improved by writing it in the so-called Breit-Wigner form

$$\frac{1}{s - m_W^2} \to \frac{1}{s - m_W^2 + i\Gamma m_W} \tag{123}$$

where Γ is the total decay width (around 2 GeV) of the W. We see from this that a substantial enhancement of the cross section is possible for $s \simeq m_W^2$. This is an example of a resonant enhancement in the s-channel. For a target electron at rest, this resonance occurs at around 6.3 PeV and is sometimes called the Glashow resonance. If astrophysical sources exist which produce electron antineutrinos with such high energies, the prospects of detecting them would be correspondingly enhanced. However, well above the resonance, the cross section will again start to decrease like $1/s$, just as in the electromagnetic case, $e^+e^- \to \mu^+\mu^-$.

It should be noted that the latter process, $e^+e^- \to \mu^+\mu^-$, also receives a contribution from an intermediate Z boson. At low energies this is negligible, but due

[3] Enrico Fermi is well-known today as the one who has been honoured by giving the γ-ray satellite, FERMI, its name. This has to do with his description of acceleration processes in astrophysics.

to the resonant enhancement it will dominate near $s \simeq m_Z^2$. This is the principle behind the Z studies performed at the LEP accelerator at CERN (where all other fermion-antifermion pairs of the Standard Model were also produced except for $t\bar{t}$, which was not kinematically allowed). In a full calculation, the two contributions have to be added coherently and may in fact interfere in interesting ways, producing for example, a backward-forward asymmetry between the outgoing muons.

A detailed calculation for neutrino energies above around 5 MeV shows that the total cross section for the reaction $\nu_X e^- \rightarrow \nu_X e^-$ is well approximated by [18]:

$$\sigma_{\nu e} = C_X \cdot 9.5 \cdot 10^{-45} \cdot \left(\frac{E_\nu}{1 \text{ MeV}} \right) \text{ cm}^2 \tag{124}$$

where the flavour-dependent constants C_X are

$$C_e = 1 \tag{125}$$

and

$$C_\mu = C_\tau = \frac{1}{6.2} \tag{126}$$

The cross section is larger for electron neutrinos as they can, unlike the other neutrino species, couple to the electrons in the target through both NC and CC interactions.

Laboratory experiments have, so far, not succeeded in directly measuring the mass of any neutrino. Instead, the negative results have been expressed in the form of upper limits, due to the finite resolution of the experiments. The best (lowest) upper limits on the mass of the electron neutrino come from the studies of the electron energy spectrum in tritium decay:

$$^3\text{H} \rightarrow ^3\text{He} + e^- + \bar{\nu}_e$$

As the minimum amount of energy taken by the ν_e is its mass, the end-point energy of the emitted electron is a measurement of m_{ν_e}. According to these experiments the mass of the electron neutrino is lower than 3 eV at the 95 % confidence level [19]. With the KATRIN experiment being constructed in Karlsruhe, Germany, one hopes to decrease this upper limit (or find a non-zero value) by an order of magnitude [20].

The discovery of the tau neutrino was announced in 2000 by the DONUT collaboration at Fermilab, through appearance in charm meson decays in photographic emulsion.

Mixing of neutrino species is a very interesting quantum mechanical effect which may occur if the weak-interaction eigenstates ν_e, ν_μ and ν_τ are not the mass eigenstates that propagate in vacuum. We can then express a flavour or weak-interaction neutrino eigenstate, ν_f, as a linear superposition of orthogonal mass eigenstates, ν_m:

$$|\,\nu_f\rangle = \sum_m c_{fm}\,|\,\nu_m\rangle.$$

Of course, all three neutrinos may mix, but it is instructive to see what happens if just two of the neutrinos mix, e.g, $\nu_\mu \leftrightarrow \nu_e$ mixing with mixing angle θ. The time evolution of a muon neutrino wave function, produced e.g. in pion decays, with momentum p is then

$$|\,\nu_e(t)\rangle = -\sin\theta e^{-iE_1t}|\,\nu_1\rangle + \cos\theta e^{-iE_2t}|\,\nu_2\rangle \tag{127}$$

where E_1 and E_2 are the energies of the two mass eigenstates. Two energy levels arise if ν_1 and ν_2 have different masses, for the same momentum, p. Then, for small neutrino masses $m_i \ll E_i$,

$$E_i = p + \frac{m_i^2}{2p} \tag{128}$$

The probability $P(\nu_e \to \nu_e) = |\langle\nu_e\,|\,\nu_e\rangle|^2$, that an electron neutrino remains a ν_e after a time t then becomes

$$P(\nu_e \to \nu_e) = 1 - \sin^2(2\theta)\sin^2\left[\frac{1}{2}(E_2 - E_1)t\right] \tag{129}$$

For very small neutrino masses, using (128),

$$P(\nu_e \to \nu_e) = 1 - \sin^2(2\theta)\sin^2\left[\left(\frac{m_2^2 - m_1^2}{4E}\right)t\right] \tag{130}$$

where E is the energy of ν_e.

Thus the probability the electron neutrino transforms to a muon neutrino at a time t is

$$P(\nu_e \to \nu_\mu) = \sin^2(2\theta)\sin^2\left[\frac{\Delta m^2}{4E}t\right] \tag{131}$$

where $\Delta m^2 = |m_2^2 - m_1^2|$.

From (131) it is seen that the probability function for flavour change oscillates, with an amplitude given by $\sin^2(2\theta)$ and oscillation frequency $\sim\Delta m^2/E$. This is now the generally accepted reason for the deficit of solar electron neutrinos, as deduced by combining data from the Super-Kamiokande experiment in Japan (most recently [21]), which sees the deficit of electron neutrinos, with SNO in Canada, which has measured the neutral current cross section, which shows no deficit [22]. As the neutral current has the same strength for all three neutrinos, this is strong evidence that the total flux is unchanged, but the flux of electron neutrinos has decreased due to mixing.

Numerically, the oscillation length becomes

$$L_\nu = 1.27\left(\frac{E}{1\,\text{MeV}}\right)\left(\frac{1\,\text{eV}^2}{\Delta m^2}\right)\text{m}. \tag{132}$$

In fact, a direct proof that oscillations occur in the (anti-) neutrino sector is given by recent results from the KamLAND experiment [23], where reactor antineutrinos have been shown to oscillate over more than one period of oscillation in L/E.

4.8 Atmospheric Neutrinos

Neutrinos are copiously produced in the atmosphere by hadronic and muonic decays following the interaction of cosmic rays with atomic nuclei N,

$$\begin{cases} p/n + N \to \pi^+/K^+ + \cdots \\ \qquad\qquad\qquad\quad \pi^+/K^+ \to \mu^+ + \nu_\mu \\ \qquad\qquad\qquad\qquad\quad \mu^+ \to e^+ + \bar{\nu}_\mu + \nu_e, \end{cases}$$
$$\begin{cases} p/n + N \to \pi^-/K^- + \cdots \\ \qquad\qquad\qquad\quad \pi^-/K^- \to \mu^- + \bar{\nu}_\mu \\ \qquad\qquad\qquad\qquad\quad \mu^- \to e^- + \nu_\mu + \bar{\nu}_e \end{cases} \tag{133}$$

Studying the end result of these reactions one expects that there are about twice as many muon neutrinos than electron neutrinos produced in the atmosphere:

$$\frac{\phi_{\nu_\mu} + \phi_{\bar{\nu}_\mu}}{\phi_{\nu_e} + \phi_{\bar{\nu}_e}} = 2 \tag{134}$$

This expectation holds at low energies. At higher energies, additional effects have to be taken into account: for example, the competition between scattering and decay of the produced pions, and also time dilation. As the energy spectrum of the primary nuclei reaches out to $\sim 10^{20}$ eV, one expects neutrinos to be produced up to comparable energies.

Due to the complicated chain of reactions in the cascade, computer simulations are needed to find the differential spectrum of atmospheric neutrinos. One finds that there is a broad peak around 0.1 GeV (~ 1 cm^{-2} s^{-1}) and at very high energies, E_ν much larger than TeV, a falling flux $\sim E^{-3.7}$.

The cross section for neutrino-nucleon interactions in a target can be calculated by inserting the nucleon mass instead of m_e in our previous example. In the region of the maximum flux of atmospheric neutrinos the cross section is $\sigma_{\nu N} \sim 10^{-39}$ cm^2. The Super-K experiment showed that also atmospheric neutrinos oscillate, and that part of the muon neutrinos disappear due to $\nu_\mu \to \nu_\tau$ mixing taking place. (Due to the high $\tau^\pm$ lepton mass (1.8 GeV) the ν_τs generated by mixing will not have enough energy on average to make the charged current interaction $\nu_\tau + N \to \tau + X$ kinematically possible. Their contribution to the neutral current events is too small to be easily detected.) The Super-K data on the angular and energy dependence of the oscillation is in excellent agreement with the E/L ratio given by (132).

4.9 Neutrinos as Tracers of Particle Acceleration

A kiloton-size detector is necessary to observe neutrinos from sources as close as the Earth's atmosphere, or the Sun (this actually gave a Nobel Prize to Davies and Koshiba, in 2002). To be able to search other astrophysical objects, the required detector mass becomes very large, megaton or even gigaton (or volume of order km^3).

Consider the $\nu_\mu \to \mu$ charged current weak interaction in a medium,

$$\nu_\mu + N \to \mu + \cdots,$$

where N is a nucleon in the medium in or surrounding the detector. The muon range rises with energy, and around 1 TeV (10^{12} eV) it is more than 1 km. The detection area is therefore greatly enhanced at high energies. In water or ice, a good approximation of the muon range as a function of energy is given by

$$R_\mu \approx 2.5 \ln\left(2 \cdot \frac{E_\mu}{1\ \mathrm{TeV}} + 1\right) \mathrm{km} \tag{135}$$

The produced muon conserves, on average, the direction of the incoming neutrino. The average of the square of the ν_μ-μ angle is approximately (see [1])

$$\sqrt{\langle\theta^2\rangle} \approx 2\left(\frac{1\ \mathrm{TeV}}{E_\nu}\right)^{\frac{1}{2}} \quad \mathrm{deg.} \tag{136}$$

The cross section for neutrino interaction with a fixed target rises linearly with energy. Neutrino telescopes for very high energies become efficient at a few GeV, where the product of the neutrino-matter cross section and the muon range rises approximately as E_ν^2. Above 1 GeV, the induced flux of muons from atmospheric neutrinos, for example, is about 1 m^{-2} year^{-1}.

This detection scheme does not work as well for other types of neutrinos. Electrons (from $\nu_e + \mathrm{N} \to \mathrm{e} + \cdots$) have a very short range as they lose energy through radiative processes, due to their small mass. On the other hand τ leptons, the heaviest known charged leptons with $m_\tau = 1.78$ GeV, are produced in charged current interactions of ν_τ, but they are very short lived ($t_\tau \sim 10^{-13}$ s). Therefore they are not suitable for detection, except for the fraction of times where the τ decays into $\mu\bar{\nu}_\mu\nu_\tau$, which happens in roughly 20 % of the cases. However, in large neutrino detectors such as the IceCube, one may perhaps detect ultra-high-energy electron and τ neutrino events by the intense cascade of light that is produced by secondary electrons, positrons and photons. In the case of τ neutrinos, special relativity may help to produce a good signature. If sources of PeV (10^{15} eV) τ neutrinos exist, the produced charged τ lepton would have a relativistic γ factor as large as

$$\gamma \sim \frac{E_\nu}{m_\tau} \sim 10^6 \tag{137}$$

which means, thanks to time dilation, that in the detector reference frame the τ lepton will travel a distance $\gamma c t_\tau \sim 10\,\text{m}$. The "double bang" created by the charged current interaction and the subsequent decay of the τ lepton, separated by 10 m, would be the signature of PeV τ neutrinos.

Since neutrinos oscillate, very energetic τ neutrinos could be produced by mixing with muon neutrinos created in high-energy pion decays in cosmic accelerators. This is, e.g., the basis for the experiments OPERA [24] at Gran Sasso and MINOS [25] at Fermilab, where a few events of produced τ leptons have in fact been reported.

In present detectors, only neutrino-induced muons moving upwards in the detectors (or downwards but near the horizon) are safe tracers of neutrino interactions. Most muons moving downwards have their origin in cosmic-ray nuclei interacting with the Earth's atmosphere and produce a very difficult background. At the surface of the Earth, the flux of downward-going muons produced in the atmosphere is about 10^6 times larger than the flux of neutrino-induced upward-moving muons.

By going underground, the material (rock, water, ice, etc.) above the detector attenuates the flux of atmospheric muons considerably. In addition, if it is experimentally possible to select events where a muon is moving upwards the Earth itself acts as a filter since only neutrino-induced muons can be produced upward-going close to the detector.

4.10 AMANDA, IceCube and Direct Detection of WIMPs

Neutrinos may give clues to the dark matter problem in another way than just being a small part of the dark matter due to their tiny mass. If the dark matter has a component that is massive and weakly coupled (electrically neutral) it will be non-relativistic at freeze-out, which is of course the WIMP paradigm of cold dark matter. A good template for a dark matter WIMP candidate is as we mentioned the lightest supersymmetric particle—plausibly the neutralino χ (see Sect. 5 for more details).

Neutralinos (or other WIMPs) have interactions with ordinary matter which are equally as small as those of neutrinos. However, since they move with non-relativistic velocity there is a chance that they become gravitationally trapped inside, for example, the Sun or the Earth. A neutralino scattering e.g., in the Sun will lose energy and fall further inside the solar volume, and successive scatterings in the solar medium will soon make it lose more and more energy. In the end, neutralinos will assemble near the centre. As they are their own antiparticles (they are Majorana fermions), they can annihilate with each other, resulting in ordinary particles (quarks, leptons, gauge particles).

As the annihilation rate is proportional to the scattering rate, and the interior of the Earth is almost entirely spin-0 nuclei, constraints on the spin-independent scattering rate from experiments described below in Sect. 8 mean that neutrinos from the center

of the Earth are not a very promising signal for canonical WIMPs. However, as the Sun consists to some 75 % of single protons (i.e., hydrogen nuclei) with spin-1/2, spin-dependent scattering is important and searching for neutrinos from the Sun stands well in competition with other experiments. We will return also to this later.

Most of the annihilation products in the Sun create no measurable effect; they are just stopped and contribute somewhat to the energy generation. However, neutrinos have the unique property that they can penetrate the whole Sun without being much absorbed, at least for WIMPs less massive than a few hundred GeV. An annihilating neutralino pair of mass m_χ would thus give rise to high-energy neutrinos of energy around $m_\chi/3$ or so (the reason that $E_\nu \neq m_\chi$ is that other particles created in the annihilation process share the energy). The signal of high-energy neutrinos (tens to hundreds of GeV—to be compared with the 'ordinary' MeV solar neutrinos) from the centre of the Sun would be an unmistakable signature of WIMP annihilation.

The detection of muons in IceCube, for instance, relies on the Cherenkov effect. This coherent emission of light follows a characteristic angle given by the Mach relation

$$\cos\theta = \frac{1}{\beta n}$$

where β is the speed of the particle traversing the medium in units of the speed of light and n is the index of refraction of the medium. The Cherenkov effect takes place when

$$\beta > \frac{1}{n}.$$

Cherenkov radiation constitutes a very small fraction of the total energy loss of a charged particle as it crosses a medium. The superluminal condition is fulfilled only between the UV and near-infrared region of the electromagnetic spectrum. In water or ice, for example, where the index of refraction for UV and optical wavelengths averages around 1.3, the Cherenkov radiation cut-off in the UV region is around 70 nm. The differential energy loss into Cherenkov photons in water or ice is a few percent of the total differential energy loss of a charged track moving with a speed very close to c.

4.11 Water and Ice Cherenkov Telescopes

Neutrinos can thus be detected indirectly by the Cherenkov radiation from charged leptons and hadrons produced in neutrino interactions with matter. The extremely large detector volumes needed to detect neutrinos from distances beyond our Sun makes the use of any other material than water or ice very difficult.

A typical detector consists of an array of light sensors (photomultipliers, PM) with good time resolution ($\sim$1 ns) distributed in the medium. The pattern of the hit PMs, and relative arrival times, are then used to fit the direction of the particle that

generated the Cherenkov radiation. The correlation between the original direction of the neutrino and the produced charged lepton means that one may reconstruct the direction of the incoming neutrino.

Antares is a good prototype, for a larger detector being planned with the working name KM3NET, near Toulon in the Mediterranean. The AMANDA experiment at the South Pole was similarly an excellent working prototype, where the disadvantages related to the remote location of the telescope were compensated by the virtues of the glacier ice, found to be the clearest natural solid on Earth. The Cherenkov photons emitted along the path of a muon at some wavelengths can be selected hundreds of metres away from the muon track.

The AMANDA detector was a great success, but was too small and has recently been abandoned, replaced by a much larger detector, the IceCube, with 80 strings encompassing roughly a cubic kilometer of ice. Construction was finished in 2010, and at that time also a smaller and denser inset, the DeepCore detector, was completed. This allows a lower detection energy threshold which is particularly beneficial for the WIMP search. Unfortunately, despite the heroic effort to build the first large neutrino detector in this remote location, no astrophysical neutrino source including WIMPs has yet been detected, but it is only a year that data have been collected (for a recent review of dark matter detection in neutrino telescopes, see [26]).

5 Supersymmetric Dark Matter

As we have mentioned several times already, one of the prime candidates for the non-baryonic cold dark matter particle is provided by the lightest supersymmetric particle, most likely the lightest neutralino χ. Even if it would be that supersymmetry were not realized in nature, the neutralino is still important as a nice, calculable template for a generic WIMP.

In most versions of the low-energy theory which results from the largely unknown mechanism of supersymmetry breaking, there is a conserved multiplicative quantum number, R-parity:

$$R = (-1)^{3(B-L)+2S}, \tag{138}$$

where B is the baryon number, L the lepton number and S the spin of the particle. This implies that $R = +1$ for ordinary particles and $R = -1$ for supersymmetric particles. In fact, for phenomenological reasons, this symmetry is required, as its conservation protects the proton from decaying through the mediation of R-symmetry breaking interactions. The R-symmetry means that supersymmetric particles can only be created or annihilated in pairs in reactions of ordinary particles. It also means that a single supersymmetric particle can only decay into final states containing an odd number of supersymmetric particles. In particular, this makes the lightest supersymmetric particle stable, since there is no kinematically allowed state with negative R-parity which it can decay to. This is of course of utmost importance for the dark matter problem. Also other WIMP models of dark matter needs some

mechanism to prevent decay, and the simplest mechanism is a discrete symmetry like the double-valued (Z_2) R-symmetry. (Another reason for stability could be the quantum numbers of the particles in the theory. There are in fact models with high spin or isospin multiplets which also have a stable particle which could act as dark matter [27].)

Pair-produced neutralinos in the early universe which left thermal equilibrium as the universe kept expanding should, due to their stability, have a non-zero relic abundance today. If the scale of supersymmetry breaking is related to that of electroweak breaking, the neutralino will act as a WIMP and therefore a dark matter candidate with a relic density of the same order of magnitude as the value implied by the WMAP measurements. This is a very elegant and economical method to solve two of the most outstanding problems in fundamental science, dark matter and the unification of the basic forces, if they have a common element of solution—supersymmetry.

5.1 Supersymmetric Dark Matter Particles

If R-parity is conserved, the lightest supersymmetric particle should be stable. The most plausible candidate is the lightest neutralino χ. As we will see in Sect. 5.2 it is a mixture of the supersymmetric partners of the photon, the Z and the two neutral CP-even Higgs bosons present in the minimal extension of the supersymmetric standard model (MSSM). It is electrically neutral and thus neither absorbs nor emits light, and is stable, surviving since earliest epoch after the big bang. Its gauge couplings and mass means that for a large range of parameters in the supersymmetric sector a relic density is predicted in the required range to explain the observed $\Omega_\chi h^2 \sim 0.11$. Its electroweak couplings to ordinary matter also means that its existence as dark matter in our galaxy's halo may be experimentally tested.

Unfortunately, very little is known about how supersymmetry is broken (for a discussion, see [28]), and therefore any given supersymmetric model contains a large number of unknown parameters (of the order of 100). Such a large parameter space is virtually impossible to explore by present-day numerical methods, and therefore simplifying assumptions are needed. Fortunately, most of the unknown parameters such as CP violating phases influence the properties relevant for cosmology, and for detection, very little.

Usually, when scanning the large space of a priori unknown parameters in supersymmetry, one thus makes reasonable simplifying assumptions and accepts solutions as cosmologically appropriate if they give a neutralino relic density in the range

$$0.09 \lesssim \Omega_\chi h^2 \lesssim 0.12 \tag{139}$$

Recently, there has been a number of analyses where the relic density, and other parameters or experimental quantities known within some error bounds are allowed to vary. By using so-called Markov Chain Monte Carlo methods (MCMC), one can get a "global fit" of the best-fit models using statistical methods [29, 30]. Usually,

one employs what is called a Bayesian method which needs some assumption about the prior distribution of probabilities. In the case of mass parameters one may, for instance, choose linear or logarithmic scans. If experimental data are good enough, it can be shown that the choice of priors is not crucial. However, so far there has been a lack of experimental information, meaning that the predicted most likely regions in parameter space may depend quite sensitively on priors (see, e.g., [31]). Hopefully, the situation may soon change with new results from the LHC. A drawback of the method of global fits is that it is very computer intensive, meaning that only very simplified models of supersymmetry have been fully investigated so far.

Besides its interesting implications for cosmology, the motivation from particle physics for supersymmetric particles at the electroweak mass scale has become stronger due to the apparent need for 100 GeV–10 TeV scale supersymmetry to achieve unification of the gauge couplings in view of LEP results. (For an extensive review of the literature on supersymmetric dark matter up to mid-1995, see Ref. [32]. More recent reviews are [33] and [34]).

A great virtue of supersymmetry at the phenomenological level is that it gives an attractive solution to the so-called hierarchy problem, which is to understand why the electroweak scale at a few hundred GeV is so much smaller than the Planck scale $\sim 10^{19}$ GeV despite the fact that there is nothing in non-supersymmetric theories to cancel the severe quadratic divergences of loop-induced mass terms. In supersymmetric theories, the partners of differing spin would exactly cancel those divergencies (if supersymmetry were unbroken). Of course, supersymmetric models are not guaranteed to contain good dark matter candidates, but in the simplest models R-parity is conserved and the neutralino naturally appears as a good candidate.

The MSSM

The minimal supersymmetric extension of the standard model (MSSM) is defined by the particle content and gauge couplings required by supersymmetry and a gauge-invariant superpotential. Thus, to each particle degree of freedom in the non-supersymmetric Standard Model, there appears a supersymmetric partner with the same charge, colour etc, but with the spin differing by half a unit. The only addition to this doubling of the particle spectrum of the Standard Model concerns the Higgs sector. It turns out that the single scalar Higgs doublet is not enough to give masses to both the u- and d-like quarks and their superpartners (since supersymmetry forbids using both a complex Higgs field and its complex conjugate at the same time, which one does in the non-supersymmetric Standard Model). Thus, two complex Higgs doublets have to be introduced. After the usual Higgs mechanism, three of these states disappear as the longitudinal components of the weak gauge bosons leaving five physical states: two neutral scalar Higgs particles H_1 and H_2 (where by convention H_2 is the lighter state), one neutral pseudoscalar state A, and two charged scalars $H^{\pm}$.

The Z boson mass gets a contribution from the vacuum expectation values v_i of both of the doublets,

$$\left\langle H_1^1 \right\rangle = v_1, \qquad \left\langle H_2^2 \right\rangle = v_2, \tag{140}$$

with $g^2(v_1^2 + v_2^2) = 2m_W^2$. One assumes that vacuum expectation values (VEVs) of all other scalar fields (in particular, squark and sleptons) vanish, as this avoids color and/or charge breaking vacua.

The supersymmetric theory also contains the supersymmetric partners of the spin-0 Higgs doublets. In particular, two Majorana fermion states, higgsinos, appear as the supersymmetric partners of the electrically neutral parts of the H_1 and H_2 doublets. These can mix quantum mechanically with each other and with two other neutral Majorana states, the supersymmetric partners of the photon (the photino) and the Z (the zino). When diagonalizing the mass matrix of these four neutral Majorana spinor fields (neutralinos), the lightest physical state becomes an excellent candidate for cold dark matter.

The one-loop effective potential for the Higgs fields has to be used to obtain realistic Higgs mass estimates. The minimization conditions of the potential allow one to trade two of the Higgs potential parameters for the Z boson mass $m_Z^2 = \frac{1}{2}(g^2 + g'^2)(v_1^2 + v_2^2)$ (where $g = e/\sin\theta_W$, $g' = e/\cos\theta_W$) and the ratio of VEVs, $\tan\beta$. This ratio of VEVs

$$\tan\beta \equiv \frac{v_2}{v_1} \tag{141}$$

always enters as a free parameter in the MSSM, although it seems unlikely to be outside the range between around 1.1 and 60, with some preference for the higher values. The third parameter can further be re-expressed in terms of the mass of one of the physical Higgs bosons, for example m_A.

5.2 Higgs and Supersymmetry

At the ATLAS and CMS experiments at the CERN Large Hadron Collider (LHC), a discovery of the Higgs particle has not yet been claimed (by the end of 2011), as the statistical significance is still below the wanted 5 σ (standard deviations). However, there are intriguing indications showing up at more than 3 σ at a mass value around 125 GeV. If this would stand when more statistics is gathered in 2012, it could means that the Standard Model of particles and fields would be completed with a most wanted spin-0 boson, the Higgs particle. Moreover, a mass below 130 GeV is a firm prediction of supersymmetry, so it may also show the way to a whole new phenomenology, including a very interesting dark matter candidate—the lightest supersymmetric particle, generally thought to be the neutralino. As mentioned in Sect. 5.1, this is a quantum mechanical mixture of the supersymmetric partner of the photon, the neutral weak gauge boson Z and the neutral spin-1/2 partners of each of the two Higgs doublets which are needed by supersymmetry. In supersymmetric

theories, the most likely dark matter candidate is a quantum mechanical superposition, called the neutralino χ of electrically neutral supersymmetric fermions.

Of course, if the 125 GeV Higgs also signals the presence of supersymmetry, then a rich spectrum of particles, several of which may be in reach kinematically at the LHC, is expected. Even if supersymmetry is not realized in nature, it will continue to play a role as an important template for dark matter, as the neutralino is a very attractive, calculable candidate for a generic WIMP. We will return to this later.

5.3 The Neutralino Sector

The neutralinos $\tilde{\chi}_i^0$, of which the lightest is the dark matter candidate, are linear combination of the neutral gauge bosons $\tilde{B}$, $\tilde{W}_3$ (or equivalently $\tilde{\gamma}$, $\tilde{Z}$) and of the neutral higgsinos $\tilde{H}_1^0$, $\tilde{H}_2^0$. In this basis, their mass matrix

$$\mathcal{M} = \begin{pmatrix} M_1 & 0 & -\frac{g'v_1}{\sqrt{2}} & +\frac{g'v_2}{\sqrt{2}} \\ 0 & M_2 & +\frac{gv_1}{\sqrt{2}} & -\frac{gv_2}{\sqrt{2}} \\ -\frac{g'v_1}{\sqrt{2}} & +\frac{gv_1}{\sqrt{2}} & 0 & -\mu \\ +\frac{g'v_2}{\sqrt{2}} & -\frac{gv_2}{\sqrt{2}} & -\mu & 0 \end{pmatrix} \tag{142}$$

can be diagonalized to give four neutral Majorana states,

$$\tilde{\chi}_i^0 = a_{i1}\tilde{B} + a_{i2}\tilde{W}^3 + a_{i3}\tilde{H}_1^0 + a_{i4}\tilde{H}_2^0 \tag{143}$$

($i = 1, 2, 3, 4$) the lightest of which, χ_1^0 or simply χ, is then the candidate for the particle making up the dark matter in the universe.

The coefficients in (143) are conveniently normalized such that for the neutralino

$$\sum_{j=1}^{4} |a_{1j}|^2 = 1. \tag{144}$$

The properties of the neutralino are quite different depending on whether it consists mainly of gaugino ($j = 1, 2$) or higgsino ($j = 3, 4$) components. We therefore define a parameter, Z_g, which tells the size of the gaugino fraction:

$$Z_g = \sum_{j=1}^{2} |a_{1j}|^2. \tag{145}$$

A neutralino is often said to be gaugino-like if $Z_g \gtrsim 0.99$, higgsino-like if $Z_g \lesssim 0.01$, and mixed otherwise.

To simplify, one often makes a diagonal ansatz for the soft supersymmetry-breaking parameters in the sfermion sector. This allows the squark mass matrices to be diagonalized analytically. Such an ansatz implies the absence of tree-level flavor changing neutral currents (FCNC) in all sectors of the model. In models inspired by low-energy supergravity with a universal scalar mass at the grand-unification (or Planck) scale the running of the scalar masses down to the electroweak scale generates off-diagonal terms and tree-level FCNC's in the squark sector.

In the estimates of detection rates here, we will adhere to a purely phenomenological approach, where the simplest unification and scalar sector constraints are assumed, and no CP violating phases outside those of the Standard Model, but no supergravity relations are used. This reduces the number of free parameters to be scanned over in numerical calculations to seven: $\tan\beta$, M_1, μ, m_A, and three parameters related to the sfermion sector (the exact values of the latter are usually not very important). In fact, on can reduce the number of parameters further by choosing, e.g., explicit supergravity models, but this only corresponds to a restriction to a subspace of our larger scan of parameter space. In fact, data from the LHC have already excluded large sectors of the simplified models.

The non-minimal character of the Higgs sector may well be the first experimental hint at accelerators of supersymmetry. At tree level, the H_2^0 mass is smaller than m_Z, but radiative (loop) corrections are important and shift this bound by a considerable amount. However, even after allowing for such radiative corrections it can hardly be larger than around 130 GeV. When there were some weak indications of a Higgs signature at 140 GeV in LHC data reported in mid-2011, this looked like bad news for the MSSM. However, with further data, the preferred mass is now around 125 GeV, which is easily accommodated.

5.4 Experimental Limits

The successful operation of the CERN accelerator LHC at centre of mass energies above 7 TeV without observing any supersymmetric particles, in particular squarks of gluinos, puts important constraints on the parameters of the MSSM. However, it may be that the mass scale of neutralinos is decoupled from the other supersymmetric particle masses (e.g, in "split susy" models [35]).

It has proven to be very difficult, however, to put very tight lower limits on the mass of the lightest neutralino, because of the multitude of couplings and decay modes of the next-to-lightest supersymmetric particle. The lightest neutralino can in general only be detected indirectly in accelerator experiments through the missing energy and momentum it would carry away from the interaction region.

The upper limit of dark matter neutralino masses in the MSSM is of the order of 7 TeV [11]. Above that mass, which is still far from the unitarity bound of 340 TeV [36], the relic density becomes larger than the allowed WMAP upper limit. To get

values for the lightest neutralino mass larger than a few hundred GeV, however, some degree of "finetuning" is necessary. (On the other hand, we have seen that for the other important unknown part of the energy density of the universe, the cosmological constant Λ, a "finetuning" of many orders of magnitude seems also to be necessary.)

By making additional well-motivated but not mandatory restrictions on the parameter space, such as in supergravity-inspired models or in simplified constrained MSSM models (CMSSM), one gets in general masses below 600 GeV [37, 38] for the lightest neutralino, but as mentioned these models are feeling some tension from early LHC data.

5.5 *Supersymmetry Breaking*

Supersymmetry is a mathematically beautiful theory, and would give rise to a very predictive scenario, if it were not broken in an unknown way which unfortunately introduces a large number of unknown parameters.

Breaking of supersymmetry has to be present since no supersymmetric particle has as yet been detected, and unbroken supersymmetry requires particles and sparticles to have the same mass. This breaking can be achieved in the MSSM by a soft potential which does not reintroduce large radiative mass shifts (and which indicates that the lightest supersymmetric particles should perhaps not be too much heavier than the 250 GeV electroweak breaking scale). The origin of the effective low-energy potential need not be specified, but it is natural to believe that it is induced through explicit breaking in a hidden sector of the theory at a high mass scale. The supersymmetry breaking terms could then be transmitted to the visible sector through gravitational interactions.

Another possibility is that supersymmetry breaking is achieved through gauge interactions at relatively low energy in the hidden sector. This is then transferred to the visible sector through some messenger fields which transform non-trivially under the Standard Model gauge group. However, we shall assume the "canonical" scenario in most of the following.

Since one of the virtues of supersymmetry is that it may establish grand unification of the gauge interactions at a common mass scale, a simplifying assumption is often used for the gaugino mass parameters,

$$M_1 = \frac{5}{3}\tan^2\theta_W M_2 \simeq 0.5 M_2, \tag{146}$$

and

$$M_2 = \frac{\alpha_{\rm em}}{\sin^2\theta_W \alpha_s} M_3 \simeq 0.3 M_3, \tag{147}$$

where θ_W is the weak mixing angle, $\sin^2\theta_W \approx 0.22$.

When using the minimal supersymmetric standard model in calculations of relic dark matter density, one should make sure that all accelerator constraints on supersymmetric particles and couplings are imposed. In addition to the significant restrictions on parameters given by LEP and LHC, the measurement of the $b \to s\gamma$ quark flavour changing process is providing important bounds, since supersymmetric virtual particles may contribute significantly to this loop-induced decay. There are also constraints arising if one wants to attribute the slightly abnormal value of $(g-2)$ for the muon [39] to supersymmetric contributions from virtual particles. The relic density calculation in the MSSM for a given set of parameters is nowadays accurate to a few percent or so [2].

5.6 Other Supersymmetric Candidates

Although the neutralino is considered by most workers in the field to be the preferred supersymmetric dark matter candidate, we mention briefly here also some other options.

If the axion, the spin-0 pseudoscalar field which solves the strong CP problem exists, and if the underlying theory is supersymmetric, there should also exist a spin-1/2 partner, the axino. If this is the lightest supersymmetric particle and is in the multi-GeV mass range, it could compose the cold dark matter of the universe (for a review, see [40]).

A completely different type of supersymmetric dark matter candidate is provided by so-called Q-balls [41], non-topological solitons predicted to be present in many versions of the theory. These are produced in a non-thermal way and may have a large lepton or baryon number. They could produce unusual ionization signals in neutrino telescopes, for example. However, the unknown properties of their precise formation mechanism means that their relic density may be far below the level of observability, and a value around the observationally favoured $\Omega_Q \sim 0.22$ may seem fortuitous (for a recent review of the physics of Q-balls, see [42]).

Of course, the possibility of dark matter being non-supersymmetric WIMPs still remains. However, the interaction cross sections should then be quite similar as for supersymmetric particles. Since, the rates in the MSSM are completely calculable once the supersymmetry parameters are fixed, these particles, in particular neutralinos, serve as important templates for reasonable dark matter candidates when it comes to designing experiments with the purpose of detecting dark matter WIMPs.

6 Detection Methods for Neutralino Dark Matter

The ideal situation would appear if supersymmetry were discovered at accelerators, so that direct measurements of the mass of the lightest supersymmetric particle, its couplings and other properties could be performed. This would give a way to

check from very basic principle if this particle is a good dark matter candidate—if it is electrically neutral and has the appropriate mass and couplings to give the required relic density to provide $\Omega_\chi h^2 \sim 0.11$. So far, no signal of supersymmetry has been found at either LEP, Fermilab, or LHC. An indirect piece of evidence for supersymmetry would be the discovery of a Higgs particle below around 130 GeV, since this is the maximal value of the lightest Higgs mass after radiative corrections, in the MSSM. In the non-supersymmetric Standard Model the Higgs could be much heavier. It is indeed encouraging that the first signs of the Higgs at LHC seems to correspond to a mass of 125 GeV.

If we assume a local neutralino halo density of $\rho_\chi = \rho_\odot \sim 0.4$ GeV/cm^3 [43], and a typical galactic velocity of neutralinos of $v/c \sim 10^{-3}$, the flux of particles of mass 100 GeV at the location of a detector at the Earth is roughly 10^9 m^{-2} s^{-1}. Although this may seem as a high flux, the interaction rate has to be quite small, since the correct magnitude of $\Omega_\chi h^2 \sim 0.11$ is only achieved if the annihilation cross section, and therefore by expected crossing symmetry also the scattering cross section, is of weak interaction strength.

The rate for direct detection of galactic neutralinos, integrated over deposited energy assuming no energy threshold, is

$$R = \sum_i N_i n_\chi \langle \sigma_{i\chi} v \rangle, \tag{148}$$

where N_i is the number of nuclei of species i in the detector, n_χ is the local galactic neutralino number density, $\sigma_{i\chi}$ is the neutralino-nucleus elastic cross section, and the angular brackets denote an average over v, the neutralino speed relative to the detector.

The most important non-vanishing contributions for neutralino-nucleon scattering are the scalar-scalar coupling giving a spin-independent (SI) effective interaction, and the spin-dependent (SD) axial-axial interaction,

$$\mathcal{L}_{\text{eff}} = f_{SI} \left(\bar{\chi}\chi\right) \left(\bar{N}N\right) + f_{SD} \left(\bar{\chi}\gamma^\mu\gamma^5\chi\right) \left(\bar{N}\gamma_\mu\gamma^5 N\right). \tag{149}$$

Usually, it is the spin-independent interaction that gives the most important contribution in realistic target materials (such as Na, Cs, Ge, I, or Xe), due to the enhancement caused by the coherence of all nucleons in the target nucleus.

The neutralino-nucleus elastic cross section can be written as

$$\sigma_{i\chi} = \frac{1}{4\pi v^2} \int_0^{4m_{i\chi}^2 v^2} \mathrm{d}q^2 G_{i\chi}^2(q^2), \tag{150}$$

where $m_{i\chi}$ is the neutralino-nucleus reduced mass, q is the momentum transfer and $G_{i\chi}(q^2)$ is the effective neutralino-nucleus vertex. One may write

$$G_{i\chi}^2(q^2) = A_i^2 F_{SI}^2(q^2) G_{SI}^2 + 4\lambda_i^2 J(J+1) F_{SD}^2(q^2) G_{SD}^2, \tag{151}$$

which shows the coherent enhancement factor A_i^2 for the spin-independent cross section. A reasonable approximation for the gaussian scalar and axial nuclear form factors is

$$F_{SI}(q^2) = F_{SD}(q^2) = \exp(-q^2 R_i^2/6\hbar^2), \tag{152}$$

$$R_i = (0.3 + 0.89 A_i^{1/3})\ \text{fm}, \tag{153}$$

which gives good approximation to the integrated detection rate [44] (but is less accurate for the differential rate [45]). Here λ_i is related to the average spin of the nucleons making up the nucleus. For the relation between G_{SI}, G_{SD} and f_{SI}, f_{SD} as well as a discussion of the several Feynman diagrams which contribute to these couplings, see e.g. [46–48]. One should be aware that these expressions are at best approximate. A more sophisticated treatment (see discussion and references in [32]) would, however, plausibly change the values by much less than the spread due to the unknown supersymmetric parameters.

For a target consisting of N_i nuclei the differential scattering rate per unit time and unit recoil energy E_R is given by

$$S_0(E_R) = \frac{dR}{dE_R} = N_i \frac{\rho_\chi}{m_\chi} \int d^3v\, f(\boldsymbol{v})\, v \frac{d\sigma_{i\chi}}{dE_R}(v, E_R). \tag{154}$$

The nuclear recoil energy E_R is given by

$$E_R = \frac{m_{i\chi}^2 v^2 (1 - \cos\theta^*)}{m_i} \tag{155}$$

where θ^* is the scattering angle in the center of mass frame. The range and slope of the recoil energy spectrum is essentially given by non-relativistic kinematics. For a low-mass χ, the spectrum is steeply falling with E_R; interaction with a high-mass χ gives a flatter spectrum with higher cutoff in E_R.

The total predicted rate integrated over recoil energy above a given (generally detector-dependent) threshold can be compared with upper limits coming from various direct detection experiments. In this way, limits on the χ-nucleon cross section can be obtained as a function of the mass m_χ [49–52]. The cross section on neutrons is usually very similar to that on protons, so in general only the latter is displayed below. Major steps forward have been taken in recent years. For example, the CDMS-II experiment [53] and XENON100 [54] have been pushing the limits down by a large factor, reaching now 10^{-44} cm^2 for masses around 50 GeV. This together with a larger detector mass (for XENON, 1 tonne is presently being installed) and other improvements will enable a thorough search well beyond the present range of WIMP-nucleon cross sections. In Europe there are several other ambitious endeavours underway, such as DARWIN, a large liquid noble gas detector, and EURECA, a solid state detector.

The rate in (154) is strongly dependent on the velocity v of the neutralino with respect to the target nucleus. Therefore an annual modulation of the counting rate is in principle possible, due to the motion of the Earth around the Sun [55]. One can thus write

$$S(E_R, t) = S_0(E_R) + S_m(E_R) \cos\left[\omega(t - t_0)\right], \tag{156}$$

where $\omega = 2\pi/365\,\text{days}^{-1}$. Starting to count time in days from January 1st, the phase is $t_0 = 153$ days since the maximal signal occurs when the direction of motion of the Earth around the Sun and the Sun around the galactic center coincide maximally, which happens on June 2nd every year [55]. Similarly, the counting rate is expected to be the lowest December 2nd every year. Here $S_0(E_R)$ is the average differential scattering rate in Eq. (154) and $S_m(E_R)$ is the modulation amplitude of the rate. The relative size of $S_m(E_R)$ and $S_0(E_R)$ depends on the target and neutralino mass as well as on E_R. Typically $S_m(E_R)$ is of the order of a few percent of $S_0(E_R)$, but may approach 10 % for small m_χ (below, say, 50 GeV) and small E_R (below some 10 keV).

Since the basic couplings in the MSSM are between neutralinos and quarks, there are uncertainties related to the hadronic physics step which relates quarks and gluons with nucleons, as well the step from nucleons to nuclei. These uncertainties are substantial, and can plague all estimates of scattering rates by at least a factor of 2, maybe even by an order of magnitude [56, 57]. The largest rates, which as first shown in [46] could be already ruled out by contemporary experiments, are generally obtained for mixed neutralinos, i.e. with Z_g neither very near 0 nor very near 1, and for relatively light Higgs masses (since Higgs bosons mediate a scalar, spin-independent exchange interaction).

The experimental situation is becoming interesting as several direct detection experiments after many years of continuing sophistication are starting to probe interesting parts of the parameter space of the MSSM, given reasonable, central values of the astrophysical and nuclear physics parameters. Perhaps most striking is the 8 σ evidence for an annual modulation effect claimed to be seen in the NaI experiment DAMA/LIBRA [58] (see Sect. 8 where present data are summarized).

Many of the present day detectors are severely hampered by a large background of various types of ambient radioactivity or cosmic-ray induced activity (neutrons are a particularly severe problem since they may produce recoils which are very similar to the expected signal). A great improvement in sensitivity would be acquired if one could use directional information about the recoils. There are some very interesting developments also along this line, but a full-scale detector is yet to be built.

Direction-sensitive detectors would have an even bigger advantage over pure counting experiments if the dark matter velocity distribution is less trivial than the commonly assumed maxwellian.

6.1 Indirect Searches

Besides these possibilities of direct detection of supersymmetric dark matter (with even present indications of the existence of a signal [58]), one also has the possibility of indirect detection through neutralino annihilation in the galactic halo. This is becoming a promising method thanks to very powerful new detectors for cosmic gamma rays and neutrinos planned and under construction. Also, with time more has become known about the distribution of dark matter thanks to very ambitious N-body simulations [59–61], and a large amount of substructure has been found. This would enhance indirect detection, as it is proportional to the line-of-sight integral of the square of the number density.

There has been a balloon-borne detection experiment [62], with increased sensitivity to eventual positrons from neutralino annihilation, where an excess of positrons over that expected from ordinary sources was found. However, due to the rather poor quality of the data, it was not very conclusive.

In 2008, however, this changed completely when the data on the positron to electron ratio, rising with energy, from the satellite PAMELA was presented [63]. Somewhat later, FERMI-LAT reported a rise above the expectation from secondary production (by cosmic rays) also for the sum of positrons and electrons [64].

An unexpectedly high ratio of positrons over electrons was measured by PAMELA, in particular in the region between 10 and 100 GeV, where previously only weak indications of an excess had been seen [65–69]. This new precision measurement of the cosmic ray positron flux, which definitely disagrees with a standard background [70] has opened up a whole new field of speculations about the possible cause of this positron excess. Simultaneously, other data from PAMELA indicate that the antiproton flux is in agreement with standard expectations [71].

There are a variety of astrophysical models proposed for the needed extra primary component of positrons, mainly based on having nearby pulsars as a source [72, 73]. Although pulsars with the required properties like distance, age, and energy output are known to exist, it turns out not to be trivial to fit both FERMI and PAMELA data with these models (see, for example, [74, 75]). For this and other reasons, the dark matter interpretation, which already had been applied to the much more uncertain HEAT data [62] was one of the leading hypotheses.

It was clear from the outset that to fit the PAMELA positron data and FERMI's sum of positrons and electrons with a dark matter model a high mass is needed (on the order of 600 GeV to several TeV). However, since the local average dark matter density is well-known to be around 0.4 GeV/cm^3 [43], the number density decreases as $1/M_X$ and therefore the annihilation rate goes as $1/M_X^2$ with M_X the mass of the annihilating particle. This means that with $\langle \sigma v \rangle = 3 \cdot 10^{-26}$ cm^3/s, which is the standard value of the annihilation rate in the halo for thermally produced WIMPs (see Eq. (69)), the rate of positrons, even for a contrived model which annihilates to e^+e^- with unit branching ratio is much too small to explain the measured result.

To a good approximation, the local electron plus positron flux for such a model is given by, assuming an energy loss of $10^{-16}E^2$ GeVs^{-1} (with E in GeV) from

inverse Compton and synchrotron radiation,

$$E^3 \frac{d\phi}{dE} = 6 \cdot 10^{-4} E \left(\frac{1\,\text{TeV}}{M_X} \right)^2 \theta(M_X - E) B_{\text{tot}}\ \text{m}^{-2}\,\text{s}^{-1}\,\text{sr}^{-1}\,\text{GeV}^2, \qquad (157)$$

which means that the boost factor B_{tot} must be of about 200 for a 600 GeV particle, that may otherwise explain the positron excess. Similar boost factors seem to be generic, also for supersymmetric models giving e^+e^- through internal bremsstrahlung [76].

Such a boost factor can in principle be given by a large inhomogeneity in the DM distribution which has to be very local, since positrons and electrons of several hundred GeV do not diffuse very far before losing essentially all their energy. Although not excluded, this would seem to be extremely unlikely in most structure formation scenarios. Therefore, most models rely on the Sommerfeld enhancement factor (see Sect. 6.3). This means a non-negligible amount of fine-tuning of the mass spectrum, in particular also for the degeneracy between the lightest and next-to-lightest particle in the new sector. For a detailed discussion of the required model-building, see [77]. Similar fine-tuning is needed for the decaying dark matter scenario, where the decay rate has to be precisely tuned to give the measured flux. Since the antiproton ratio seems to be normal according to the PAMELA measurements [71], the final states should be mainly leptons (with perhaps intermediate light new particles decaying into leptons). For an interesting such model, which may in fact contain an almost standard axion, see [78].

It seems that at present it is possible to construct models of the Sommerfeld enhanced type [79] which do marginally not contradict present data. However, constraints are getting severe and the dark matter solution to the positron excess is currently not as fashionable as a couple of years ago. It will be interesting, however, to see the first results from the AMS-02 experiment [80] on the International Space Station, which should appear in the summer of 2012.

A very rare process in proton-proton collisions, antideuteron production, may be less rare in neutralino annihilation [81]. However, the fluxes are so small that the possibility of detection seems marginal even in the AMS-02 experiment, and probably a dedicated space probe has to be employed [82].

6.2 Indirect Detection by γ-Rays from the Halo

With the problem of a lack of clear signature of positrons and antiprotons, one would expect that the situation of gamma rays and neutrinos is similar, if they only arise from secondary decays in the annihilation process. For instance, the gamma ray spectrum arising from the fragmentation of fermion and gauge boson final states is quite featureless and gives the bulk of the gamma rays at low energy where the cosmic gamma ray background is severe. However, an advantage is the directional

information that photons carry in contrast to charged particles which random walk through the magnetic fields of the Galaxy [83].

For annihilation into quark-antiquark pairs, or W and Z bosons, the continuous energy spectrum one gets after fragmentation into SM particles can rather well and conveniently be parametrized as

$$dN_{\rm cont}(E_\gamma)/dE_\gamma = (0.42/m_\chi)e^{-8x}/(x^{1.5} + 0.00014), \tag{158}$$

where m_χ is the WIMP mass and $x = E_\gamma/m_\chi$. For more detailed spectra, one may for instance use standard particle physics codes like PYTHIA [84] (as is done in [2]). One should note that for τ leptons in the final state (158) is not a good approximation, as this gives a harder spectrum.

Gamma-Ray Lines

An early idea was to look for a spectral feature, a line, in the radiative annihilation process to a charm-anticharm bound state $\chi\chi \to (\bar{c}c)_{\rm bound} + \gamma$ [85]. However, as the experimental lower bound on the lightest neutralino became higher it was shown that form factor suppression rapidly makes this process unfeasible [86]. The surprising discovery was made that the loop-induced annihilations $\chi\chi \to \gamma\gamma$ [86–88] and $\chi\chi \to Z\gamma$ [89–91] do not suffer from any form factor suppression.

The rates of these processes are difficult to estimate because of uncertainties in the supersymmetric parameters, cross sections and halo density profile. However, in contrast to the other proposed detection methods they have the virtue of giving very distinct, "smoking gun" signals of monoenergetic photons with energy $E_\gamma = m_\chi$ (for $\chi\chi \to \gamma\gamma$) or $E_\gamma = m_\chi(1 - m_Z^2/4m_\chi^2)$ (for $\chi\chi \to Z\gamma$) emanating from annihilations in the halo.

The detection probability of a gamma-ray signal, either continuous or line, will of course depend sensitively on the density profile of the dark matter halo. To illustrate this point, let us consider the characteristic angular dependence of the γ-ray line intensity from neutralino annihilation $\chi\chi \to \gamma\gamma$ in the galactic halo. Annihilation of neutralinos in an isothermal halo with core radius a leads to a γ-ray flux along the line-of-sight (l.o.s.) direction $\hat{n}$ of

$$\frac{d\mathcal{F}}{d\Omega}(\hat{n}) \simeq (0.94 \times 10^{-13}{\rm cm}^{-2}{\rm s}^{-1}{\rm sr}^{-1}) \left(\frac{\sigma_{\gamma\gamma} v}{10^{-29}{\rm cm}^{-3}{\rm s}^{-1}}\right) \left(\frac{\rho_\chi}{0.3{\rm GeV\,cm}^{-3}}\right)^2 \times \left(\frac{100{\rm GeV}}{m_\chi}\right)^2 \left(\frac{R}{8.5{\rm kpc}}\right) J(\hat{n}) \tag{159}$$

where $\sigma_{\gamma\gamma} v$ is the annihilation rate, ρ_χ is the local neutralino halo density and R is the distance to the galactic center. The integral $J(\hat{n})$ is given by

$$J(\hat{n}) = \frac{1}{R\rho_\chi^2} \int_{\text{l.o.s.}} \rho^2(\ell) d\ell(\hat{n}), \tag{160}$$

and is evidently very sensitive to local density variations along the line-of-sight path of integration. In the case of a smooth halo, its value ranges from a few at high galactic latitudes to several thousand for a small angle average towards the galactic center in the Navarro, Frenck and White (NFW) [105] model [92].

Since the neutralino velocities in the halo are of the order of 10^{-3} of the velocity of light, the annihilation can be considered to be at rest. The resulting gamma ray spectrum is a line at $E_\gamma = m_\chi$ of relative linewidth 10^{-3} (coming from the Doppler effect caused by the motion of the WIMP) which in favourable cases will stand out against background.

Detection of a γ-rate line signal would need a detector with very good energy resolution, like 1 % or better. This may be achieved by FERMI (although only upper limits have been presented so far [93]). However, the Russian satellite GAMMA-400 [94] seems to have very promising characteristics for this type of dark matter search, when it is launched by the end of this decade. This could be a very interesting new instrument in the search for γ-ray lines from annihilation (or decay) of dark matter.

The calculation of the $\chi\chi \to \gamma\gamma$ cross section is technically quite involved with a large number of loop diagrams contributing. A full calculation in the MSSM was performed in [95, 96]. Since the different contributions all have to be added coherently, there may be cancellations or enhancements, depending on the supersymmetric parameters. The process $\chi\chi \to Z\gamma$ is treated analogously and has a similar rate [89–91].

An important contribution, especially for neutralinos that contain a fair fraction of a higgsino component, is from virtual W^+W^- intermediate states. This is true both for the $\gamma\gamma$ and $Z\gamma$ final state for very massive neutralinos [89–91]. In fact, thanks to the effects of coannihilations [11], neutralinos as heavy as several TeV are allowed without giving a too large Ω. These extremely heavy dark matter candidates (which, however, would require quite a degree of finetuning in most supersymmetric models) are predominantly higgsinos and have a remarkably large branching ratio into the loop-induced $\gamma\gamma$ and $Z\gamma$ final states (the sum of these can be as large as 30 %). If there would exist such heavy, stable neutralinos, the gamma ray line annihilation process may be the only one which could reveal their existence in the foreseeable future (since not even LHC would be sensitive to supersymmetry if the lightest supersymmetric particle weighs several TeV). In fact the high branching ratio for higgsino annihilation to 2γ was the reason that Hisano et al. [97] took a closer look at the process and discovered the effect of Sommerfeld enhancement.

Internal Bremsstrahlung

The $\gamma\gamma$ process appears in a closed loop meaning that it is suppressed by powers of the electromagnetic coupling constant. An amusing effect appears, however, for Majorana fermions at even lower order. It was early realized that there could be important spectral features [98], and recently it has been shown that internal bremsstrahlung

(IB) from produced charged particles in the annihilations could yield a detectable "bump" near the highest energy for heavy gauginos or Higgsinos annihilating into W boson pairs, such as expected in split supersymmetry models [99]. In [100], it was furthermore pointed out that IB often can be estimated by simple, universal formulas and often gives rise to a very prominent step in the spectrum at photon energies of $E_\gamma = m_\chi$ (such as in lightest Kaluza-Klein particle (LKP) models [101] (see Sect. 7.8)). The IB process was thoroughly treated in [102], and here we summarize the main results.

In [98] it was shown that the radiative process $\chi^0\chi^0 \to f\bar{f}\gamma$ may circumvent the chiral suppression, i.e., the annihilation rate being proportional to m_f^2. This is normally what one would get for annihilation into a fermion pair from an S-wave initial state [103], as is the case in lowest order for non-relativistic dark matter Majorana particles in the Galactic halo (see also [104]). Since this enhancement mechanism is most prominent in cases where the neutralino is close to degenerate with charged sleptons, it is of special importance in the so-called stau coannihilation region.

A fermion final state containing an additional photon, $f\bar{f}\gamma$, is thus not subject to a helicity suppression. The full analytical expressions are lengthy, but simplify in the limit of $m_f \to 0$. Then one finds

$$\frac{\mathrm{d}N_{f^+f^-}}{\mathrm{d}x} = \lambda \times \left\{ \frac{4x}{\mu(\mu-2x)} - \frac{2x}{(\mu-x)^2} - \frac{\mu(\mu-2x)}{(\mu-x)^3} \log\frac{\mu}{\mu-2x} \right\}, \quad (161)$$

with

$$\lambda = (1-x)\alpha_{\mathrm{em}} Q_f^2 \frac{|\tilde{g}_R|^4 + |\tilde{g}_L|^4}{64\pi^2} \left(m_\chi^2 \langle\sigma v\rangle_{\chi\chi\to f\bar{f}} \right)^{-1}.$$

where $\mu \equiv m^2_{\tilde{f}_R}/m^2_\chi + 1 = m^2_{\tilde{f}_L}/m^2_\chi + 1$ and $\tilde{g}_R P_L$ ($\tilde{g}_L P_R$) is the coupling between neutralino, fermion and right-handed (left-handed) sfermion. This confirmed the result found in [98] for photino annihilation. Note the large enhancement factor m_χ^2/m_f^2 due to the lifted helicity suppression (from $\langle\sigma v\rangle_{\chi\chi\to f\bar{f}} \propto m_f^2 m_\chi^{-4}$), and another large enhancement that appears at high photon energies for sfermions degenerate with the neutralino.

Internal bremsstrahlung from the various possible final states of neutralino annihilations is included in DarkSUSY [2]. The total γ-ray spectrum is given by

$$\frac{dN^{\gamma,\mathrm{tot}}}{dx} = \sum_f B_f \left(\frac{dN_f^{\gamma,\mathrm{sec}}}{dx} + \frac{dN_f^{\gamma,\mathrm{IB}}}{dx} + \frac{dN_f^{\gamma,\mathrm{line}}}{dx} \right), \quad (162)$$

where B_f denotes the branching ratio into the annihilation channel f. The last term in the above equation gives the contribution from the direct annihilation into photons, $\gamma\gamma$ or $Z\gamma$, which result in a sharp line feature [89–91, 95, 96]. The first term is the contribution from secondary photons from the fragmentation of the fermion pair.

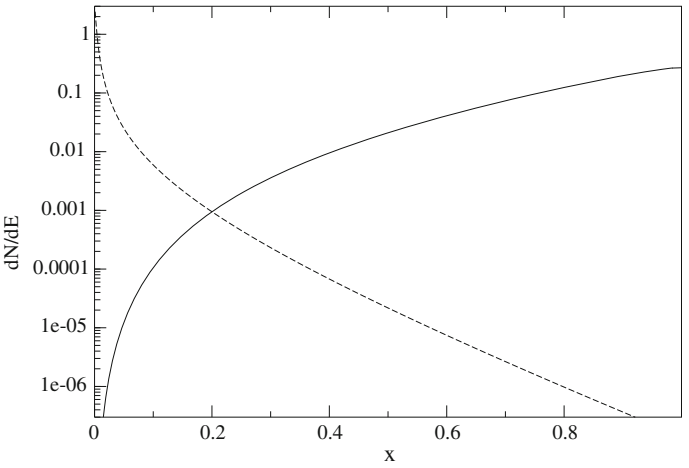

Fig. 6 The distribution of γ-rays from the internal bremsstrahlung process $\chi^0\chi^0 \to f\bar{f}\gamma$ is shown as the *solid line*, and compared to the standard case, (158) (*dashed line*). As can be seen, the internal bremsstrahlung process gives a very hard spectrum, which may counteract the fact that radiation of a photon always is suppressed by a factor of $\sim\alpha_{em}/\pi$

This "standard" part of the total γ-ray yield from dark matter annihilations shows a feature-less spectrum with a rather soft cutoff at $E_\gamma = m_\chi$.

In Fig. 6 an example of the energy distribution of photons given by (161) is shown.

Density Profile and γ-Ray Detection

To compute $J(\hat{n})$ in (160), a model of the dark matter halo has to be chosen. The universal halo profile found in simulations by Navarro, Frenk and White (NFW) [105] has a rather significant enhancement $\propto 1/r$ near the halo centre,

$$\rho_{\rm NFW} = \frac{c}{r(a+r)}, \tag{163}$$

where c is a concentration parameter and a a typical length scale for the halo. In fact, more detailed later simulations have given a slightly different shape, the so-called Einasto profile,

$$\rho_{\rm Einasto} = \rho_s e^{-\frac{2}{\alpha}\left[\left(\frac{r}{a}\right)^\alpha - 1\right]}, \tag{164}$$

with $\alpha \sim 0.17$ for the Milky Way. Except near $r = 0$, this profile is actually quite similar to the NFW profile, and it has slightly higher density outside the very center. The local dark matter density near the solar system can be quite well determined [43] and is $\rho_0 \simeq 0.4$ GeV/cm^3. If these forms of the density can be applied to the Milky Way, this would lead to a much enhanced annihilation rate towards the galactic centre,

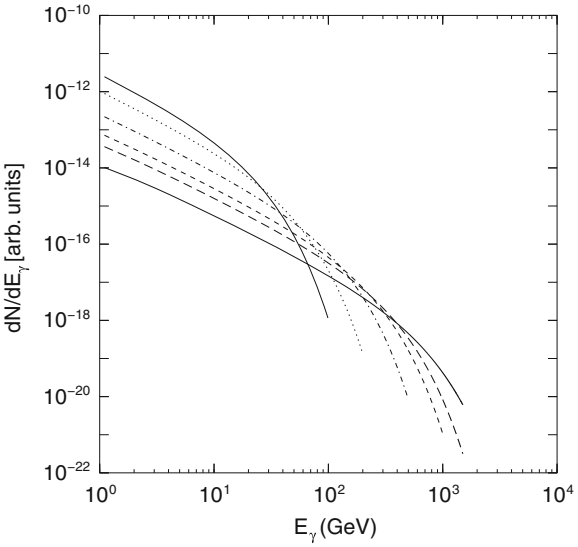

Fig. 7 The energy distribution of γ-rays from WIMP dark matter annihilation into a $b\bar{b}$ pair, for a dark matter particle mass of 100, 200, 500, 1000, 1500, and 3000 GeV, respectively. One can see that the bulk of the signal is at low energies. (Here the line signals from $\gamma\gamma$ and $Z\gamma$ have not been included)

and also to a very characteristic angular dependence of the line signal. This would be very beneficial when discriminating against the extragalactic γ ray background, and Imaging Air Cherenkov Telescope Arrays (IACTAs) are be eminently suited to look for these signals since they have an angular acceptance which is well matched to the angular size of the Galactic central region where a cusp is likely to be. Both H.E.S.S. [106], MAGIC [107] and Whipple [108] have searched for a signal at the galactic center or in other dark matter concentrations, but are still a couple of orders of magnitude above the flux which would correspond to the canonical WIMP flux, Eq. (69). Maybe with the planned CTA project [109] one may get to the interesting region of parameter space for supersymmetric or other WIMPs.

Also the energy threshold of present-day IACTAs is too high (of the order of 50 GeV or higher) to be very useful for WIMPs of 100 GeV or lighter. There have been discussions about a high-altitude detector with lower threshold, perhaps as low as 5 GeV [110], which would be very beneficial for dark matter detection, see Fig. 7.

Space-borne gamma-ray detectors, like the FERMI satellite have a much smaller area (on the order of 1 m^2 instead of $10^4 - 10^5$ m^2 for IACTAs), but a correspondingly larger angular acceptance so that the integrated sensitivity is in fact similar. This is at least true if the Galactic center does not have a very large dark matter density enhancement which would favour IACTAs. The total rate expected in FERMI can be computed with much less uncertainty because of the angular integration [111]. Directional information is obtained and can be used to discriminate against the diffuse

extragalactic background. A line signal can be searched for with high precision, since the energy resolution of FERMI is at the few percent level.

Indirect Detection Through Neutrinos

The density of neutralinos in the halo is not large enough to give a measurable flux of secondary neutrinos, unless the dark matter halo is very clumpy [112–114]. In particular, the central Galactic black hole may have interacted with the dissipationless dark matter of the halo so that a spike of very high dark matter density may exist right at the Galactic centre [115]. However, the existence of these different forms of density enhancements are very uncertain and depend extremely sensitively on presently completely unknown aspects of the formation history of the Milky Way.

More model-independent predictions (where essentially only the relatively well-determined local halo dark matter density is of importance) can be made for neutrinos from the centre of the Sun or Earth, where neutralinos may have been gravitationally trapped and therefore their density enhanced. As they annihilate, many of the possible final states (in particular, $\tau^+\tau^-$ lepton pairs, heavy quark–antiquark pairs and, if kinematically allowed, $W^\pm H^\mp$, $Z^0 H_i^0$, W^+W^- or Z^0Z^0 pairs) give after decays and perhaps hadronization energetic neutrinos which will propagate out from the interior of the Sun or Earth. (For neutrinos from the Sun, energy loss of the hadrons in the solar medium and the energy loss of neutrinos have to be considered [116, 117]). In particular, the muon neutrinos are useful for indirect detection of neutralino annihilation processes, since muons have a quite long range in a suitable detector medium like ice or water. Therefore they can be detected through their Cherenkov radiation after having been produced at or near the detector, through the action of a charged current weak interaction $\nu_\mu + A \to \mu + X$.

Detection of neutralino annihilation into neutrinos is one of the most promising indirect detection methods, and will be subject to extensive experimental investigations in view of the new neutrino telescopes (IceCube, ANTARES, KM3NET) planned or under construction [118]. The advantage shared with gamma rays is that neutrinos keep their original direction. A high-energy neutrino signal in the direction of the centre of the Sun or Earth is therefore an excellent experimental signature which may stand up against the background of neutrinos generated by cosmic-ray interactions in the Earth's atmosphere.

The differential neutrino flux from neutralino annihilation is

$$\frac{dN_\nu}{dE_\nu} = \frac{\Gamma_A}{4\pi D^2} \sum_f B_\chi^f \frac{dN_\nu^f}{dE_\nu} \tag{165}$$

where Γ_A is the annihilation rate, D is the distance of the detector from the source (the central region of the Earth or the Sun), f is the neutralino pair annihilation final states, and B_χ^f are the branching ratios into the final state f. dN_ν^f/dE_ν are the energy distributions of neutrinos generated by the final state f. Detailed calculations

of these spectra can be made using Monte Carlo methods [117, 119–121]. Effects of neutrino oscillations have also been included [122].

The neutrino-induced muon flux may be detected in a neutrino telescope by measuring the muons that come from the direction of the centre of the Sun or Earth. For a shallow detector, this usually has to be done in the case of the Sun by looking (as always the case for the Earth) at upward-going muons, since there is a huge background of downward-going muons created by cosmic-ray interactions in the atmosphere. The flux of muons at the detector is given by

$$\frac{dN_\mu}{dE_\mu} = N_A \int_{E_\mu^{\rm th}}^{\infty} dE_\nu \int_0^{\infty} d\lambda \int_{E_\mu}^{E_\nu} dE'_\mu \; P(E_\mu, E'_\mu; \lambda) \; \frac{d\sigma_\nu(E_\nu, E'_\mu)}{dE'_\mu} \; \frac{dN_\nu}{dE_\nu}, \tag{166}$$

where λ is the muon range in the medium (ice or water for the large detectors in the ocean or at the South Pole, or rock which surrounds the smaller underground detectors), $d\sigma_\nu(E_\nu, E'_\mu)/dE'_\mu$ is the weak interaction cross section for production of a muon of energy E'_μ from a parent neutrino of energy E_ν, and $P(E_\mu, E'_\mu; \lambda)$ is the probability for a muon of initial energy E'_μ to have a final energy E_μ after passing a path-length λ inside the detector medium. $E_\mu^{\rm th}$ is the detector threshold energy, which for "small" neutrino telescopes like Baksan, MACRO and Super-Kamiokande is around 1 GeV. Large area neutrino telescopes in the ocean or in Antarctic ice typically have thresholds of the order of tens of GeV, which makes them sensitive mainly to heavy neutralinos (above 100 GeV) [123]. Convenient approximation formulas relating the observable muon flux to the neutrino flux at a given energy exist [124].

The integrand in (166) is weighted towards high neutrino energies, both because the cross section σ_ν rises approximately linearly with energy and because the average muon energy, and therefore the range λ, also grow approximately linearly with E_ν. Therefore, final states which give a hard neutrino spectrum (such as heavy quarks, τ leptons and W or Z bosons) are usually more important than the soft spectrum arising from light quarks and gluons.

The rate of change of the number of neutralinos N_χ in the Sun or Earth is governed by the equation

$$\dot{N}_\chi = C_C - C_A N_\chi^2 \tag{167}$$

where C_C is the capture rate and C_A is related to the annihilation rate Γ_A, $\Gamma_A = C_A N_\chi^2$. This has the solution

$$\Gamma_A = \frac{C_C}{2} \tanh^2\left(\frac{t}{\tau}\right), \tag{168}$$

where the equilibration time scale $\tau = 1/\sqrt{C_C C_A}$. In most cases for the Sun, and in the cases of observable fluxes for the Earth, τ is much smaller than a few billion years, and therefore equilibrium is often a good approximation ($\dot{N}_\chi = 0$ in (167)).

This means that it is the capture rate which is the important quantity that determines the neutrino flux.

The capture rate induced by scalar (spin-independent) interactions between the neutralinos and the nuclei in the interior of the Earth or Sun is the most difficult one to compute, since it depends sensitively on Higgs mass, form factors, and other poorly known quantities. However, this spin-independent capture rate calculation is the same as for direct detection. Therefore, there is a strong correlation between the neutrino flux expected from the Earth (which is mainly composed of spin-less nuclei) and the signal predicted in direct detection experiments [123, 125]. It seems that even the large (kilometer-scale) neutrino telescopes planned will not be competitive with the next generation of direct detection experiments when it comes to detecting neutralino dark matter, searching for annihilations from the Earth. However, the situation concerning the Sun is more favourable. Due to the low counting rates for the spin-dependent interactions in terrestrial detectors, high-energy neutrinos from the Sun constitute a competitive and complementary neutralino dark matter search. Of course, even if a neutralino is found through direct detection, it will be extremely important to confirm its identity and investigate its properties through indirect detection. In particular, the mass can be determined with reasonable accuracy by looking at the angular distribution of the detected muons [126, 127].

For the Sun, dominated by hydrogen, the axial (spin-dependent) cross section is important and relatively easy to compute. A good approximation is given by [32]

$$\frac{C_{\odot}^{\mathrm{sd}}}{(1.3\cdot 10^{23}\,\mathrm{s}^{-1})} = \left(\frac{\rho_{\chi}}{0.3\ \mathrm{GeV\,cm}^{-3}}\right)\left(\frac{100\,\mathrm{GeV}}{m_{\chi}}\right)\left(\frac{\sigma_{p\chi}^{\mathrm{sd}}}{10^{-40}\ \mathrm{cm}^{2}}\right)\left(\frac{270\ \mathrm{km/s}}{\bar{v}}\right), \tag{169}$$

where $\sigma_{p\chi}^{\mathrm{sd}}$ is the cross section for neutralino-proton elastic scattering via the axial-vector interaction, $\bar{v}$ is the dark-matter velocity dispersion, and ρ_{χ} is the local dark matter density. The capture rate in the Earth is dominated by scalar interactions, where there may be kinematic and other enhancements, in particular if the mass of the neutralino almost matches one of the heavy elements in the Earth. For this case, a more detailed analysis is called for, but convenient approximations are available [32]. In fact, also for the Sun the spin-dependent contribution can be important, in particular iron may contribute non-negligibly.

A neutrino telescope of area around 1 km^2, which is roughly the size of IceCube, has discovery potential for a range of supersymmetric models, which cannot easily be probed using other methods, see [123].

6.3 Antimatter Detection of Dark Matter

Antimatter does not seem to be present in large quantities in the universe, as can be inferred from the absence of γ-ray radiation that would have been created in large amounts if astrophysical anti-objects would annihilate on their matter counterparts

(this would also cause deviations from the pure black-body form of the cosmic microwave background, something which is very severely limited by WMAP data and will be further probed by the Planck satellite). In fact, both the analysis of primordial nucleosynthesis and the CMB, give a non-zero number around 10^{-10} for the baryon-antibaryon asymmetry, which means that matter dominated over antimatter already in the very early universe. On the other hand, dark matter annihilation in almost all models occurs from a matter-antimatter symmetric initial state and thus equal amounts of matter and antimatter is created. This leads to an interesting possible new primary source of positrons and antiprotons (i.e. the stable anti-particles of protons) in the cosmic rays of dark matter halos, including the one where the Milky Way resides. (There is always a small amount of antimatter produced as secondary particles in collisions with galactic gas and dust by ordinary cosmic rays, of course.) As discussed extensively at conferences in 2009 (see, e.g., [128]) this was an extremely hot topic then. This was due to the PAMELA and FERMI collaborations just having discovered an anomalously high ratio of positrons over electrons up to 100 GeV [63], and sum of positrons and electrons up to 1 TeV [64], respectively. During the last two years, this anomaly, although possible to explain by dark matter annihilation, needs such large boost factors (e.g., from Sommerfeld enhancement to be discussed below), and somewhat contrived, leptophilic models, that these models are feeling severe pressure from other detection methods, e.g, γ-rays from the central parts of the Galaxy [129]. Alternative astrophysical explanations are on the other hand possible with quite standard assumptions. One cannot say that the dark matter explanation is yet completely ruled out, but it is in strong tension from other measurements.

Returning to more standard WIMP models, there have recently been improvements in the computations of the annihilation rate at low velocity as is the case in galaxies, where $v/c \sim 10^{-3}$. An amusing effect is caused due to the suppression of the ${}^3S_1$ for an initial state of two Majorana spinors (such as neutralinos) at zero velocity, due to the requirement of Fermi statistics. Namely, one cannot have two identical fermions in the same spin state. This means that annihilation only occurs from the pseudoscalar ${}^1S_0$ state where one of the particles has spin up, the other spin down. This causes for instance the annihilation amplitude into a light fermion-antifermion pair, like e^+e^-, to be suppressed by an explicit helicity factor of the fermion mass (as in the limit of zero mass, the vertices are helicity-preserving, and to cause a spin flip a mass term is needed). Direct annihilation into e^+e^- was thus thought to be very subdominant. However, it was realized [130, 131] (building on an old idea [132]), that a spin-flip by one of the Majorana fermions caused by emitting a photon could first of all relieve the helicity suppression of the process to a mere α/π ordinary radiative factor. And, in addition, the spectral shape of the emitted photon is very favorable for detection, causing a shoulder which peaks close to the dark matter particle mass. In particular, for heavy (TeV-scale) WIMPs this could be quite important, and using the radiative peak would help extracting the signal over background [133]. Recently, these radiative processes have been generalized also to emission of other gauge bosons, and have been shown to be quite important generally [134, 135].

The Sommerfeld Effect

The possibility of an enhanced annihilation rate due to DM halo substructure has been realized for a long time [112–114]. However, it seems hard to produce a boost factor of the order of a few hundred to a thousand in the solar neighborhood, as would be needed to explain the PAMELA and FERMI excesses. This is because substructure survives in numerical simulations mostly in the outer portions of the halo, due to tidal stripping in the inner part.

Another potentially very important effect, Sommerfeld enhancement, which may explain the large boost had been found a few years earlier. This effect, was computed for electromagnetism by Arnold Sommerfeld many years ago [136], but it was rediscovered [77, 97] in the quantum field theory of very heavy dark matter particles in the limit when the gauge particles, γ, Z^0 and $W^{\pm}$ are essentially massless, or at least have a Compton wavelength that is sufficiently large compared to the would-be bound state caused by the attractive gauge forces. (Of course, a bound state is never really formed due to the fast time scale of annihilation.)

In the quantum mechanical calculation of electron scattering and e^+e^- annihilation, Sommerfeld enhancement is caused by the distortion of the plane wave describing the relative motion of the annihilating particle pair through the near formation of a bound state caused by photon exchange. In the so-called ladder approximation for QED (where one sums only certain types of Feynman diagrams), one obtains this Sommerfeld effect, and the square of the wave function at the origin in relative coordinates $r_1 - r_2$, which enters into the probability for the short-distance process of annihilation, is increased by the factor [77]

$$S = \frac{|\Psi(0)|^2}{|\Psi_{(0)}(0)|^2} = \frac{\left(\frac{\pi\alpha}{\beta}\right)}{1 - e^{-\left(\frac{\pi\alpha}{\beta}\right)}}, \tag{170}$$

with α the fine-structure constant, and β the relative velocity. This can be expanded to $S_{QED} = \pi\alpha/\beta$ for small relative velocities. In the Milky Way halo, velocities are typically $\beta \sim 10^{-3}$, so this limit is certainly relevant. For smaller galaxies or DM substructure, velocities (as measured by velocity dispersions) are even smaller. Of course, there is no direct photon exchange between DM particles, since they are electrically neutral. However, if there are charged states nearby in mass, the neutral pair may momentarily, before annihilation, transform into a charged pair which in turn may exchange a photon between then. These are the basic processes that have to be summed to all orders in the ladder approximation, and which lead to Sommerfeld enhancement (see Fig. 8).

One could of course also have a Yukawa-like particle (i.e., spinless) of mass m_Y, mediating a weak attractive force with coupling constant α_Y between DM particles of mass m_χ. The small velocity limit of the enhancement then becomes

$$S_Y \propto \frac{\alpha_Y m_\chi}{m_Y}. \tag{171}$$

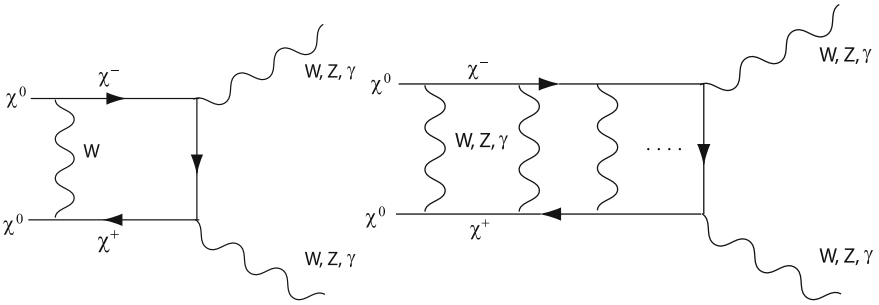

Fig. 8 Diagrams illustrating the field-theoretical reason for the Sommerfeld enhancement. The figure is drawn for a supersymmetric neutralino (which is the case where the effect was first found in dark matter physics [97]), but similar diagrams apply for any dark matter candidate which first of all is heavy compared to the exchanged particle in the t-channel (i.e. in the "ladder"), and where there is a near degeneracy between the neutral state being the dark matter and the virtual states (in this case charged particles, charginos). On the *left* is shown the lowest order contribution, which gets very important for large masses, and which is further enhanced by the ladder diagrams of the type shown on the *right*. The net result could be an "explosive annihilation", to quote [97]

In some cases, depending on the detailed nature of the mediating particles, the enhancement factor S can indeed be as high as several hundred to a few thousand, depending on the exact parameters. The effect is generally strongly velocity-dependent, depending on velocity as $1/\beta$ or even (near resonance) $1/\beta^2$ but in the Yukawa case the $1/\beta$ scaling is valid only for $\beta > m_Y/m_\chi$. At smaller velocities and outside resonances, the effect saturates at m_Y/m_χ [137].

Important bounds come from γ-rays, but also from the non-observation of energy distortions in the cosmic microwave background. It may still be possible to (marginally) fit the PAMELA/FERMI excess, if one takes astrophysical uncertainties into account [79].

It should be noted that the Sommerfeld effect has a solid theoretical backing and is important, if the mass and coupling parameters are in the right range. For supersymmetric models, however, it occurs only for very heavy neutralinos (generally higgsinos) and the phenomenology has only been partly investigated [138].

To conclude this section on detection methods of WIMPs, we have seen that supersymmetric particles, which are the theoretically most plausible WIMPs have many interesting features which may make them detectable in the not too distant future. Supersymmetry, in particular MSSM, invented already in the 1970s, and obtained as a phenomenological manifestation of the most realistic string theories, has since the early 1980s, when the CDM paradigm first won universal acclaim, been the prime template for a WIMP [103, 139].

Even in the MSSM, however, there are in principle more than a hundred free parameters, meaning that for practical reasons the templates, for instance used at the LHC experiments, are drastically simplified versions, like constrained MSSM (CMSSM) or the even more constrained minimal super gravity (mSUGRA), which do not, in contrast to the full MSSM, correspond very well to more recent thinking

about supersymmetry breaking [140]. This has to be kept in mind when discussing the impressive LHC limits. Even in still simplified versions, like the 19 to 24-parameter "phenomenological MSSM", pMSSM [141, 142], the bounds on particle masses given, e.g., by fulfilling the WMAP relic density, are not very constraining at the moment [143]. Of course, the outlook for the MSSM would be much bleaker if a light Higgs (with mass below roughly 130 GeV) were not to be established by the end of the 7 TeV run, in 2012.

With the freely available [144] DarkSUSY package [2], one can compute in detail the relic density, not only for supersymmetric models, but since the package has a modular design, one can insert any favourite model one has for WIMP-like dark matter. Of course, DarkSUSY is mostly used for the supersymmetric case, and it has been originally set up for a general pMSSM model, with large freedom in the choice of parameters.

7 Particular Dark Matter Candidates

7.1 WIMP Models

The particle physics connection is particularly striking in the WIMP scenario, namely that for typical gauge couplings and a mass at the weak interaction scale of a few hundred GeV, consistent with the relic density computed using standard big bang thermodynamics, as we saw in Sect. 3. This is rather well tested by the calculation of the abundances of hydrogen and helium in the early universe, through big bang nucleosynthesis. The calculation of these abundances turns out to be in amazingly good agreement with the measured ones. Using the same early universe thermodynamics and solving the Boltzmann equation for hypothetical dark matter particles of mass m_χ, we found that the annihilation rate $\langle \sigma v \rangle$ needed to explain $\Omega_\chi h^2 \sim 0.11$ (as determined by WMAP), naturally appears for ordinary gauge couplings and a mass between around 20 GeV to a few TeV—a WIMP.

Although this is not a completely convincing argument for WIMP dark matter—it may perhaps be a coincidence—it nevertheless gives WIMP candidates a flavour of naturalness. For non-WIMP candidates there is, on the other hand, usually a fine tuning involved, or use of non-standard cosmology, to obtain the correct relic density. Even limiting oneself to WIMP models for dark matter, the literature is extensive, and among some recent developments, which cannot be discussed in this review in any detail, can be mentioned:

7.2 Dark Stars

Since cosmological structure in WIMP models occurs hierarchically, starting from scales as small as 10^{-12}–$10^{-6} M_{\odot}$ [145], the idea has been put forward that the earliest dense, small structures created by dark matter may play a role in star formation and if the dark matter particles annihilate within the stars, unusual stellar evolution may result [146–149].

7.3 Inelastic Dark Matter

These are dark matter candidates which may be excited to a state with slightly higher mass and therefore cause a higher than usual direct detection rate [150–155], and also relieve the tension between the different direct detection experiments.

7.4 Dynamical Dark Matter

As it is not obvious that there is only one type of particle making up the dark matter (neutrinos should, for example contribute up to a few percent), an extreme solution could be to have a very large number, with different spins, masses, etc. [156].

7.5 Leptophilic Dark Matter

As we have mentioned, there was an almost explosion of suggestions of this kind of models in 2009, when the dark matter interpretation of the anomalous positron ratio measured by PAMELA [63] and FERMI [64] was proposed to be explained by dark matter annihilation. Leptophilic means that these dark matter particles annihilate mainly to leptons, for example by proceeding through axion-like particles below the pion mass [157–163]. Although the original motivation for these models has become somewhat weaker, the concept has established itself in the dark matter community.

7.6 Supersymmetric Models Beyond the MSSM

Of course, even though the minimal supersymmetric version of the standard model, the MSSM, has more than 100 free parameters, models having, e.g., motivation from new scenarios of supersymmetry breaking, are of course logically possible. These "beyond the MSSM" or BMSSM models [164–167] may among other things give a higher Higgs mass than the limit of 130 GeV given by minimal SUSY models. In the summer of 2011, this was perhaps a favoured scenario, as the first indications

of the Higgs mass was around 140 GeV. However, with more data, the preferred range (not yet significant enough by the end of 2011 to be called a discovery) is now 124–126 GeV which is more easily encompassed in the MSSM.

7.7 Asymmetric Dark Matter

This is a class of dark matter models which may also explain the baryon (or lepton) asymmetry of the universe [168–173]. This generally only works for masses around or below 10 GeV, and this mass range has been in focus recently due to a (possible) signal in direct detection experiments [58, 174–176], and maybe also in γ-ray detection in the direction near the Galactic centre [177]. However, it remains to see whether these indications will stand the test of time. A similar model is "emergent dark matter". This is a recent version of asymmetric DM with larger possible parameter range, such as a DM mass up to 100 GeV [168–173].

7.8 Kaluza-Klein Models

A candidate for dark matter, the so-called LKP (for lightest Kaluza-Klein particle) has been identified. This appears in theories with extra dimensions, and has a rich phenomenology which we will not enter into here (for a review, see [178]). The main difference with supersymmetry is that the dark matter candidate has spin-1, and can give the correct relic density for a mass in the range from 600 GeV to 1 TeV.

7.9 Inert Higgs Doublet

Interesting are also versions of the Standard Model with an enlarged Higgs sector. If there would be, for instance, a second Higgs doublet which does not couple directly to Standard Model particles (an "inert doublet"), there turns out to be a stable spin-0 state which then would be the dark matter particle (see [179], and references therein).

7.10 Non-WIMP Models

WIMPs are arguably the leading candidates for Dark Matter, due to lack of fine-tuning to get correct relic density. In most models, the annihilation cross section which sets the relic density also implies observable rates in various DM detection experiments.

A word of caution is in place here, however. There are many non-WIMP models that also have good particle physics motivation, and may be detectable, like: axions,

gravitinos, superWIMPS, non-thermal dark matter, decaying dark matter, sterile Neutrinos, Q-balls... The literature is extensive, but a good summary of both WIMP and non-WIMP models has recently appeared, namely, a 700-page book giving details of most dark matter scenarios [180].

7.11 The Axion

Another, rather different candidate [181] for dark matter is provided by the axion, a hypothetical light boson which was introduced for theoretical reasons to explain the absence of CP violation in the strong interactions (as far as we know, CP violations only take place in the weak interactions). It turns out that for a mass range between 10^{-6} and 10^{-3} eV, the axion could give a sizable contribution to Ω_M. It couples very weakly to ordinary matter, but it may be converted into a photon in a cavity containing a strong magnetic field (the basic coupling is to two photons, but here the magnetic field takes the role of one photon). Experiments in the USA and Japan are currently probing parts of the interesting mass region. A section about the axion should always be inserted when describing dark matter candidates, since the axion has, as has the lightest supersymmetric particle, a good particle physics motivation for its existence.

8 Dark Matter Detection: Status

As we have mentioned, there are basically three different, and complementary methods for detecting WIMPs. First, the dark matter particle may be directly produced at accelerators, in particular at the LHC, which today is the only high-energy accelerator running (although data from Fermilab's Tevatron collider will still be analyzed and may give surprises in the coming year or so). Of course, it is not clear that the particle will be kinematically allowed, and even if it is produced, one will not know that the lifetime is of the required cosmological order of magnitude. Anyway, detecting a candidate and determining its mass would be a great gain when combining with the other two search methods of dark matter, namely direct and indirect detection. In particular, direct detection experiments have seen an impressive gain of sensitivity during the last few years. The idea is to register rare events giving a combination of scintillation, ionization and nuclear recoil signals in chunks of matter shielded from cosmic rays in underground sites.

In indirect detection, one rather registers products of dark matter annihilation from regions in the surrounding universe with a high dark matter density like the galactic centre, dwarf spheroidal galaxies, or the interior of the Earth or the Sun. An interesting feature of indirect detection is that the expression for the local annihilation rate of a pair of DM particles χ (here assumed, like in supersymmetry, to be self-charge-conjugate, of relative velocity v_{rel}

$$\Gamma_{ann} \propto n_\chi^2 \sigma_{ann}(v_{rel}) v_{rel} \tag{172}$$

is the dependence on the square of the number density. Also, the cross section may depend in non-trivial ways on the relative velocity. In particular, for low velocities the rate may be much higher than at high velocity, for models containing an attractive force between the annihilating particles. This is in particular true for models with so-called Sommerfeld enhancement [97], a resonant enhancement by in some cases orders of magnitude (see Sect. 6.3). This means that dwarf galaxies (dark matter subhalos) may be particularly interesting objects to study, as they are completely dark matter dominated with low rate of cosmic-ray induced γ-rays, and their low mass means a relatively low velocity dispersion, meaning higher possible rates if Sommerfeld enhancement is active.

So far, indirect methods have not been as competitive as direct detection, but recently the FERMI collaboration has started to probe the interesting WIMP region by stacking data from several dwarf galaxies [182].

For non-WIMP dark matter, like sterile neutrinos (warm DM), the production rate in the early universe generally has to be tuned to give the observed relic density, but phenomenologically warm DM is possible, and according to some analyses even preferred in cosmological data [183]. However, the significance is weak and may be influenced by statistical bias [184]. Ordinary, active neutrinos have too small mass to contribute significantly to the dark matter density, although in the extreme case may contribute a couple of percent to the critical density today.

A very interesting effect for direct detection of dark matter WIMPs in terrestrial detectors comes about due to the motion of the solar system in the Galaxy [55]. This circular speed is around 200 km/s, and the direction of the "wind" of dark matter particles varies in between seasons. This is due to the detector following the Earth's motion around the Sun and sometimes (actually around June 2) having "headwind" of WIMPs and sometimes (December 2) "tailwind". As the cross section between a WIMP and the detector target depends strongly on their relative velocity, this causes a few percent annual modulation of the detection rate, something that is a very distinct signature. The DAMA/LIBRA experiment in the Gran Sasso tunnel [58] has in fact seen an annual modulation, which has a statistical significance of more than 8 standard deviations. However, since no other experiment has found the same effect (see Table 1), the effect can still not be taken as an established detection of dark matter. There have been attempts to interpret the DAMA signal as possibly being due to a neutralino of the MSSM [185, 186]. It seems premature, however, to draw strong conclusions from this experiment alone. Besides some cloudy experimental issues, the implied scattering rate seems somewhat too high for the MSSM or any other canonical WIMP, given the strong Higgs mass bounds from LEP and LHC unless one stretches the astrophysical and nuclear physics quantities. Also, it is disturbing that neither XENON100 nor CDMS-II see an effect despite their nominally higher sensitivity. Clearly, even more sensitive experiments, preferably also using NaI, seem to be needed to settle this issue. An interesting idea, DM-Ice [187], uses the IceCube site to deploy crystals of NaI with ice as a very calm surrounding medium. If an annual modulation could be measured also there one could check whether it has the

Table 1 Some of the recent experimental claims for possible dark matter detection, and a comment on the present status

Experiment	Status of claim
DAMA/LIBRA annual modulation [58]	Unexplained at the moment; not confirmed by other experiments [54, 188]
CoGeNT excess events and annual modulation [174, 175]	Tension with other data [54, 188]
EGRET excess of GeV photons [189, 190]	Due to instrument error (?)—not confirmed by FERMI [191]
INTEGRAL 511 keV γ-line from galactic centre region [192]	Does not seem to have spherical symmetry—shows an asymmetry which follows the disk (?) [193]
PAMELA: Anomalous ratio of cosmic ray positrons/electrons [63]	May be due to DM [194, 195], or pulsars [72, 73]—energy signature not unique for DM
FERMI positrons + electrons excess [64]	May be due to DM [194, 195], or pulsars [72, 73]—energy signature not unique for DM
FERMI γ-ray excess towards galactic centre [196, 197]	Unexplained at the moment—astrophysical explanations possible [198, 199], no statement from the FERMI collaboration
WMAP radio "haze" [200]	Has a correspondence in "FERMI bubbles" [201]—probably caused by outflow from the galactic center

same phase as that of DAMA, or if it rather follows the seasons (which are opposite on the southern hemisphere).

There have recently been a number of claimed possible detections of dark matter, see Table 1. Of the items in Table 1, it seems that only the positron excess at high energy (20 GeV–1 TeV) and the γ-ray excess towards the galactic center, inferred by an analysis of FERMI public data [196, 197], can be due to dark matter annihilation without tension from other data. However, they may both perhaps more naturally be explained by ordinary astrophysical processes. In addition, the DM explanation of the PAMELA and FERMI data as we have seen needs a leptophilic particle of TeV-scale mass and a very much boosted cross section. Although this may perhaps be obtained, stretching all uncertainties involved [202], and employing Sommerfeld enhancement [79], the remaining window seems quite tight.

The DAMA/LIBRA annual modulation is a statistically very strong signal (significance of the order of 8σ), however the lack of supporting data from other experiments is disturbing. The annual modulation hinted at by CoGeNT [174, 175] is statistically much weaker, and the purported excess unmodulated signal may in fact be incompatible with the level of modulation reported. Also, it seems that the DAMA/LIBRA and GoGeNT signals, if interpreted as being due to dark matter, may be in tension with each other, even if one uses freedom in isospin violation, inelastic scattering, and non-standard halo properties [203–206]. At the moment this is one of the unsolved, frequently debated issues in the dark matter community.

The recent improvement of the upper limits on the WIMP-nucleon scattering cross section reported by CDMS II [188] and, in particular, XENON100 [54] are

truly impressive. Not only does it cast some doubt on other reported experimental results, the sensitivity is also good enough to start probing the parameter space of supersymmetric models [2]. The new calibration of the sensitivity to low-energy recoils of Xenon adds to the credibility of the new limits. The very good news is also that the installation of the next stage, a 1 ton liquid Xenon detector, has already started in the Gran Sasso experimental halls in Italy.

Of course, a much more decisive claim of detection of dark matter would result if any of the other methods, like a suitable new particle candidate being detected at the LHC, or a signature in γ-rays from the Galactic dark matter halo would be discovered.

In the first runs at LHC, no signs of a Higgs particle, nor supersymmetry or any other of the prime candidates for dark matter, have been discovered. On the other hand, the mass region 115–130 GeV, interesting for the lightest Higgs boson in the simplest versions of supersymmetry, was yet to be investigated, and in fact a weak indication around 125 GeV seem to have been found.

One possible scenario might be that such a Higgs particle is indeed found, but the particles carrying non-trivial R-parity all have masses beyond reach with the LHC. This is not impossible, depending on the amount of fine-tuning one is willing to tolerate. In fact, if one puts no prior constraints on the supersymmetric parameter space other than one should have the WMAP-measured relic density, and fulfill all other experimental constraints (cf. [143]), a mass for the lightest supersymmetric neutralino in the TeV region is generic. For such heavy dark matter neutralinos, the rate for direct detection will also be small, and it would seem impossible to test such a scenario. However, for this particular case indirect detection through gamma rays turns out to have an interesting advantage, as the new imaging air Cherenkov arrays like CTA will have their peak sensitivity in the energy range between a few hundred GeV to a few TeV [207].

Depending on the particular model realized in nature, Sommerfeld enhancement of indirect detection may also be operative. However, these large arrays will be served by a large astrophysical community which will be very much interested in transient or periodic events, meaning that a "boring" search for a stationary dark matter spectral signature during hundreds or even thousands of hours seem out of question. One may therefore consider a dedicated particle physics experiment, the "Dark Matter Array", DMA [208] only used for dark matter search. This would have great, and complementary, potential to the large direct detection experiments that are presently being planned. In fact, we mentioned, and you heard at the lectures by F. Aharonian (see Sect. 2.3 in his part), that there are ideas [110] on how to decrease the lower threshold for detection, something that could increase the sensitivity for DM detection considerably (see Fig. 7). If such a working prototype could be built, this idea may materialize in the next decade as a new way to search for phenomena beyond the Standard Model—with an expensive dedicated detector, still far below the cost of a new high-energy accelerator.

Of course, LHC data has already started to exclude some regions of supersymmetric parameter space, although not very much. This may be surprising, but is in fact due to the relative independence of the squark and gluino sector of supersymmetry,

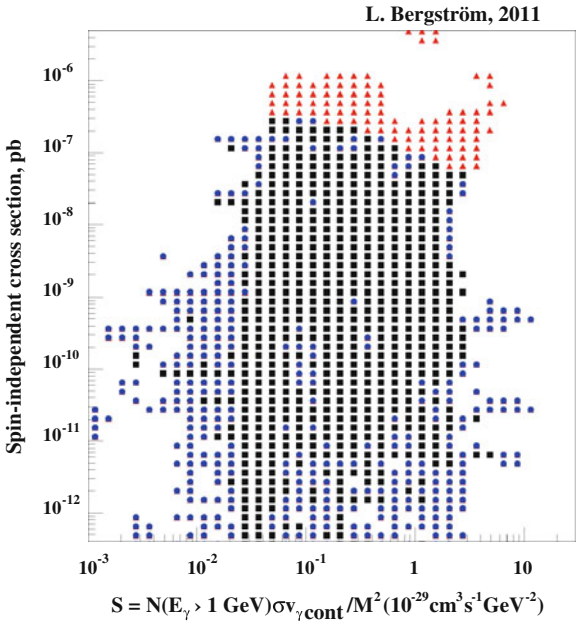

Fig. 9 Scan of the MSSM parameter space showing the direct detection cross section versus indirect detection through gamma rays. The *uppermost points* are excluded by XENON100, and points which survive also the LHC 2011 data are shown in *black*

and the neutralino sector, which hosts the dark matter candidate. In fact, as mentioned, there are so-called split supersymmetry models, which have this dichotomy explicitly postulated [35].

The complementarity of direct and indirect detection is shown in Fig. 9, where also the effects on the parameter space caused by the XENON100 bounds and LHC 2011 bounds, respectively, are shown.

9 A Detailed Calculation: The Saas-Fee WIMP

An interesting question came up during the Saas-Fee Course: Could there be a cosmological contribution to the γ-ray spectrum making up the deficit in the diffuse γ-ray emission measured by FERMI? As we heard, this is not readily explained by adding the well-known sources like AGNs, millisecond pulsars and star-forming galaxies described by C. Dermer.

Here we will outline the simple steps in making the dark matter prediction for this flux, based on [209] (see [210] for a much more thorough treatment). We will see how that could lead us to predict a several hundred GeV dark matter particle—the Saas-Fee particle as we named it at the Saas-Fee Course in 2010. This was only published in online slides from my talk,[4] and should not be taken too seriously. However, as a

[4] Available on the website of the Course: http://isdc.unige.ch/sf2010/.

pedagogical example of a surprising effect of the accumulated dark matter structure in the universe it is quite instructive.

As we have seen, in the presently most successful model for structure formation, ΛCDM, most of the matter is in the form of non-relativistic cold dark matter (CDM), but with a contribution to the present-day energy density also from a cosmological constant (Λ). As shown by detailed N-body simulations (see, e.g., [59–61] and references therein), in such a picture large structures form by the successive merging of small substructures, with smaller objects generally being denser. N-body simulations also show that the dark matter density profile in clusters of galaxies and in single galaxies develops an enhancement of the density near the centre, although it is at present unclear how steep this increase is, and whether it even shows a cusp near the center like in the popular parametrization of NFW, Eq. (163), $\rho_{\rm CDM}(r) \sim r^{-\alpha}$ with α close to 1 [105] (a very similar profile, the Einasto profile, Eq. (164), does not show a singularity, but behaves rather similarly on moderate length scales).

At present, it is not clear whether these N-body predictions are in agreement or not with all available data (one recently acknowledged problem is, for example, the apparent lack of a halo mass threshold for dwarf galaxies [211]). On large scales, however, the ΛCDM scenario gives excellent agreement with observations. On smaller scales, the dynamical range of the simulations is not enough, and one of the main puzzles is how to properly include the non-linearities induced by baryonic matter in the form of supernova explosions and other feedback mechanisms.

Let us assume that the ΛCDM picture is basically correct and that structure forms hierarchically, with the number density of halos of mass M being distributed as $dN/dM \propto M^{-\beta}$ with $\beta \sim 1.9-2$, as predicted by the Press-Schechter theory [212] and also verified in N-body simulations. Furthermore, the concentration of halos grows in these simulations with decreasing mass.

It is interesting that the averaging involved in computing the integrated signal of annihilation γ-rays of unresolved cosmological dark matter gives results which are more robust to changes in the details of how the dark matter is distributed on small scales. (The same is actually also true for all sources which are completely encompassed by the angular resolution cone of a given γ-ray experiment, for the obvious source of the galactic centre, the prediction of fluxes differ by up to 4 orders of magnitude for different models: in particular they are very sensitive to the presence or not of a central cusp.)

Let us consider annihilation of a WIMP such as the lightest neutralino χ of the MSSM, as a template. The mass range is from around 20 GeV up to several TeV [2]. For the sake of pedagogy, let us start with the unrealistic case of all the dark matter is smoothly distributed with the density distribution being just a number, the average density, at all redshifts. The idea is that since the dark matter was more dense in the early universe, one may get a large (red-shifted) flux by integrating over the line of sight from 0 to very high redshifts. Actually, in papers preceding [209] this was the only effect considered. We will soon modify the results by introducing the effects of structure, which indeed increases the flux by many orders of magnitude.

9.1 The Flux in a Smooth Universe

The comoving number density n_c of WIMPS, after decoupling from chemical equilibrium ("freeze-out") at very large temperatures ($T \sim m_\chi/20$) is depleted only slightly due to self-annihilations, governed by the Boltzmann equation

$$\dot{n}_c = -\langle \sigma v \rangle (1+z)^3 n_c^2, \tag{173}$$

where $\langle \sigma v \rangle$ is the thermal- and angular-averaged annihilation rate, which, to an excellent approximation after freeze-out, is velocity independent, since the neutralinos move non-relativistically, and are always in a dominant S-wave component (at least for our supersymmetric WIMP templates).

Each pair of χ particles that disappears through annihilation give rise to N_γ photons on the average, with an energy distribution in the rest frame of the annihilation pair,

$$\frac{dN_\gamma(E)}{dE} = \frac{dN_{\rm cont}}{dE}(E) + b_{\gamma\gamma}\delta\left(m_\chi - E\right). \tag{174}$$

Here the first term gives the average continuum gamma ray distribution per annihilating χ and we have also added a term for the possible $\gamma\gamma$ line contribution, with $b_{\gamma\gamma}$ being the branching ratio into $\gamma\gamma$ (one could also have an additional $Z\gamma$ channel).

A γ-ray observed today, at redshift $z = 0$, of energy E_0 would correspond to an energy at the emission redshift z of $E = (1+z)E_0$. We can now track, using the Boltzmann equation, the number of WIMPs that have disappeared from redshift z until now, and fold in the energy distribution (174). Thus we get a first estimate of the level of the diffuse extragalactic γ-ray flux. As usual, H_0 is the Hubble parameter, and we use the relation between time and redshift (see, e.g., [1]) $d/dt = -H_0(1+z)h(z)d/dz$ with

$$h(z) = \sqrt{\Omega_M(1+z)^3 + \Omega_K(1+z)^2 + \Omega_\Lambda} \sim \sqrt{\Omega_M(1+z)^3 + \Omega_\Lambda}. \tag{175}$$

Here Ω_M, Ω_Λ and $\Omega_K = 1 - \Omega_M - \Omega_\Lambda$ are the present fractions of the critical density given by matter, vacuum energy and curvature. We can here use the result from Sect. 2 that the universe to an excellent approximation is flat, $\Omega_K = 0$. We then obtain

$$\frac{dn_c(z)}{dz} = \frac{\langle \sigma v \rangle}{H_0}\left(\frac{(1+z)^2}{h(z)}\right) n_c(z)^2. \tag{176}$$

The differential energy spectrum of the number density n_γ of photons generated by WIMP annihilations is then given by

$$\frac{dn_\gamma}{dz} = N_\gamma \frac{dn_c}{dz} = \int_0^{m_\chi} \frac{dN_\gamma(E)}{dE}\frac{dn_c}{dz}dE. \tag{177}$$

Here, dn_c/dz can be computed directly from (176) to excellent accuracy, replacing the exact solution $n_c(z)$ by the present average number density of neutralinos n_0 on the right hand side. This we can do since the comoving number density does not change appreciably after freeze-out.

Neglecting the baryon contribution (as we will see, factors of order unity will not make a difference here, due to much larger uncertainties in structure formation), $\Omega_\chi \sim \Omega_M$, we obtain

$$n_0 = \rho_\chi/m_\chi = \rho_c \Omega_M/m_\chi. \tag{178}$$

Here $\rho_c = 1.06 \cdot 10^{-5}\, h^2$ GeV/cm^3 and h as before is the scaled Hubble parameter in units of 100 km s^{-1} Mpc^{-1}, $h \sim 0.7$. There are a few more effects we have to include. We have to use the fact that all photons move with velocity c and that the average flux is isotropic from each volume element where annihilation takes place, giving a factor $1/4\pi$ per steradian. The cross section times velocity average should, for Majorana particles, also be divided by 2, something which was missing in the original derivation [209], but added in [210] (see the published version). Some of the photons will be absorbed after travelling over cosmological distances. This can to the level of our approximate calculation be handled by introducing a simple energy- and redshift-dependent factor $e^{-z/z_{\max}}$ (or the more detailed calculation in [210] a more complicated factor depending on z and E_0).

The resulting γ-ray flux at the detector is then given by:

$$\begin{aligned}\phi_\gamma = \frac{c}{8\pi}\frac{dn_\gamma}{dE_0} &= 4.2 \cdot 10^{-14}\ \mathrm{cm}^{-2}\mathrm{s}^{-1}\mathrm{sr}^{-1}\mathrm{GeV}^{-1} \\ &\times \frac{\Gamma_{26}\Omega_M^2 h^3}{m_{100}^2}\int_0^{z_{up}} dz \frac{(1+z)^3 e^{-z/z_{\max}}}{h(z)}\frac{dN_\gamma(E_0(1+z))}{dE}.\end{aligned} \tag{179}$$

where we defined $\Gamma_{26} = \langle\sigma v\rangle/(10^{-26}\ \mathrm{cm}^3\,\mathrm{s}^{-1})$ and m_{100} the mass in units of 100 GeV.

For the energies we are interested in, 1 GeV $< E_0 <$ 500 GeV, it is the starlight and (more poorly known) infrared background radiation which is most important, whereas the CMBR may be important for higher energies. An optical depth of order unity is reached for a redshift which in [210] was approximated by $z_{\max}^{\mathrm{old}}(E_0) \sim 3.3(E_0/10\ \mathrm{GeV})^{-0.8}$, which represented older results. However, the newer data discussed in the lectures by C. Dermer (see Sect. 7.3 in his part), indicate much less absorption. As a representative of the more recent evaluation of this absorption [213], we take instead the simple approximation $z_{\max}^{\mathrm{new}}(E_0) \sim 2.3(E_0/50\ \mathrm{GeV})^{-1.1}$.

The exponential form is a good approximation for small values of $z_{\max}$ as is dominant in most of the cases we study here. The upper limit of integration is given by kinematics, $z_{up} = m_\chi/E_0 - 1$, as the maximum rest frame energy of a photon in an annihilation event is $E = m_\chi$. The gamma line contribution to (179) is particularly simple, just picking out the integrand at $z + 1 = m_\chi/E_0$; it has the very distinctive and potentially observable signature of being asymmetrically smeared to lower energies (due to the redshift) and of suddenly dropping just above m_χ. Unfortunately,

for most models the branching ratio for this channel is too small to be measurable with present-day energy resolution, and we will drop it from now on. (This may however change when the high-resolution instrument GAMMA-400 [94] is operational towards the end of this decade. This is specified to have an energy resolution of 1 %, which will be a perfect instrument for searching for γ lines from annihilation, and also from models where dark matter decays radiatively [214].) The continuum emission will produce a characteristic, although less conspicuous feature, a smooth "bump" below around one tenth of the neutralino mass, and may be more difficult to detect. One should notice that there are particular models where radiative corrections ("internal bremsstrahlung") may give a significantly harder spectrum near $E_\gamma = m_\chi$, facilitating discrimination against most backgrounds [130, 131].

9.2 Including Effects of Cosmic Structure

To give an example of the results (which in [209] contained both obsolete SUSY models and not very accurate data from the old EGRET experiment), we take a generic model with mass 600 GeV, and the canonical WIMP averaged cross section times velocity of $\langle \sigma c \rangle = 3 \cdot 10^{-26}$ cm^3 s^{-1}, in the "concordance" cosmology $\Omega_M = 0.3, \Omega_\Lambda = 0.7, h = 0.7$. The continuous γ-ray rest frame energy distribution per annihilating particle comes mainly from hadronization and decay of π^0s and is conveniently parametrized to reasonable accuracy as (see Eq. (158))

$$dN_{\rm cont}(E)/dE = (0.42/m_\chi)e^{-8x}/(x^{1.5} + 0.00014)$$

where $x = E/m_\chi$. This is valid for most quark jet final states, except for the top. Also, τ lepton decays give a somewhat harder γ-ray spectrum, and as mentioned internal bremsstrahlung may be important for certain types of models.

The most difficult, but also most important and interesting part of the calculation is to include the effects of structure formation. Following [209], we consider first a halo of mass M whose radial density profile can be described by $\rho_{DM}(r) = \rho'_{DM} f\,(r/a)$, with ρ'_{DM} being a characteristic density and a a length scale. These are found in N-body simulations not to be independent parameters, as smaller halos are generally associated with higher densities.

As a simple first model for structure formation, assume that the halo of mass M accreted from a spherical volume of radius R_M, determined by requiring that the average cosmological density times that volume is equal to M, $\rho_0 \cdot 4\pi R_M^3/3 = M$ (with $\rho_0 \sim 1.3 \cdot 10^{-6}$ GeV/cm^3). The increase of average squared overdensity per halo, which is what enters the annihilation rate, is given by:

$$\Delta^2 \equiv \left\langle \left(\frac{\rho_{DM}}{\rho_0} \right)^2 \right\rangle_{r<R_M} = \left(\frac{\rho'_{DM}}{\rho_0} \right) \frac{I_2}{I_1}, \tag{180}$$

where $I_n \equiv \int_0^{R_M/a} y^2 dy (f(y))^n$ with $y \equiv r/a$. Here the dependence on the limits of integration is rather weak, at least for profiles less cuspy than the NFW profile [105] (see Eq. (163)).

Computing I_2/I_1 numerically, and using values of ρ'_{DM}/ρ_0 as determined for Milky Way size halos we find values of Δ^2 of $1.5 \cdot 10^4$ for the NFW profile, and $7 \cdot 10^3$ for a cored, modified isothermal profile (modified so that the density falls as $1/r^3$ at large radii). The flux ratio, 2:1 for these two models should be compared with the ratios roughly 100:1 obtained within a few-degree cone encompassing the galactic center, showing the announced relative insensitivity to halo density profiles.

We should now also take into account that the number density of halos is scaling like $\sim 1/M^{1.9}$, and that small-mass halos are denser. We can resort to the highest-resolution N-body simulations available to date [215]. Fitting the concentration parameter of halos by

$$c \sim 100 \, (M_{\rm vir}/h^{-1} M_\odot)^{-0.08}, \tag{181}$$

one finds to a good approximation

$$\Delta^2 \sim 2 \cdot 10^5 M_{12}^{-0.2}, \tag{182}$$

where M_{12} is the halo mass in units of 10^{12} solar masses. This means that the total flux from a halo of mass M scales as $M^{0.8}$. Since the number density of halos goes as $M^{-1.9}$, the fraction of flux coming from halos of mass M scales as $M^{-1.1}$. Thus the γ-ray flux will dominantly come from the smallest CDM halos. In simulations, substructure has been found on all scales (being limited only by numerical resolution). For very small dark matter clumps, however, no gain in overdensity is expected, since once the matter power spectrum enters the k^{-4} region a constant density is expected. There are arguments [216] that structure is present in cold dark matter models all the way down to 10^{-6} or smaller [217]. We conservatively set $1 M_\odot$ as the minimal scale. In a more detailed treatment, one should also include effects of clumps within clumps, which increase the enhancement. However, destruction of DM clumps near large central densities of halos should also be included.

Finally, regarding redshift dependencies, we assumed in [209] a constant enhancement factor Δ^2 out to $z \sim 1$, and somewhat arbitrarily imposed quadratic growth in the enhancement factor from $z \sim 10$ to the fully developed epoch $z = 1$. (The computed flux is not very sensitive to this assumption.) Furthermore, in (179) we make the replacement $(1+z)^3 \to 1$, reflecting the fact that the we are now dealing with a clumped, rather than a smooth distribution with density scaling $\sim (1+z)^3$.

We thus arrive at the following expression for the flux including structure formation

$$\begin{aligned} \phi_\gamma = \frac{c}{8\pi} \frac{dn_\gamma}{dE_0} &= 4.2 \cdot 10^{-14} \, {\rm cm}^{-2} \, {\rm s}^{-1} \, {\rm sr}^{-1} \, {\rm GeV}^{-1} \\ &\times \frac{\Gamma_{26} \Omega_M^2 h^3}{m_{100}^2} \int_0^{z_{up}} dz \frac{\Delta^2(z) e^{-z/z_{\rm max}}}{h(z)} \frac{dN_\gamma(E_0(1+z))}{dE}. \end{aligned} \tag{183}$$

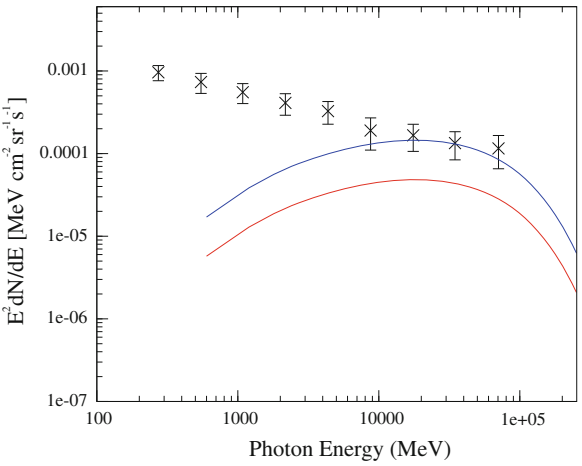

Fig. 10 The predicted diffuse extragalactic γ-ray flux computed using the methods described in the text, for a 600 GeV WIMP with a cross section compatible with the WMAP-inferred relic density and with different assumptions for the effects of structure. The diffuse extragalactic data was measured by FERMI-LAT [191]

9.3 The Saas-Fee WIMP

We find using (183) (see also [218]) that the flux from small halo structure is enhanced by roughly a factor $(4-10)\cdot 10^7$ compared to the smooth case, giving in the upper range observability for the annihilation parameters as used above. The uncertainties reside mainly in the still poorly known factor $\Delta^2(z)$ and its extrapolation to small halo masses (and also the effects of DM clumps within clumps, for instance).

In Fig. 10, we show the results for this 600 GeV WIMP model. The results are compared with the measurements from FERMI-LAT [191], and despite the fact that there is this uncertainty in the absolute rates, it is amusing, as I discussed at the Saas-Fee course, that the possible break in the FERMI data may be caused by a new contribution from 500–600 GeV mass annihilating dark matter ("The Saas-Fee WIMP", of which there would be one per 2 litres in the lecture hall at Les Diablerets as in all other places on Earth) setting in. It will obviously be interesting to follow the development of this data set during the next few years, to see if this model survives or even becomes more convincing.

It has of course to be remembered that the strength of the annihilation signal can be much lower than the proof-of-existence example chosen for Fig. 10 in which case a detection would be correspondingly more difficult. On the other hand, there may be particle physics effects (such as Sommerfeld enhancement) which could give a higher flux.

As a recent illustration of the importance of adding up all structure present, e.g., in galaxy clusters, can be mentioned the results of [219–223] and [224], where it was shown that by choosing particularly favourable, not too distant clusters, one is very

close to the current observational limits from FERMI-LAT. Indeed, there may even be (weak) indications from FERMI data of a signal [225].

A related type of analysis for the diffuse extragalactic case is performed in a similar way as when analyzing the angular fluctuations in the CMB. Also using this method of analysis, the conclusion is that with FERMI-LAT data one may be very near detection [226–229].

10 Primordial Black Holes as Dark Matter?

Sometimes one gets the question from lay persons, when telling that we are interested in the problem of dark matter: *Could it be black holes?* Black holes are in some sense dark: they do not emit light from within the event horizon, so the question is not completely out of context. However, the only black holes which we are relatively certain to exist are those around 2–20 solar masses, and the supermassive ones like the one residing at the Galactic center (of mass a few times $10^6 M_\odot$). We also know of even more massive ones (of mass up to a few times $10^9 M_\odot$) making up active galactic nuclei (AGNs). However, the galactic halos in which even the most massive, "supermassive", black holes reside have a factor of at least 1000 more total mass. Thus their influence on the cosmic energy balance is rather marginal. Also the solar mass type black holes which are produced as end results of stellar evolution constitute a small fraction, by far too small to explain the abundant and omnipresent dark matter. Finally, most black holes are in practice not very dark, as their concentrated mass has an effect on surrounding matter, causing various types of radiation processes, as ordinary matter is "eaten" by the black hole.

However, very massive black holes may be important for dark matter detection: if left undisturbed for a long time, they may adiabatically attract surrounding dark matter, changing the NFW-type distribution to a much more spiky cusp [230]. As the annihilation rate grows with the square of the dark matter density, this could give a dramatically increased rate of γ-rays, and in particular neutrinos (which are unlikely to be absorbed by surrounding matter). More extreme versions of this scenario are in fact ruled out already, due to the lack of unambiguous dark matter signals from the galactic centre. An interesting possibility is that intermediate mass black holes exist, where this type of signal could be close to detection, e.g., with FERMI-LAT [231].

10.1 Primordial Black Holes

There is also a small, be definite probability that small mass black holes would have been formed in the early universe. These "primordial" black holes would have to have been formed with a rather peculiar mass spectrum not to overclose the universe, and not to create too much radiation due to the interesting spontaneous emission of Hawking radiation, named after its discoverer (in theory).

Let us first remind ourselves of the metric surrounding a point mass M,

$$ds^2 = \left(1 - \frac{r_S}{r}\right) dt^2 - \frac{1}{1 - \frac{r_S}{r}} dr^2 - r^2 \left(d\theta^2 + \sin^2 \theta d\varphi^2\right), \tag{184}$$

where r_S is the Schwarzschild radius, $r_S = 2GM$ (here G is Newton's constant, and as usual we set $c = 1$). A radial photon trajectory in this metric is given by $ds^2 = 0$, which gives

$$dt = \frac{dr}{1 - \frac{r_S}{r}}, \tag{185}$$

for $\theta = \phi = const$. The time for the photon to travel from r_i to r_f is thus

$$t_f - t_i = \int_{r_i}^{r_f} \frac{dr}{1 - \frac{r_S}{r}} = r_f - r_i + r_S \ln\left(\frac{r_f - r_S}{r_i - r_S}\right). \tag{186}$$

This diverges as $r_i \to r_S$, so that a light ray which starts at $r < r_S$ will never reach an outside observer: we have a black hole! If we define the sphere at $r = r_S$ as the areas A_{BH} of the black hole, we find

$$A_{BH} = 4\pi r_S^2 = 4\pi (2GM)^2 = 16\pi G^2 M^2. \tag{187}$$

It is interesting to contrast this with the behaviour of a solid sphere in classical physics, where $M \sim R^3$ which gives $R \sim M^{\frac{1}{3}}$, so that $A_{\text{class}} \sim M^{\frac{2}{3}}$. This difference is due to the strong curvature of space-time near the black hole.

As we noted, known black hole candidates either have a mass of a few solar masses (probably remnants of stellar collapse, as the maximal mass of a neutron star is somewhere between 1.4 solar masses—the Chandrasekhar mass—and a few solar masses), or a few million solar masses (Milky Way centre) to billions of solar masses (AGNs). There is no known present formation mechanism for BHs of mass less than a solar mass, so these, if they exist, must be primordial (PBHs), i.e. produced in the early universe, e.g. at some phase transition after inflation. There are various limits restricting formation scenarios, in general one has to "cook up" a power spectrum of density fluctuations which peaks at a particular mass length scale. When the horizon passes that scale, copious production of BHs may occur in such a scenario. An example can be found in a recent paper [232] where one tries to explain all of dark matter with PBHs, by having a power spectrum with a huge peak ($\delta\rho/\rho \sim 0.1$) at a scale corresponding to a black hole mass of $10^{-7} M_\odot$.

10.2 Hawking Radiation

If PBHs exist, one may detect them through Hawking radiation, as Hawking discovered in a remarkable 1975 paper [233] that a black hole should emit thermal radiation. This can be explained as a tunneling phenomenon [234].

Let us make an extremely simplified heuristic version of the derivation. Let us say that we have an isolated black hole. We can then for certain say that it is inside the Schwarzschild radius r_S. This uncertainty in the position of the radiation gives an uncertainty of the time $\Delta t \sim r_S/c = 2GM/c^3$, but the uncertainty relation between time and energy, $\Delta E \Delta t \sim \hbar/2$ gives

$$\Delta E \sim \frac{\hbar c^3}{4GM} \sim E_{th} = k_B T \rightarrow k_B T \sim \frac{\hbar c^3}{4GM} = \frac{1}{4GM}. \tag{188}$$

Thus, in our units, where also $k_B = 1$, the temperature $T = 1/(4GM)$. This is only a factor of 2π different from Hawking's result:

$$T_H = \frac{1}{8\pi GM}. \tag{189}$$

Of course, Hawking's derivation is much more beautiful, by explaining the radiation by mixing of positive and negative energy states due to the strong space-time curvature near the black hole. Another way to understand the process is that for a virtual particle pair created just at the horizon, one of the particles will be dragged into the black hole, releasing gravitational binding energy to the other particle, which can then appear as a real propagating state outside the horizon.

An interesting consequence of Hawking radiation and the equivalence principle is that an uniformly accelerated observer, with acceleration a, in empty space should see a thermal distribution of particles—the Unruh effect. The Unruh temperature is $T = a/2\pi$. Attempts have been made to measure the Unruh effect at accelerators, but present-day accelerations are not large enough. It has been argued, however, that the so-called Sokolov-Ternov effect (depolarization of electrons in a storage ring due to synchrotron radiation) really has the same origin as the Unruh effect—and it has been experimentally verified [235].

10.3 Thermodynamics of Black Holes

If we regard the Hawking temperature as a true thermodynamical temperature $T(M) = T(E)$, there should also be an entropy (Bekenstein entropy) associated with the BH:

$$T(E) = \frac{1}{8\pi GE}; \quad dS = \frac{dE}{T(E)} \rightarrow S = \int_0^M 8\pi GE dE = 4\pi GM^2 = \frac{1}{4}\frac{A_{BH}}{G}. \tag{190}$$

If we remember that $G = 1/M_{Pl}^2 = l_{Pl}^2$, we see that each "Planck area" of the surface of the BH contributes one quarter unit of entropy, and one gets huge numbers. This is still mysterious—what are the degrees of freedom describing the black hole, and why does ordinary matter that forms a BH suddenly increase its entropy enormously?

To describe black hole evaporation, it is useful to remember the form of a thermal distribution for a particle species

$$f_i(\mathbf{p}) = \frac{1}{e^{\frac{E_i-\mu_i}{k_B T}} \pm 1} = \frac{1}{e^{\frac{E_i-\mu_i}{T}} \pm 1}. \tag{191}$$

This means that for the rate of mass loss we can analogously write [236]

$$\frac{dM}{dt} = -\sum_j \frac{1}{2\pi}\int_{m_j}^{\infty} \Gamma_j \frac{EdE}{e^{8\pi GME} \pm 1} = \ldots = -5 \cdot 10^{25} f(M) M^{-2}\, gs^{-1}. \tag{192}$$

Here Γ_j is the absorption rate for particle of type j and the sum is over all particle-antiparticle pairs. This gives the evaporation time

$$\tau_{evap} \sim \int_{M_{min}}^{M_{max}} \frac{M^2}{f(M)} dM \sim \frac{6 \cdot 10^{-27}}{f(M_i)} \left(\frac{M_i}{1\ g}\right)^3 s. \tag{193}$$

Thus, only BHs with mass $>10^{15}$ g are stable on cosmological time scales (so don't worry about BHs produced at LHC—they would evaporate immediately—if they exist!) Upper limits of γ-ray emission from EGRET and FERMI-LAT gives the approximate bound for light PBHs:

$$\Omega_{PBH}(M < 10^{15}\ g) < 10^{-8}. \tag{194}$$

Actually, since the temperature increases with decreasing mass, all particles, even more massive than those presently produced at accelerators, may give a contribution in the final "Hawking explosion". In particular, if supersymmetry is realized in nature, the end-time evolution may have interesting differences from the scenario with only Standard Model particles [237].

10.4 Formation of Primordial Back Holes

Let us discuss how primordial black holes formed in the early universe (see [238]). The relevant length scale is the particle horizon length, so that

$$M = \gamma M_{\text{particle horizon}} = 2 \cdot 10^5 \gamma \left(\frac{t}{1\ s}\right) M_\odot, \tag{195}$$

where $\gamma \sim 0.2$ depends on the detailed formation scenario. We can now compute the fraction of total energy density in black holes at formation:

$$\beta(M) \equiv \frac{\rho_{PBH}(t_i)}{\rho(t_i)} = 8 \cdot 10^{-29} \frac{1}{\sqrt{\gamma}} \left(\frac{g_i}{106.75}\right)^{\frac{1}{4}} \left(\frac{M}{M_\odot}\right)^{\frac{3}{2}} \left(\frac{n_{PBH}(t_0)}{1\ \text{Gpc}^{-3}}\right). \tag{196}$$

This means a contribution to Ω today of

$$\Omega_{PBH} = \frac{M n_{PBH}(t_0)}{\rho_c} = \left(\frac{\beta(M)}{1.2 \cdot 10^{-8}}\right) \sqrt{\gamma} \left(\frac{g_i}{106.75}\right)^{-\frac{1}{4}} \left(\frac{M}{M_\odot}\right)^{-\frac{1}{2}}. \tag{197}$$

The WMAP bound (the PBHs would behave gravitationally as cold dark matter) $\Omega < 0.25$, gives

$$\beta(M) < 2 \cdot 10^{-18} \frac{1}{\sqrt{\gamma}} \left(\frac{g_i}{106.75}\right)^{\frac{1}{4}} \left(\frac{M}{10^{15}\ g}\right)^{\frac{1}{2}}. \tag{198}$$

(This is valid for BHs that have not evaporated today, i.e., for $M > 10^{15}$ g.) It is convenient to divide out the cosmology/formation factors and consider the simpler expression for the energy density limit from WMAP:

$$\beta'(M) < \sqrt{\gamma} \left(\frac{g_i}{106.75}\right)^{-\frac{1}{4}} \beta(M) = 2 \cdot 10^{-18} \left(\frac{M}{10^{15}\ g}\right)^{\frac{1}{2}}. \tag{199}$$

Limits on $\beta'(M)$ can be obtained from a variety of data, from BBN and CMB in the early universe to the galactic and diffuse extragalactic γ-ray emission, gravitational lensing data and large scale structure. The limits we just computed on Ω_{PBH} is also important in the region $M \sim 10^{15}$–10^{27} g (for a detailed summary of the situation, see [238]).

To conclude: PBHs of mass less than around 10^{15} g cannot be the dark matter due to important constraints from the absence of Hawking radiation in 1–100 MeV γ-rays, but may still be a subdominant component. It is worthwhile to look for γ-ray signatures—a discovery of Hawking radiation would be truly wonderful!

At all masses, there are important bounds from a variety of methods. In principle, there are mass ranges where PBHs can still be the dark matter—all of dark matter, but one needs contrived production mechanisms such as a strongly peaked, and fine-tuned, density power spectrum.

11 Gravitational Waves

We will now, in view of the multi-messenger aspects of this lecture series, discuss one more type of radiation which is deeply linked to the theory of general relativity on which modern cosmology rests: gravitational radiation.

Due to the nonlinearity of Einstein's equations, it is virtually impossible to find exact solutions to the metric tensor $g^{\mu\nu}(\mathbf{r}, t)$ corresponding to the dynamics, for example, of a massive star which collapses to a black hole near the strong gravitational field of the star (using supercomputers, numerical studies can, however, be made). Far from the source of the gravitational field, it is on the other hand reasonable to use a first-order approximation. The gravitational deformation of space-time near celestial bodies like the Earth or the Sun due to conceivable astrophysical processes happening elsewhere in the Galaxy is indeed as we will see extremely tiny, which justifies such a perturbative approach. The same smallness of the effect unfortunately also make detection of gravitational radiation very challenging.

11.1 The Gauge Choice for Electromagnetism

Recall the way one derives the existence of electromagnetic waves in Maxwell's theory. One inserts the vector potential A^μ in the equations of motion for a vanishing current j^μ (since we are dealing with propagation in vacuum) to obtain

$$\Box A^\mu - \partial^\mu \left(\partial_\nu A^\nu\right) = 0 \tag{200}$$

Through the use of the gauge freedom $A^\mu \rightarrow A^\mu + \partial^\mu f$, we can choose A^μ to fulfill $A^0 = 0$ and also the so-called Lorentz condition $\partial_\nu A^\nu = 0$. This leads to the wave equation

$$\Box A^\mu = 0 \tag{201}$$

with solutions of the form

$$A^\mu(\mathbf{r}, t) = \epsilon^\mu e^{\pm i(\omega t - \mathbf{k}\cdot\mathbf{r})} = \epsilon^\mu e^{\pm i k^\mu x_\mu} \tag{202}$$

where $k^\mu k_\mu = 0$ (light-like propagation) and the gauge conditions $A^0 = 0$ and $\partial_\nu A^\nu = \nabla \cdot \mathbf{A} = 0$ translate into $\epsilon^0 = 0$ and $\mathbf{k} \cdot \epsilon = 0$. This means that the two physical degrees of freedom are transverse to the direction of propagation, and there is no time-like mode of propagation (this is deeply connected to the masslessness of the photon).

11.2 Gauge Choice for the Metric Perturbation

In the case of gravity waves in Einstein's theory of general relativity, we can similarly make a first-order expansion of the dynamical degrees of freedom, which are the components of the metric tensor field $g_{\mu\nu}$, around the constant Minkowski metric $\eta_{\mu\nu}$:

$$g_{\mu\nu} = \eta_{\mu\nu} + h_{\mu\nu}, \tag{203}$$

and work to the first non-vanishing order in $h_{\mu\nu}$.

Now we have a spin-2 field $h_{\mu\nu}$ instead of the vector quantity A^μ, but again we can use a gauge-like invariance (which in this case rather is re-parametrization invariance)

$$x_\mu \to x_\mu + \xi_\mu(x) \tag{204}$$

translating into

$$h_{\mu\nu} \to h_{\mu\nu} - \partial_\mu \xi_\nu - \partial_\nu \xi_\mu. \tag{205}$$

Using this we may impose the so-called traceless gauge condition

$$h^\mu_{\ \mu} = 0 \tag{206}$$

The analogy of $A_0 = 0$ is

$$h_{0\nu} = h_{\nu 0} = 0, \tag{207}$$

and of the transversality condition

$$\nabla \cdot \mathbf{A} = 0 \tag{208}$$

is

$$\nabla_i h^{i\nu} = \nabla_i h^{\nu i} = 0. \tag{209}$$

The Einstein equation (neglecting back-reaction, i.e. the contribution to the energy-momentum tensor by the gravitational field itself) becomes simply

$$\Box h_{\mu\nu} = 0. \tag{210}$$

11.3 Solutions to the Wave Equation

Exactly like for photons we can write for the wave solutions to Einstein's equation

$$h_{\mu\nu} = E_{\mu\nu} e^{\pm i(\omega t - \mathbf{k}\cdot\mathbf{x})} \tag{211}$$

with $k^2 = \omega^2$, i.e. massless propagation, with the speed of light. (There have been brave attempts to replace Einstein's gravity with a massive theory, with the extra component having extremely small mass. This would lead to many interesting differences, perhaps even explaining the small value of the cosmological constant. So far, there has not appeared any generally accepted way to do this, however.)

We can represent $E_{\mu\nu}$ by a 4×4 matrix, which, exactly like for A_μ, should reflect the gauge choice. We know already that the $E_{0\nu}$ row and $E_{\mu 0}$ columns are zero. Also E has to be symmetric in the two indices (since the metric is). Further, $k^i E_{i\nu} = k^j E_{\mu j} = 0$, meaning that also the elements of the $E_{3\nu}$ column and $E_{\mu 3}$ row are zero for a wave propagating in the z-direction. So, we really just have zeros for our perturbative solution apart from a symmetric, traceless 2×2 matrix. A general such matrix is a linear combination of

$$E^+_{\mu\nu} = \begin{pmatrix} 0\,0 & 0 & 0 \\ 0\,1 & 0 & 0 \\ 0\,0 & -1 & 0 \\ 0\,0 & 0 & 0 \end{pmatrix} \tag{212}$$

and

$$E^\times_{\mu\nu} = \begin{pmatrix} 0\,0\,0\,0 \\ 0\,0\,1\,0 \\ 0\,1\,0\,0 \\ 0\,0\,0\,0 \end{pmatrix} \tag{213}$$

For a given value of the 3-component z, and at time t, we can then write

$$E_{\mu\nu}(t) = h_+(t) E^+_{\mu\nu} + h_\times(t) E^\times_{\mu\nu}. \tag{214}$$

Look at the case

$$h_+ \neq 0, \quad h_\times = 0. \tag{215}$$

At a given time, we have in the unperturbed case

$$\Delta s^2 = \eta_{\mu\nu} \Delta x^\mu \Delta x^\nu = (\Delta t)^2 - \sum_i (\Delta x^i)^2 = -\sum_i (\Delta x^i)^2 \tag{216}$$

For two diametrically opposed points on the unit circle,

$$\Delta x^i = (2\cos\theta, 2\sin\theta, 0) \tag{217}$$

and their distance is

$$d_0 = \sqrt{-\eta_{ij}(\Delta x^i)(\Delta x^j)} = 2\sqrt{\sin^2\theta + \cos^2\theta} = 2. \tag{218}$$

In the perturbed case (i.e., if a gravity wave passes)

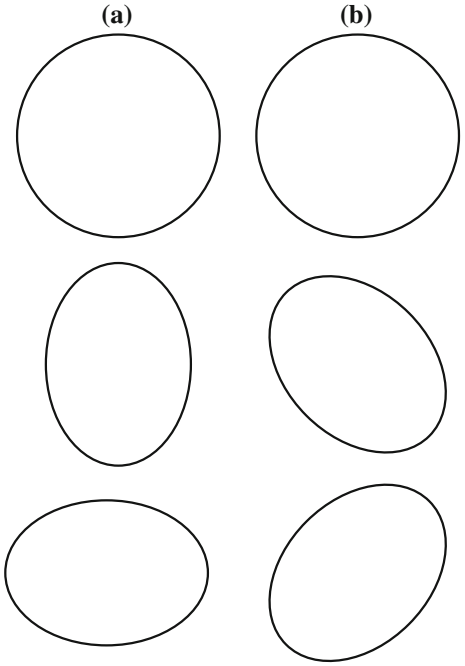

Fig. 11 **a** The deformation of the unit circle caused by gravity waves proportional to the polarization amplitude h_+. Shown are the unperturbed circle and the maximally stretched configurations along the two axes of symmetry, the x and y axes. **b** The corresponding pattern for the orthogonal polarization state described by the amplitude $h_\times$. Note that the axes along which stretching and compression occur form 45-degree angles to the x and y axes

$$d_+ = \sqrt{-(\eta_{ij} + h_+ E^+_{ij})\Delta x^i \Delta x^j} = \sqrt{4 - h_+(t) 4(\cos^2\theta - \sin^2\theta)} \tag{219}$$

$$\simeq 2 - h_+(t)(\cos^2\theta - \sin^2\theta) = 2 - h_+(t)\cos 2\theta. \tag{220}$$

For simplicity, we may work with real h by combining as usual the waves with the two signs in the exponential, giving

$$h^+_{\mu\nu} = E^+_{\mu\nu} h_+(t) = E^+_{\mu\nu} \cos(\omega t - \mathbf{k}\cdot\mathbf{r}) \tag{221}$$

and we see that the unit circle will be successively "compressed" or "squeezed" depending on the sign of the last factor (see Fig. 11, where the corresponding deformation caused by $h_\times$ is also shown).

These are the two independent quadrupole deformations of a circle. This means that the source of the gravitational field giving gravity waves has to have a quadrupole moment, Q. From dimensional reasoning,

$$h \sim \frac{G_N \ddot{Q}}{d} \sim \frac{4 G_N E_{\rm kin}}{d}, \tag{222}$$

which is obtained by the crude estimate

$$Q \sim Ml^2 \Rightarrow \dot{Q} = M2l\dot{l} = 2Mlv \Rightarrow \ddot{Q} \sim 2Mv^2 = 4E_{kin}. \tag{223}$$

For objects in the Milky Way, typically $d \sim 10$ kpc, and with $E_{\rm kin} \sim M_\odot$ we find

$$h \sim 10^{-17}. \tag{224}$$

On the other hand, for the distance appropriate for the Virgo galaxy cluster,

$$h \sim 10^{-20}. \tag{225}$$

These extremely tiny deformations is the reason for the non-detection so far of gravitational radiation, although there are promising objects like coalescing neutron stars which should have amplitudes nearing the experimental upper limits.

In a sense, gravity waves have already been indirectly detected, however, by comparing the slowing-down of the rotation rate of the binary pulsar system PSR 1913–16 by Hulse and Taylor (Nobel Prize of 1993):

$$\frac{dP}{dt} = (-2.4225 \pm 0.0056) \cdot 10^{-12}, \tag{226}$$

with the general relativistic calculation (with energy loss due to gravitational radiation):

$$\frac{dP_{GR}}{dt} = -2.40 \cdot 10^{-12}. \tag{227}$$

This excellent agreement has put severe limits on possible modifications of Einstein gravity. But effects of gravity waves have so far never been detected directly on Earth, despite an impressive increase in sensitivity of the LIGO experiment in the US, and VIRGO in Italy. Actually by combining several experiments and searching for time-coincident effects, one may both decrease various noise sources and increase the sensitivity for a signal. This is presently done by LIGO, VIRGO and GEO600 in Germany. All three detector are presently being upgraded to more advanced versions. However, it may be that a space experiment, LISA, will be needed to detect a significant signal. Its status is, however, at present unclear due to the difficult financial situation in most countries of the world.

We finally remind that there is also a possibility of detecting gravitational waves that are relics of dramatic processes in the early universe, such as during the epoch of inflation or during the formation of cosmic strings, if such exist. In that case, the most promising method is through analyzing the imprints they have made in the CMBR. As gravitational waves carry a quadrupole moment it is possible to distinguish their effects through studies of CMBR polarization. With the Planck satellite it is possible

to search for gravitational waves of very long wavelength generated through these hypothetical processes. Results are expected in early 2013.

12 Conclusions

This finishes our trip through the universe, looking at fundamental processes of similar interest to particle physicists, cosmologists, astrophysicists and astroparticle physicists alike. As hopefully has becomes clear, by combining information from all messengers that we have available: photons of all wavelengths, neutrinos, antimatter and perhaps gravitational waves, we may study from the Earth some of the most energetic and interesting processes in the universe. If we are lucky, we may even solve the problem of the nature of the dark matter, which has been with us since the times of Fritz Zwicky. Let us remind ourselves of his prophetic words from 1933 [8], after observing the rapid movement of the galaxy members of the Coma cluster, which pointed to an overdensity of matter in the cluster:

If this over-density is confirmed we would arrive at the astonishing conclusion that dark matter is present with a much greater density than luminous matter...

Acknowledgments The author is grateful to several colleagues, including G. Bertone, T. Bringmann, J. Conrad, J. Edsjö, P. Gondolo, A. Goobar, P.O. Hulth, E. Mörtsell, F. Aharonian and C. Dermer as well as the participants of the 2010 Saas-Fee Course for many useful suggestions and discussions. A particular thanks to the organizers of the School, chaired by Roland Walter, for making the School such an enjoyable and memorable event, and to Marc Türler for a careful reading of the manuscript.

References

1. L. Bergström, A. Goobar, *Particle Astrophysics and Cosmology*, 2nd edn. (Springer, Dordrecht, 2006). ISBN-13: 978-3540329244
2. P. Gondolo, J. Edsjö, P. Ullio, L. Bergström, M. Schelke, E.A. Baltz, JCAP **0407**, 008 (2004) . [astro-ph/0406204]
3. L. Bergström, G. Bertone, in *Particle Dark Matter*, ed. by Bertone, G. (Cambridge University Press, Cambridge, 2010) pp. 491–506. ISBN-13: 978-0521763684
4. L. Bergström, invited talk at the EPS-HEP Conference, to appear in the Proceedings (Grenoble, 2011)
5. L. Bergström, *Dark Matter and Imaging Air Cherenkov Arrays*, to appear in Astroparticle Physics, special issue for the Cherenkov Telescope Array (2012)
6. M. Blomqvist, E. Mortsell, JCAP **1005**, 006 (2010). [arXiv:0909.4723 [astro-ph.CO]]
7. E. Komatsu et al. WMAP Collaboration. Astrophys. J. Suppl. **192**, 18 (2011). [arXiv:1001.4538 [astro-ph.CO]]
8. F. Zwicky, Helv. Phys. Acta **6**, 110 (1933)
9. D. Clowe, M. Bradac, A.H. Gonzalez, M. Markevitch, S.W. Randall, C. Jones, D. Zaritsky, Astrophys. J. **648**, L109–L113 (2006). [astro-ph/0608407]
10. P. Binetruy, G. Girardi, P. Salati, Nucl. Phys. B **237**, 285 (1984)
11. J. Edsjö, P. Gondolo, Phys. Rev. D **56**, 1879 (1997). [hep-ph/9704361]
12. A. Linde, Phys. Lett. **B129**, 177 (1983)
13. C. Itzykson, J.B. Zuber, *Quantum Field Theory*, (McGraw-Hill, New York, 1980)
14. L.J. Reinders, H. Rubinstein, S. Yazaki, Phys. Rept. **127**, 1 (1985)

15. J.B. Kogut, Rev. Mod. Phys. **55**, 775 (1983)
16. G. Altarelli, G. Parisi, Nucl. Phys. B **126**, 298 (1977)
17. M. Shaposhnikov, I. Tkachev, Phys. Lett. B **639**, 414 (2006). [hep-ph/0604236]
18. G.G. Raffelt, *Stars as Laboratories for Fundamental Physics*, (University of Chicago Press, Chicago, 1996)
19. K. Nakamura et al., Particle data group collaboration. J. Phys. G G **37**, 075021 (2010)
20. A. Osipowicz et al., KATRIN Collaboration. hep-ex/0109033
21. K. Abe et al., Super-Kamiokande collaboration. Phys. Rev. D **83**, 052010 (2011).[arXiv:1010.0118 [hep-ex]]
22. B. Aharmim et al., SNO collaboration. Phys. Rev. C **81**, 055504 (2010). [arXiv:0910.2984 [nucl-ex]]
23. S. Abe et al., KamLAND collaboration. Phys. Rev. Lett. **100**, 221803 (2008). [arXiv:0801.4589 [hep-ex]]
24. R. Acquafredda et al., OPERA collaboration. New J. Phys. **8**, 303 (2006). [hep-ex/0611023]
25. P. Adamson et al., MINOS collaboration. Phys. Rev. Lett. **107**, 011802 (2011). [arXiv:1104.3922 [hep-ex]]
26. F. Halzen, D. Hooper, New J. Phys. **11**, 105019 (2009). [arXiv:0910.4513 [astro-ph.HE]]
27. M. Cirelli, A. Strumia, M. Tamburini, Nucl. Phys. B **787**, 152 (2007). [arXiv:0706.4071 [hep-ph]]
28. K.A. Intriligator, N. Seiberg, Class. Quant. Grav. **24**, S741 (2007). [hep-ph/0702069]
29. R.R. de Austri, R. Trotta, L. Roszkowski, JHEP **0605**, 002 (2006). [hep-ph/0602028]
30. P. Scott, J. Conrad, J. Edsjö, L. Bergström, C. Farnier, Y. Akrami, JCAP **1001**, 031 (2010). [arXiv:0909.3300 [astro-ph.CO]]
31. C. Strege, G. Bertone, D.G. Cerdeno, M. Fornasa, R.R. de Austri, R. Trotta, [arXiv:1112.4192 [hep-ph]]
32. G. Jungman, M. Kamionkowski, K. Griest, Phys. Rept. **267**, 195 (1996). [hep-ph/9506380]
33. G. Bertone, D. Hooper, J. Silk, Phys. Rept. **405**, 279 (2005) [hep-ph/0404175]
34. L. Bergström, New J. Phys. **11**, 105006 (2009) [arXiv:0903.4849 [hep-ph]]
35. G. F. Giudice, A. Romanino, Nucl. Phys. B **699**, 65 (2004). [Erratum-ibid. B **706** (2005) 65] [hep-ph/0406088]
36. K. Griest, M. Kamionkowski, Phys. Rev. Lett. **64**, 615 (1990)
37. J. Ellis, T. Falk, K.A. Olive, Phys. Lett. **B444**, 367 (1998)
38. J. R. Ellis, T. Falk, G. Ganis, K.A. Olive, M. Srednicki, Phys. Lett. B **510**, 236 (2001). [hep-ph/0102098]
39. G.W. Bennett et al., Muon G-2 collaboration. Phys. Rev. D **73**, 072003 (2006). [hep-ex/0602035]
40. L. Covi, H. -B. Kim, J.E. Kim, L. Roszkowski, JHEP **0105**, 033 (2001). [hep-ph/0101009]
41. A. Kusenko, M.E. Shaposhnikov, Phys. Lett. B **418**, 46 (1998). [hep-ph/9709492]
42. M.I. Tsumagari, [arXiv:0910.3845 [hep-th]]
43. R. Catena, P. Ullio, JCAP **1008**, 004 (2010). [arXiv:0907.0018 [astro-ph.CO]]
44. J. Ellis, R. Flores, Phys. Lett. **B263**, 259 (1991)
45. J. Engel, Phys. Lett. **B264**, 114 (1991)
46. L. Bergström, P. Gondolo, Astropart. Phys. **5**, 263 (1996)
47. M. Drees, M. Nojiri, Phys. Rev. **D48**, 3483 (1993)
48. D. Bailin, G.V. Kraniotis, A. Love, Nucl. Phys. **B556**, 23 (1999)
49. L. Baudis et al., Heidelberg-Moscow collaboration. Phys. Rev. **D59**, 022001 (1999)
50. R.W. Schnee et al., CDMS collaboration, Phys. Rep. **307**, 283 (1998)
51. P. Belli et al., DAMA collaboration. Phys. Rep. **307**, 269 (1998)
52. P. Smith et al., UKDM collaboration. Phys. Rep. **307**, 275 (1998)
53. Z. Ahmed et al., CDMS-II collaboration. Phys. Rev. Lett. **106**, 131302 (2011).[arXiv:1011.2482 [astro-ph.CO]]
54. E. Aprile et al., XENON100 collaboration. Phys. Rev. Lett. **105**, 131302 (2010). [arXiv:1005.0380 [astro-ph.CO]]
55. A.K. Drukier, K. Freese, D.N. Spergel, Phys. Rev. D **33**, 3495 (1986)

56. A. Bottino, F. Donato, N. Fornengo, S. Scopel, Astropart. Phys. **13**, 215 (2000). [hep-ph/9909228]
57. S. Andreas, T. Hambye, M.H.G. Tytgat, JCAP **0810**, 034 (2008). [arXiv:0808.0255 [hep-ph]]
58. R. Bernabei et al., DAMA collaboration. Eur. Phys. J. **C56**, 333–355 (2008). [arXiv:0804.2741 [astro-ph]]
59. V. Springel, J. Wang, M. Vogelsberger, A. Ludlow, A. Jenkins, A. Helmi, J.F. Navarro, C.S. Frenk et al., Mon. Not. Roy. Astron. Soc. **391**, 1685 (2008). [arXiv:0809.0898 [astro-ph]]
60. V. Springel, S.D.M. White, C.S. Frenk, J.F. Navarro, A. Jenkins, M. Vogelsberger, J. Wang, A. Ludlow et al., Nature **456N7218**, 73–80 (2008)
61. J. Diemand, M. Kuhlen, P. Madau, M. Zemp, B. Moore, D. Potter, J. Stadel, Nature **454**, 735 (2008). [arXiv:0805.1244 [astro-ph]]
62. S.W. Barwick et al., Phys. Rev. Lett. **75**, 390–393 (1995)
63. O. Adriani et al., PAMELA collaboration. Nature **458**, 607 (2009). [arXiv:0810.4995 [astro-ph]]
64. A.A. Abdo et al., The fermi LAT collaboration. Phys. Rev. Lett. **102**, 181101 (2009).[arXiv:0905.0025 [astro-ph.HE]]
65. D. Müller, K.K. Tang, Astrophys. J. **312**, 183 (1987)
66. R.L. Golden et al., Astrophys. J. **457**, L103 (1996)
67. H. Gast, J. Olzem, S. Schael, *Proceedings of XLIst Rencontres de Moriond. Electroweak Interactions and Unified Theories*, (La. Thuile, Italy, 2006), pp. 421–428
68. S.W. Barwick et al., Astrophys. J. **482**, L191 (1997)
69. J.J. Beatty et al., Phys. Rev. Lett. **93**, 241102 (2004)
70. I.V. Moskalenko, A.W. Strong, Astrophys. J. **493**, 694 (1998). [arXiv:astro-ph/9710124]
71. O. Adriani et al., Phys. Rev. Lett. **102**, 051101 (2009). [arXiv:0810.4994 [astro-ph]]
72. F.A. Aharonian, A.M. Atoyan, H. J. Völk, Astron. Astrophys. **294**, L41–L44 (1995)
73. D. Grasso et al., FERMI-LAT collaboration. Astropart. Phys. **32**, 140–151 (2009). [arXiv:0905.0636 [astro-ph.HE]]
74. S. Profumo, Cent. Eur. J. Phys. **10**, 1 (2011). [arXiv:0812.4457 [astro-ph]]
75. D. Malyshev, I. Cholis, J. Gelfand, Phys. Rev. D **80**, 063005 (2009). [arXiv:0903.1310 [astro-ph.HE]]
76. L. Bergström, T. Bringmann, J. Edsjö, Phys. Rev. D **78**, 103520 (2008).[arXiv:0808.3725 [astro-ph]]
77. N. Arkani-Hamed, D.P. Finkbeiner, T.R. Slatyer, N. Weiner, Phys. Rev. **D79**, 015014 (2009) [arXiv:0810.0713 [hep-ph]]
78. Y. Nomura, J. Thaler, Phys. Rev. D **79**, 075008 (2009). [arXiv:0810.5397 [hep-ph]]
79. D.P. Finkbeiner, L. Goodenough, T.R. Slatyer, M. Vogelsberger, N. Weiner, JCAP **1105**, 002 (2011) [arXiv:1011.3082 [hep-ph]]
80. K. Lubelsmeyer, A. Schultz von Dratzig, M. Wlochal, G. Ambrosi, P. Azzarello, R. Battiston, R. Becker, U. Becker et al., Nucl. Instrum. Meth. A **654**, 639 (2011)
81. F. Donato, N. Fornengo, P. Salati, Phys. Rev. D **62**, 043003 (2000). [hep-ph/9904481]
82. J.E. Koglin, T. Aramaki, S.E. Boggs, W.W. Craig, H. Fuke, F. Gahbauer, C.J. Hailey, N. Madden et al., J. Phys. Conf. Ser. **120**, 042011 (2008)
83. H.U. Bengtsson, P. Salati, J. Silk, Nucl. Phys. **B346**, 129 (1990)
84. T. Sjostrand, S. Mrenna, P.Z. Skands, JHEP **0605**, 026 (2006). [hep-ph/0603175]
85. M. Srednicki, S. Theisen, J. Silk, Phys. Rev. Lett. **56**, 263 (1986). Erratum-ibid **56**, (1986) 1883
86. L. Bergström, H. Snellman, Phys. Rev. **D37**, 3737 (1988)
87. A. Bouquet, P. Salati, J. Silk, Phys. Rev. **D40**, 3168 (1989)
88. G. Jungman, M. Kamionkowski, Phys. Rev. **D51**, 3121 (1995)
89. M. Urban et al., Phys. Lett. **B293**, 149 (1992)
90. L. Bergström, J. Kaplan, Astropart, Phys. **2**, 261 (1994)
91. P. Ullio, L. Bergström, Phys. Rev. **D57**, 1962 (1998)
92. L. Bergström, P. Ullio, J.H. Buckley, Astropart. Phys. **9**, 137–162 (1998). [astro-ph/9712318]

93. A.A. Abdo, M. Ackermann, M. Ajello, W.B. Atwood, L. Baldini, J. Ballet, G. Barbiellini, D. Bastieri et al., Phys. Rev. Lett. **104**, 091302 (2010). [arXiv:1001.4836 [astro-ph.HE]]
94. A.M. Galper, R.L. Aptekar, I.V. Arkhangelskaya, M. Boezio, V. Bonvicini, B.A. Dolgoshein, M.O. Farber, M.I. Fradkin et al., Astrophys. Space Sci. Trans. **7**, 75 (2011)
95. L. Bergström, P. Ullio, Nucl. Phys. **B504**, 27 (1997)
96. Z. Bern, P. Gondolo, M. Perelstein, Phys. Lett. **B411**, 86 (1997)
97. J. Hisano, S. Matsumoto, M.M. Nojiri, O. Saito, Phys. Rev. **D71**, 063528 (2005). [hep-ph/0412403]
98. L. Bergström, Phys. Lett. B **225**, 372 (1089)
99. L. Bergström, T. Bringmann, M. Eriksson, M. Gustafsson, Phys. Rev. Lett. **95**, 241301 (2005). [arXiv:hep-ph/0507229]
100. A. Birkedal, K.T. Matchev, M. Perelstein, A. Spray, [arXiv:hep-ph/0507194]
101. L. Bergström, T. Bringmann, M. Eriksson, M. Gustafsson, Phys. Rev. Lett. **94**, 131301 (2995). [arXiv:astro-ph/0410359]
102. T. Bringmann, L. Bergström, J. Edsjö, JHEP **0801**, 049 (2008). [arXiv:0710.3169 [hep-ph]]
103. H. Goldberg, Phys. Rev. Lett. **50**, 1419 (1983)
104. E.A. Baltz, L. Bergström, Phys. Rev. D **67**, 043516 (2003). [arXiv:hep-ph/0211325]
105. J.F. Navarro, C.S. Frenk, S.D.M. White, Astrophys. J. **462**, 563 (1996)
106. A. Abramowski et al., H.E.S.S. collaboration. Phys. Rev. Lett. **106**, 161301 (2011).[arXiv:1103.3266 [astro-ph.HE]]
107. J. Aleksic et al., The MAGIC collaboration. JCAP **1106**, 035 (2011). [arXiv:1103.0477 [astro-ph.HE]]
108. M. Wood, G. Blaylock, S.M. Bradbury, J.H. Buckley, K.L. Byrum, Y.C.K. Chow, W. Cui, I.D.l.C. Perez et al., [arXiv:0801.1708 [astro-ph]]
109. T. Bringmann, M. Doro, M. Fornasa, JCAP **0901**, 016 (2009). [arXiv:0809.2269 [astro-ph]]
110. F.A. Aharonian, A.K. Konopelko, H.J. Volk, H. Quintana, Astropart. Phys. **15**, 335–356 (2001). [astro-ph/0006163]
111. E. A. Baltz, B. Berenji, G. Bertone, L. Bergström, E. Bloom, T. Bringmann, J. Chiang, J. Cohen-Tanugi et al., JCAP **0807**, 013 (2008). [arXiv:0806.2911 [astro-ph]]
112. J. Silk, A. Stebbins, Astrophys. J. **411**, 439 (1993)
113. L. Bergström, J. Edsjö, P. Gondolo, P. Ullio, Phys. Rev. D **59**, 043506 (1999). [astro-ph/9806072]
114. B. Moore, S. Ghigna, F. Governato, G. Lake, T.R. Quinn, J. Stadel, P. Tozzi, Astrophys. J. **524**, L19 (1999). [astro-ph/9907411]
115. P. Gondolo, J. Silk, Phys. Rev. Lett. **83**, 1719 (1999)
116. S. Ritz, D. Seckel, Nucl. Phys. **304**, 877 (1988)
117. J. Edsjö, Ph.D. Thesis, Uppsala University, hep-ph/9504205
118. F. Halzen, Comments Nucl. Part. Phys. **22**, 155 (1997)
119. A. Bottino, N. Fornengo, G. Mignola, L. Moscoso, Astropart. Phys. **3**, 65 (1995)
120. V. Berezinsky et al., Astropart. Phys. **5**, 333 (1996)
121. L. Bergström, J. Edsjö, P. Gondolo, Phys. Rev. **D55**, 1765 (1997)
122. M. Blennow, J. Edsjö, T. Ohlsson, JCAP **0801**, 021 (2008). [arXiv:0709.3898 [hep-ph]]
123. L. Bergström, J. Edsjö, P. Gondolo, Phys. Rev. **D58**, 103519 (1998)
124. T.K. Gaisser, F. Halzen, T. Stanev, Phys. Rep. **258**, 173 (1995)
125. M. Kamionkowski, G. Jungman, K. Griest, B. Sadoulet, Phys. Rev. Lett. **74**, 5174 (1995)
126. J. Edsjö, P. Gondolo, Phys. Lett. **B357**, 595 (1995)
127. L. Bergström, J. Edsjö, M. Kamionkowski, Astropart. Phys. **7**, 147 (1997)
128. A. Strumia, PoS **EPS-HEP2009**, 012 (2009)
129. L. Bergström, G. Bertone, T. Bringmann, J. Edsjö, M. Taoso, Phys. Rev. D **79**, 081303 (2009). [arXiv:0812.3895 [astro-ph]]
130. T. Bringmann, L. Bergström, J. Edsjö, JHEP **0801**, 049 (2008). [arXiv:0710.3169 [hep-ph]]
131. L. Bergström, T. Bringmann, J. Edsjö, Phys. Rev. **D78**, 103520 (2008). [arXiv:0808.3725 [astro-ph]]
132. L. Bergström, Phys. Lett. **B225**, 372 (1989)

133. T. Bringmann, F. Calore, G. Vertongen, C. Weniger, [arXiv:1106.1874 [hep-ph]]
134. N.F. Bell, J.B. Dent, A.J. Galea, T.D. Jacques, L.M. Krauss, T.J. Weiler, [arXiv:1104.3823 [hep-ph]]
135. P. Ciafaloni, M. Cirelli, D. Comelli, A. De Simone, A. Riotto, A. Urbano, JCAP **1110**, 034 (2011). [arXiv:1107.4453 [hep-ph]]
136. A. Sommerfeld, Annalen der Physik **403**, 257 (1931)
137. M. Kamionkowski, S. Profumo, Phys. Rev. Lett. **101**, 261301 (2008). [arXiv:0810.3233]
138. A. Hryczuk, R. Iengo, P. Ullio, JHEP **1103**, 069 (2011). [arXiv:1010.2172 [hep-ph]]
139. J.R. Ellis, J.S. Hagelin, D.V. Nanopoulos, K.A. Olive, M. Srednicki, Nucl. Phys. **B238**, 453–476 (1984)
140. P. Meade, N. Seiberg, D. Shih, Prog. Theor. Phys. Suppl. **177**, 143–158 (2009). [arXiv:0801.3278 [hep-ph]]
141. C.F. Berger, J.S. Gainer, J.L. Hewett, T.G. Rizzo, JHEP **0902**, 023 (2009). [arXiv:0812.0980 [hep-ph]]
142. J.A. Conley, J.S. Gainer, J.L. Hewett, M.P. Le, T.G. Rizzo, [arXiv:1103.1697 [hep-ph]]
143. L. Bergström, Phys. Lett. **B225**, 372 (1989)
144. For downloading DarkSUSY, visit http://www.fysik.su.se/~edsjö/ds
145. T. Bringmann, New J. Phys. **11**, 105027 (2009a). [arXiv:0903.0189 [astro-ph.CO]]
146. D. Spolyar, K. Freese, P. Gondolo, Phys. Rev. Lett. **100**, 051101 (2008). [arXiv:0705.0521 [astro-ph]]
147. F. Iocco, Astrophys. J. **677**, L1–L4 (2008). [arXiv:0802.0941 [astro-ph]]
148. P. Scott, M. Fairbairn, J. Edsjö, Mon. Not. Roy. Astron. Soc. **394**, 82 (2009). [arXiv:0809.1871 [astro-ph]]
149. S. Sivertsson, P. Gondolo, Astrophys. J. **729**, 51 (2011). [arXiv:1006.0025 [astro-ph.CO]]
150. D. Tucker-Smith, N. Weiner, Phys. Rev. **D64**, 043502 (2001). [hep-ph/0101138]
151. J. March-Russell, C. McCabe, M. McCullough, JHEP **0905**, 071 (2009). [arXiv:0812.1931 [astro-ph]]
152. Y. Cui, D.E. Morrissey, D. Poland, L. Randall, JHEP **0905**, 076 (2009). [arXiv:0901.0557 [hep-ph]]
153. D.P. Finkbeiner, T. Lin, N. Weiner, Phys. Rev. **D80**, 115008 (2009). [arXiv:0906.0002 [astro-ph.CO]]
154. D.S.M. Alves, M. Lisanti, J.G. Wacker, Phys. Rev. **D82**, 031901 (2010). [arXiv:1005.5421 [hep-ph]]
155. M.T. Frandsen, F. Kahlhoefer, J. March-Russell, C. McCabe, M. McCullough, K. Schmidt-Hoberg, Phys. Rev. **D84**, 041301 (2011). [arXiv:1105.3734 [hep-ph]]
156. K.R. Dienes, B. Thomas, [arXiv:1106.4546 [hep-ph]]
157. Y. Nomura, J. Thaler, Phys. Rev. **D79**, 075008 (2009). [arXiv:0810.5397 [hep-ph]]
158. P.J. Fox, E. Poppitz, Phys. Rev. **D79**, 083528 (2009). [arXiv:0811.0399 [hep-ph]]
159. B. Kyae, JCAP **0907**, 028 (2009). [arXiv:0902.0071 [hep-ph]]
160. D. Spolyar, M.R. Buckley, K. Freese, D. Hooper, H. Murayama, [arXiv:0905.4764 [astro-ph.CO]]
161. A. Ibarra, A. Ringwald, D. Tran, C. Weniger, JCAP **0908**, 017 (2009). [arXiv:0903.3625 [hep-ph]]
162. T. Cohen, K.M. Zurek, Phys. Rev. Lett. **104**, 101301 (2010). [arXiv:0909.2035 [hep-ph]]
163. N. Haba, Y. Kajiyama, S. Matsumoto, H. Okada, K. Yoshioka, Phys. Lett. **B695**, 476–481 (2011). [arXiv:1008.4777 [hep-ph]]
164. A. Menon, D.E. Morrissey, C.E.M. Wagner, Phys. Rev. **D70**, 035005 (2004). [hep-ph/0404184]
165. M. Dine, N. Seiberg, S. Thomas, Phys. Rev. **D76**, 095004 (2007). [arXiv:0707.0005 [hep-ph]]
166. N. Bernal, A. Goudelis, JCAP **1003**, 007 (2010). [arXiv:0912.3905 [hep-ph]]
167. M. Berg, J. Edsjö, P. Gondolo, E. Lundström, S. Sjors, JCAP **0908**, 035 (2009). [arXiv:0906.0583 [hep-ph]]
168. D.B. Kaplan, Phys. Rev. Lett. **68**, 741–743 (1992)

169. D.E. Kaplan, M.A. Luty, K.M. Zurek, Phys. Rev. **D79**, 115016 (2009). [arXiv:0901.4117 [hep-ph]]
170. A.L. Fitzpatrick, D. Hooper, K.M. Zurek, Phys. Rev. **D81**, 115005 (2010). [arXiv:1003.0014[hep-ph]
171. M.T. Frandsen, S. Sarkar, Phys. Rev. Lett. **105**, 011301 (2010). [arXiv:1003.4505 [hep-ph]]
172. M.L. Graesser, I.M. Shoemaker, L. Vecchi, [arXiv:1103.2771 [hep-ph]]
173. S. Profumo, L. Ubaldi, JCAP **1108**, 020 (2011). [arXiv:1106.4568 [hep-ph]]
174. C. E. Aalseth et al., CoGeNT collaboration. Phys. Rev. Lett. **106**, 131301 (2011). [arXiv:1002.4703 [astro-ph.CO]]
175. C.E. Aalseth, P.S. Barbeau, J. Colaresi, J.I. Collar, J. Diaz Leon, J.E. Fast, N. Fields, T.W. Hossbach et al., Phys. Rev. Lett. **107**, 141301 (2011). [arXiv:1106.0650 [astro-ph.CO]]
176. G. Angloher, M. Bauer, I. Bavykina, A. Bento, C. Bucci, C. Ciemniak, G. Deuter, F. von Feilitzsch et al., [arXiv:1109.0702 [astro-ph.CO]]
177. D. Hooper, T. Linden, Phys. Rev. D **84**, 123005 (2011). [arXiv:1110.0006 [astro-ph.HE]]
178. D. Hooper, S. Profumo, Phys. Rept. **453**, 29 (2007). [hep-ph/0701197]
179. M. Gustafsson, E. Lundstrom, L. Bergström, J. Edsjö, Phys. Rev. Lett. **99**, 041301 (2007). [astro-ph/0703512 [ASTRO-PH]]
180. G.F. Bertone (ed.), *Particle Dark Matter*, (Cambridge University Press, Cambridge, 2010)
181. S.J. Asztalos et al., The ADMX collaboration. Phys. Rev. Lett. **104**, 041301 (2010). [arXiv:0910.5914 [astro-ph.CO]]
182. M.L. Garde, J. Conrad, J. Cohen-Tanugi, M. Kaplinghat, G. Martinez, For the Fermi-LAT collaboration. [arXiv:1111.0320 [astro-ph.HE]]
183. J. Hamann, S. Hannestad, G.G. Raffelt, I. Tamborra, Y.Y.Y. Wong, Phys. Rev. Lett. **105**, 181301 (2010). [arXiv:1006.5276 [hep-ph]]
184. A.X. Gonzalez-Morales, R. Poltis, B.D. Sherwin, L. Verde, [arXiv:1106.5052 [astro-ph.CO]]
185. A. Bottino, F. Donato, N. Fornengo, S. Scopel, Phys. Lett. **B423**, 109 (1998)
186. R. Arnowitt, P. Nath, Phys. Rev. **D60**, 044002 (1999)
187. J. Cherwinka, R. Co, D.F. Cowen, D. Grant, F. Halzen, K.M. Heeger, L. Hsu, A. Karle et al., [arXiv:1106.1156 [astro-ph.HE]]
188. Z. Ahmed et al., The CDMS-II collaboration. Science **327**, 1619–1621 (2010). [arXiv:0912.3592 [astro-ph.CO]]
189. S.D. Hunter, D.L. Bertsch, J.R. Catelli, T.M. Digel, S.W. Dingus, J.A. Esposito, C.E. Fichtel, C.E. Hartman et al., Astrophys. J. **481**, 205–240 (1997)
190. W. de Boer, C. Sander, V. Zhukov, A.V. Gladyshev, D.I. Kazakov, Astron. Astrophys. **444**, 51 (2005). [astro-ph/0508617]
191. A.A. Abdo et al., The Fermi-LAT collaboration. Phys. Rev. Lett. **104**, 101101 (2010). [arXiv:1002.3603 [astro-ph.HE]]
192. J. Knodlseder, P. Jean, V. Lonjou, G. Weidenspointner, N. Guessoum, W. Gillard, G. Skinner, P. von Ballmoos et al., Astron. Astrophys. **441**, 513–532 (2005). [astro-ph/0506026]
193. G. Weidenspointner, G. Skinner, P. Jean, J. Knodlseder, P. von Ballmoos, G. Bignami, R. Diehl, A.W. Strong et al., Nature **451**, 159–162 (2008)
194. P. Meade, M. Papucci, A. Strumia, T. Volansky, Nucl. Phys. **B831**, 178–203 (2010). [arXiv:0905.0480 [hep-ph]]
195. L. Bergström, J. Edsjö, G. Zaharijas, Phys. Rev. Lett. **103**, 031103 (2009). [arXiv:0905.0333 [astro-ph.HE]]
196. D. Hooper, L. Goodenough, Phys. Lett. **B697**, 412–428 (2011). [arXiv:1010.2752 [hep-ph]]
197. D. Hooper, T. Linden, [arXiv:1110.0006 [astro-ph.HE]]
198. M. Chernyakova, D. Malyshev, F.A. Aharonian, R.M. Crocker, D.I. Jones, Astrophys. J. **726**, 60 (2011). [arXiv:1009.2630 [astro-ph.HE]]
199. A. Boyarsky, D. Malyshev, O. Ruchayskiy, [arXiv:1012.5839 [hep-ph]]
200. D. Hooper, D.P. Finkbeiner, G. Dobler, Phys. Rev. **D76**, 083012 (2007). [arXiv:0705.3655 [astro-ph]]
201. M. Su, T.R. Slatyer, D.P. Finkbeiner, Astrophys. J. **724**, 1044–1082 (2010). [arXiv:1005.5480 [astro-ph.HE]]

202. G. Bertone, M. Cirelli, A. Strumia, M. Taoso, JCAP **0903**, 009 (2009). [arXiv:0811.3744 [astro-ph]]
203. T. Schwetz, J. Zupan, JCAP **1108**, 008 (2011). [arXiv:1106.6241 [hep-ph]]
204. P.J. Fox, J. Kopp, M. Lisanti, N. Weiner, [arXiv:1107.0717 [hep-ph]]
205. M. Farina, D. Pappadopulo, A. Strumia, T. Volansky, [arXiv:1107.0715 [hep-ph]]
206. M.T. Frandsen, F. Kahlhoefer, C. McCabe, S. Sarkar, K. Schmidt-Hoberg, [arXiv:1111.0292 [hep-ph]]
207. Cherenkov Telescope Array Consortium, [arXiv:1008.3703 [astro-ph.IM]]
208. L. Bergström, T. Bringmann, J. Edsjö, Phys. Rev. **D83**, 045024 (2011). [arXiv:1011.4514 [hep-ph]]
209. L. Bergström, J. Edsjö, P. Ullio, Phys. Rev. Lett. **87**, 251301 (2001). [astro-ph/0105048]
210. P. Ullio, L. Bergström, J. Edsjö, C.G. Lacey, Phys. Rev. D **66**, 123502 (2002). [astro-ph/0207125]
211. I. Ferrero, M.G. Abadi, J.F. Navarro, L.V. Sales, S. Gurovich, [arXiv:1111.6609 [astro-ph.CO]]
212. W.H. Press, P. Schechter, Astrophys. J. **187**, 425 (1974)
213. J.D. Finke, S. Razzaque, C.D. Dermer, Astrophys. J. **712**, 238 (2010) [arXiv:0905.1115 [astro-ph.HE]]
214. W. Buchmuller, A. Ibarra, T. Shindou, F. Takayama, D. Tran, JCAP **0909**, 021 (2009). [arXiv:0906.1187 [hep-ph]]
215. M. Boylan-Kolchin, V. Springel, S.D.M. White, A. Jenkins, G. Lemson, Mon. Not. Roy. Astron. Soc. **398**, 1150 (2009). [arXiv:0903.3041 [astro-ph.CO]]
216. S. Hofmann, D.J. Schwarz, H. Stoecker, Phys. Rev. D **64**, 083507 (2001). [astro-ph/0104173]
217. T. Bringmann, New J. Phys. **11**, 105027 (2009). [arXiv:0903.0189 [astro-ph.CO]]
218. A.A. Abdo et al., Fermi-LAT collaboration. JCAP **1004**, 014 (2010). [arXiv:1002.4415 [astro-ph.CO]]
219. A. Pinzke, C. Pfrommer, L. Bergström, Phys. Rev. Lett. **103**, 181302 (2009).[arXiv:0905.1948 [astro-ph.HE]]
220. T.E. Jeltema, J. Kehayias, S. Profumo, Phys. Rev. **D80**, 023005 (2009). [arXiv:0812.0597 [astro-ph]]
221. M.A. Sanchez-Conde, M. Cannoni, F. Zandanel, M.E. Gomez, F. Prada, [arXiv:1104.3530 [astro-ph.HE]]
222. A. Pinzke, C. Pfrommer, L. Bergström, [arXiv:1105.3240 [astro-ph.HE]]
223. L. Gao, C.S. Frenk, A. Jenkins, V. Springel, S.D.M. White, [arXiv:1107.1916 [astro-ph.CO]]
224. L. Gao, C.S. Frenk, A. Jenkins, V. Springel, S.D.M. White, Mon. Not. Roy. Astron. Soc. **419**, 1721 (2012). [arXiv:1107.1916 [astro-ph.CO]]
225. J. Han, C.S. Frenk, V.R. Eke, L. Gao, S.D.M. White, [arXiv:1201.1003 [astro-ph.HE]]
226. S. 'i. Ando, E. Komatsu, Phys. Rev. D **73**, 023521 (2006). [astro-ph/0512217]
227. P.D. Serpico, E. Sefusatti, M. Gustafsson, G. Zaharijas, [arXiv:1109.0095 [astro-ph.CO]]
228. A. Cuoco, T. Linden, M.N. Mazziotta, J.M. Siegal-Gaskins, V. Vitale, E. Komatsu, f. t. F. -L. collaboration. [arXiv:1110.1047 [astro-ph.HE]]
229. J. Zavala, M. Vogelsberger, T.R. Slatyer, A. Loeb, V. Springel, Phys. Rev. D **83**, 123513 (2011). [arXiv:1103.0776 [astro-ph.CO]]
230. P. Gondolo, J. Silk, Phys. Rev. Lett. **83**, 1719 (1999). [astro-ph/9906391]
231. G. Bertone, A.R. Zentner, J. Silk, Phys. Rev. D **72**, 103517 (2005). [astro-ph/0509565]
232. P.H. Frampton, M. Kawasaki, F. Takahashi, T.T. Yanagida, JCAP **1004**, 023 (2010). [arXiv:1001.2308 [hep-ph]]
233. S.W. Hawking, Commun. Math. Phys. **43**, 199 (1975). [Erratum-ibid. **46** (1976) 206]
234. M.K. Parikh, F. Wilczek, Phys. Rev. Lett. **85**, 5042 (2000). [hep-th/9907001]
235. E.T. Akhmedov, D. Singleton, Int. J. Mod. Phys. A **22**, 4797 (2007). [hep-ph/0610391]
236. J.H. MacGibbon, B.J. Carr, Astrophys. J. **371**, 447 (1991)
237. M. Sahlen, [astro-ph/0304478]
238. B.J. Carr, K. Kohri, Y. Sendouda, J. 'i. Yokoyama, Phys. Rev. D **81**, 104019 (2010). [arXiv:0912.5297 [astro-ph.CO]]

http://www.springer.com/978-3-642-36133-3

Astrophysics at Very High Energies
Saas-Fee Advanced Course 40. Swiss Society for Astrophysics and Astronomy
Aharonian, F.; Bergström, L.; Dermer, C. - Walter, R.; Türler, M. (Eds.)
2013, XII, 361 p., Hardcover
ISBN: 978-3-642-36133-3